HIGH FUNCTIONAL DENSITY THROUGH RIGID-FLEX

By

Vincens Gjokaj

A DISSERTATION

Submitted to
Michigan State University
in partial fulfillment of the requirements
for the degree of

Electrical Engineering – Doctor of Philosophy

2021

ABSTRACT

HIGH FUNCTIONAL DENSITY THROUGH RIGID-FLEX

By

Vincens Gjokaj

In the last decade Additive Manufacturing (AM), often referred to as 3D printing, has garnered signficant interest in systems packaging. It has proven as an effective way of producing Radio Frequency (RF) to millimeter wave (mmWave) components and modules. AM enables flexible and rapid realization of structures with arbitrary shapes and complexity. AM is considered as one of the most important emerging material processing technologies that will drive the future designs of high functional density modules and systems. This thesis investigates the us of AM for the design and fabrication of microwave and mmWave circuits and systems.

Different AM technologies are used to design and demonstrate a range of high frequency passive and active components. Stereolithography printing is utilized to create passive components in the X-band (10-18 GHz) and K-band (18-27 GHz) frequency bands. These passive component designs are then combined with active RF circuits to design transmit and receive modules. Aerosol jet printing (AJP) is used to create an entirely printed mmWave components that avoids the use of traditional photolithography fabrication methods. All the designs are compared to their counterparts fabricated using conventional techniques. It is demonstrated that self-packaged RF components 3D form can readily be produced using AM leading to high functional density systems working well into the W-band frequency band.

For my parents and siblings, Pellumb, Gjyljana, Miklovan, and Desantila.

ACKNOWLEDGMENTS

This work is funded by the Department of Energy's Kansas City National Security Campus, operated by Honeywell Federal Manufacturing & Technologies, LLC under contract number DE-NA0002839.

TABLE OF CONTENTS

LIST OF FIGURES

CHAPTER 1

INTRODUCTION

1.1 Traditional Wireless systems design and packaging

In the area of electromagnetics, a major breakthrough happened in 1873 when James Clerk Maxwell published his book Treatise on Electricity and Magnetism which theoretically explained how these phenomenon work. Following this work, German physicist Heinrich Rudolf Hertz was able to prove Maxwells ideas in experimentation. The first science experiment with millimeter waves occurred in 1897, conducted by Jagadish Chandra Bose. The first public demonstration of a functional radio system was done by Guglielmo Marconi in England. Marconi transmitted a telegraph message across the English Channel in 1899, and sequentially transmitted a long-distance message from England to Canada in 1901. The greatest surge in radio technology was in the 1920s when radio broadcasts began happening each day and in the 1930s when radios became a common home appliance. in 1957 the Soviets launched the first satellite Sputnik into orbit. With the advent of the first transistor at Bell Labs in 1947, and the first integrated circuit (IC) patented by Jack Kilby in 1959 [1]. This marked a major path forward for radio systems. They were able to become smaller and less bulky which paved the way in the 1970s for Global Positioning System (GPS) and cellular networks to become commercially available. This was followed by wireless-fidelity networks in the 1990s and in the 2010s with the development of the 5th-generation (5G) networks.

A major use for wireless systems is for radar systems. This technology stretches across many platforms in modern technology. This was mainly utilized for military purposes when it first began being studied but now spreads to commercial aviation and is being incorporated into automobiles for driver assistance. The first notable radar patented was in 1903 in Germany. It was a spark-gap transmitter that was connected to an array of dipoles [2]. It had a basic function of noting when a mateallic body was approaching. This technology functioned on the principle of a transmit (Tx) module and a receive module (Rx). This would set the groundwork for future radar systems to be

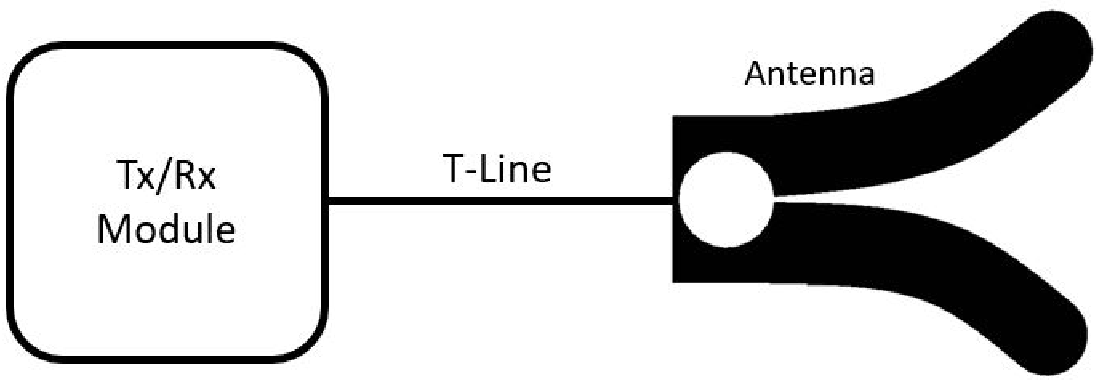

Figure 1.1: Three major parts of a system.

developed. The Tx and Rx modules can be broken down into three major parts as can be seen in Fig. 1.1. These parts of the module have been studied and developed over the years to achieve a high efficiency module. While the modules have been optimized for performance they still are expensive to produce and use. Recently, additive manufacturing (AM) has been studied to create some of these aspects of the modules to reduce the cost and make them compact. No real break through has been made to create a module that combines the standard components with the AM components to create a high efficiency module at a low cost.

1.1.1 System

The major development of radio technology can be mainly attributed to the development of packaging methods. In traditional manufacturing, remarkable changes are happening to wireless technology through miniaturization, integration, and innovation in both integrated circuits (IC) and packaging methods in order to meet on going challenges of greater functionality, higher performance, smaller size, lower cost, and faster time to market. Printed circuit boards (PCBs) are the essential parts to assemble modern electronic circuits. The PCB design and development process has a direct impact on the system cost and time to market. On average, companies report that PCB represents 31% of the overall product cost[3]. Industry uses various methods in modern day technology packaging to achieve the highest performance in a small lightweight package that is

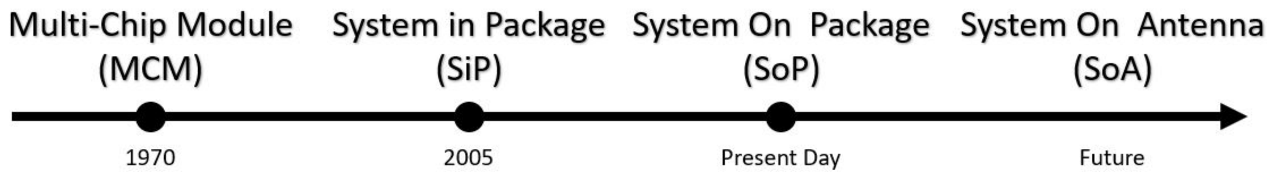

Figure 1.2: Time-line of packaging advances.

extremely cost effective to produce. The most commonly used packaging methods are System-On-A-Package (SOP), System-On-A-Chip (SOC), System-In-A-Package (SIP), and Multi-Chip-Modules (MCM). The time-line of these advances can be seen in Fig. 1.2. While high functional density has been achieved with the packaging of individual components, no solution to combing these systems to antennas without the use of bulky connectors or enlarging the circuit board or silicon die to fit the antenna.

1.1.1.1 Multi-Chip-Modules (MCM)

For the active analog/RF and digital/DSP functions, individual ICs can be interconnected using flip-chip bonding to eliminate bondwires (and their associated parasitic effects) and allow more compact MCM floor planning. An additional benefit of this approach is that complete system redesign is not necessarily needed to change one part of the subsystem/module; individual functional component dies could be upgraded as long as their interconnection scheme and footprint were kept the same to remain compatible with the MCM layout. The incorporation of microelectromechanical systems (MEMS), smart materials, smart antennas, and etc., with mixed-signal ICs in such an environment is now increasingly referred to as “mixed-technology” or “heterogeneous” integration [4]. The multilayer ceramic MCM package offers an attractive alternative to the conventional plastic QFP package in terms of significant size reduction, thickness, and performance at high frequencies for the mobile communication market [5]. A strong alternative to complete single-chip SOC integration is some advanced form of an MCM solution, which integrates antenna, filters, resonators, baluns, and other RF components. These can be integrated in either ceramic, such as low-temperature cofired ceramic (LTCC), or organic, such as multilayer

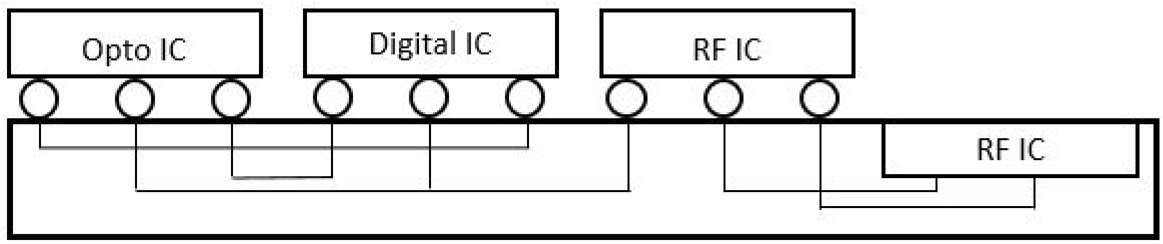

Figure 1.3: Drawing of MCM.

organic (MLO). The basic philosophy for MCM is to fabricate devices and circuits in the optimum available technology for their particular function (e.g., digital circuits in submicrometer CMOS, analog components in BiCMOS, RF components in GaAs or InP) and then integrate them into a system or subsystem using MCM technology. High-Q passive structures could potentially be embedded directly into the MCM structure. Since MCM utilizes the optimum substrates for each the devices packaged it overcomes a lot of the issues that SOC faces. A drawing of MCM can be seen in Fig. 1.3.

1.1.1.2 System-On-Chip (SOC)

Integration of complete systems of RF analog & digital functions in a single chip is typically referred to as System-On-A-Chip (SOC). But this method is facing many obstacles due to the requirements for high capacity memory devices, duplexer and filter banks, MEMS, and High Q Devices[3]. Another major limitation of SOC is the extremely high initial cost of producing the system. Developing and fabricating ICs is one of the highest expenses a manufacturer of electronic components can have. When combining many functions into one Chip, the SOC movement is ambushed by the cost of additional mask layers needed to marry digital logic with memory and analog function on one specific and optimum substrate [4]. Also if any changes are wanted to be made to the system the chip has to be completely re-fabricated from the masks and this makes it extremely expensive. SOC offers many benefits, out of all packaging methods SOC offers the smallest size & footprint, it also offers an increased sensor density[6]. Because of this SOC are most commonly used today for powering smart phones and tablets because they offer the small

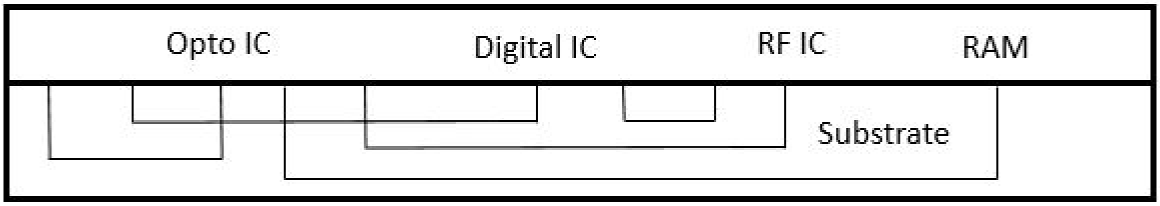

Figure 1.4: Drawing of SOC.

size needed for all the components. Typical smart phone applications for SOC package the Central Processing Unit (CPU), Graphical Processing Unit (GPU), Random Access Memory (RAM), Read Only Memory (ROM), and even the Modem for the wireless connectivity of the smart phone (LTE, Bluetooth, Cellular) into one packaged IC chip. A drawing of SOC can be seen in Fig. 1.4. A downside of utilizing SOC is that its impossible to connect wires to it; which this limits the package to be utilized only on printed circuit boards (PCBs). Also the SOC packaging method is really hurt by the cost added by additional mask layers needed to marry digitial logic with memory and analog functions on one specific substrate [4]. Another downside of SoC is the inability to add antennas that have high gain and large bandwidths because of the size of the antenna. This increases the size of the chip which increases the production cost as will as decreasing the performance of the antenna due to utilizing silicon as the substrate.

1.1.1.3 System-On-Package (SOP)

Recently, a new concept called SOP is introduced in which the package, and not the board, is the system. As such, SOP is beginning to address the shortcomings of both SOC and SIP[4]. The system-on-a-package (SOP) concept is considered as the solution of future communication modules, which would need more functionality, better performance, low cost, and more integrity[7]. The concept of SOP can be thought of a conceptual paradigm in which the package, and not the bulky board acts as the system and the package provides all the system functions in one single module, not as an assemblage of discrete components to be connected together, but as a continuous merging of various integrated thin film technologies to comprise a system solution in a small package[8]. SOP aims to utilize the best of on-chip SOC integration and package integration to

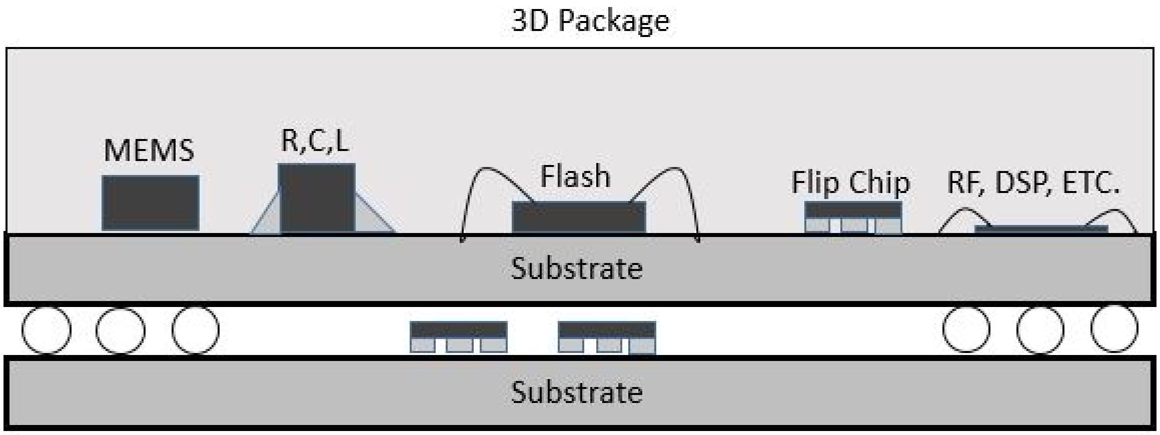

Figure 1.5: Drawing of SOP.

achieve the highest system performance at the lowest cost. Similar to a wafer-to-IC concept, the SOP packages are fabricated on panels using low cost processes used in high density organic packages and diced to smaller sizes. This leads to tremendous size and cost reduction, functionality, performance, and reliability. SOP overcomes both the computing limitations and integration limitations of SOC, SIP, MCM and traditional system packaging. The limitation of this technology is the interconnect delay is becoming a serious bottleneck for the new generation of high speed digital systems [8]. As well as one of the major issues for developing SOP is integrating an antenna with a module efficiently. Fabricating an antenna directly on the package has the advantages of reducing interconnect loss and size of an entire module. SOP goes one step beyond multichip module (MCM) by enhancing overall performances and adding more functionalities[7]. A drawing of SOP can be seen in Fig. 1.4.

1.1.2 Transmission lines

Transmission line is one of the most basic RF passive components. A transmission lines sole purpose is to carry a signal from one point to another. The three forms of transmission lines are microstrip, coaxial, and waveguide based. Hollow metallic waveguide based transmission lines have been utilized since they offer low loss characteristics. As new dielectric materials have been developed with low-loss, low tan-δ, low loss microstrip and coaxial transmission lines are commonly employed in the design of high frequency circuits.

1.1.3 Antenna fabrication

There are three main forms of antennas that are commonly employed. The most basic form of antenna is the wire antenna. This is known as the Monopole and Dipole antenna. Sometimes they are referred to as a Whip antenna and most notably found on automobiles. These are low gain antennas that have a broad beam width. These antennas are very basic antennas that are designed to be quarter wavelength long. Whip antennas offer a very narrow operating frequency band.

The second form of antenna is the the planar or microstrip patch antenna. These substrate based antennas are ground plane back antennas that offer higher gain at the expense of a smaller beamwidth, which is needed in many applications. These offer the benefit of being easily incorporated with planar circuits. Microstip antennas are dependent on substrate properties and it becomes increasingly expensive more expensive as the frequency increases the substrates need to be lower loss. These antennas allow for various designs to meet specific criteria such as operating frequency range, gain, directivity and polarization.

The third form is traveling wave antennas. The most common are Vivaldi, leaky-wave, and Yagi-Uda antennas. These offer the benefit of being very high gain, high directivity, and large bandwidth. The downside of these antennas are the size is large and typically linearly polarized. The other difficulty of these antennas are the feeding network is more complex. They are not ground plane back antennas which limits a direct microstrip feed without multilayer fabrication. Traveling wave antennas are also larger when compared to their counterparts.

1.2 Additive Manufacturing of Wireless Components

AM is a form of manufacturing in which a Computer Aided Design (CAD) model is captured and then subsequently fabricated in a layer-by-layer manner – eliminating tooling and enabling complex geometries not possible with traditional manufacturing [9]. It is revolutionizing how critical parts get manufactured, fast prototyping, reduced waste, allows custom designs, easier design adjustments, and parts can be printed as a single unit. This contrasts with traditional manufacturing, which cuts, drills, and grinds away unwanted excess from a solid piece of material, often metal. The term AM is a term that encompasses several different methods and technologies of AM. In 2015 the ISO/ASTM 529000 [10] standard was created in an effort to standardize the terminology and classify each method of AM. In total there are seven different categories of AM processes have been established and are used to identify which process of AM is used. Though in general all of the processes follow the same basic steps of generating individual physical layers and combining them together [11]. This section will introduce and describe each of the classifications with an example of a typical 3D printer that utilizes that method followed by a section on the process of blanket metallization used to metallize all the plastic AM. components. The cost of 3-D printers and the materials used in them are continuing to decrease as the technology gains in popularity and utility which makes it a promising technology for the RF world especially for small scale operations and prototyping.

1.2.1 Fused Deposition Modeling (FDM)

The most basic form of AM is FDM printing sometimes referred to as Fused Filament Fabrication (FFF). This process uses a spool of plastic filament that is fed through a printer head which is heated and the filament is pushed through the head which causes it to melt. The printer head is moved to specific points laying down the melted filament in layers on a build plate, the filament then cools down on the build-plate and solidifies into a solid object. For layers that are floating or not directly touching a layer below it; supports are also printed to support the layer in the position it is in as can seen in 1.6. This process is repeated layer by layer until the object is fully created. This method of 3D printing is very affordable, a standard FDM printer costs a few hundred dollars which has made it extremely popular among hobbyist. Typical FDM printers are the Makerbot and Flashforge.

The surface of these AM structures has a certain roughness level due to laying separate layers of the melted filament on top of each other. When looking at the root-mean-square (RMS) of

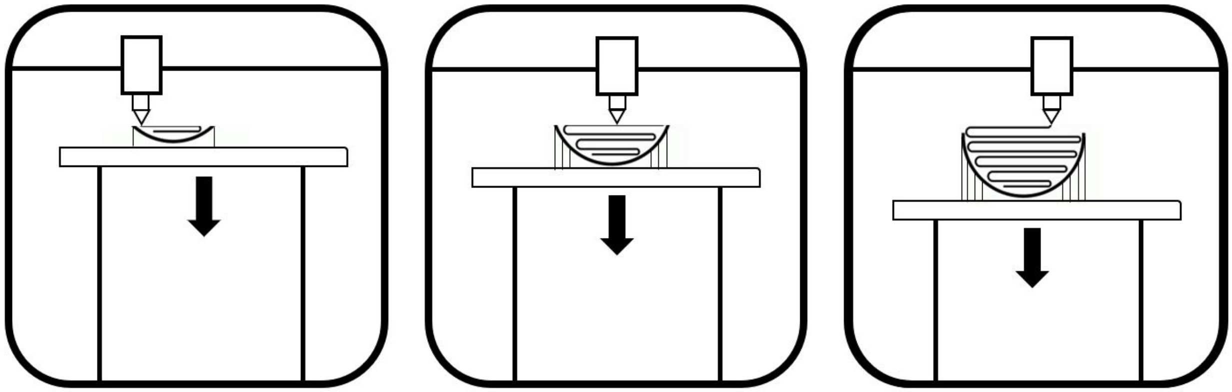

Figure 1.6: Drawing of the FDM process.

the surface roughness it is dependent on a few conditions, the printing tip diameter, the nozzle temperature, ambient temperature, and it is also dependent on which material is being printed[12]. For a 200 μm print nozzle it can be expected to have a RMS surface roughness of about 100 μm. Due to this relatively high surface roughness it makes FDM not an ideal choice of AM to use above X-band frequency range (8-12 GHz).

1.2.2 Stereolithography (SLA)

Stereolithography referred to as (SLA) is the oldest form of AM. The first patent was filed for in 1986 and the company 3D systems commercialized the technology [13]. SLA printers use mirrors in the X and Y-axis, and the mirrors aim a sold-state laser to cure a reservoir of resin selectively.The resin is a photo-polymer which is cured by light. The build platform moves up out of the reservoir and layer by layer the object is built. A drawing of this process can be seen in Fig. 1.7. The most common type of commercially available SLA printer is the Formlabs which offers SLA printers with accuracy down to 25 μm and various material choices from flexible, high temperature, and standard [14]. The high temperature materials offered with SLA printing offer an ability to maintain structure and form at over 200^{o}c.

SLA is one of the most accurate AM for large structures [11]. SLA provides a superior and smoother surface finish but with photo-curable materials that suffer from poor mechanical strength or durability and degrade or discolor with prolonged UV exposure [15]. SLA produces structures

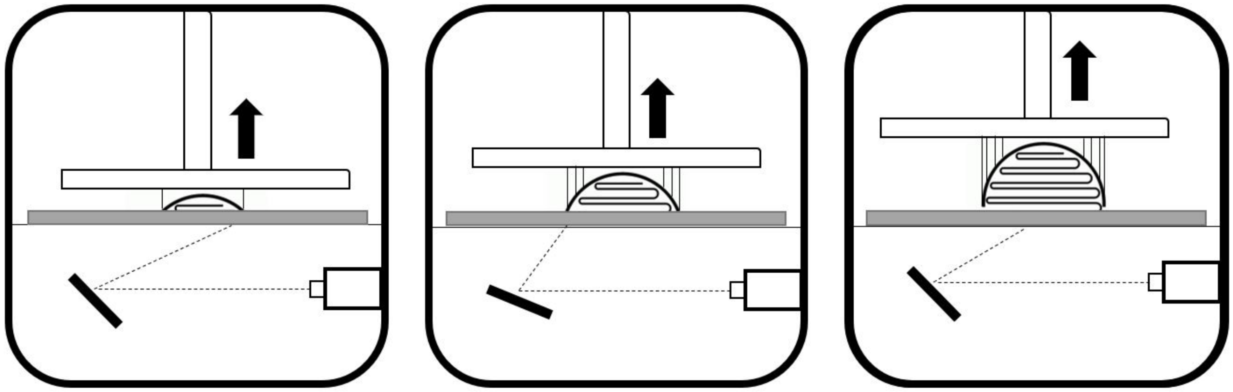

Figure 1.7: Drawing of the SLA.

with a RMS surface roughness of 25 μm which makes it an good choice to use on structures with feature as small as 100 μm [16]. This low surface roughness allows SLA to be used to create structures up to the W-band frequency Range (75-110 GHz).

1.2.3 Polyjet Printing/ Material Jetting (MJ)

Polyjet printing which is the commercial name for material jetting works very similarly to a standard home inkjet printer. Just as a inkjet printer prints a single layer of ink- Material Jetting prints multiple layers, moving the build platform down a layer thickness between each layer until the object is created. This process can be seen in a sketch in Fig. 1.8. The print-head jets hundreds of droplets of a photopolymer, which is then followed by a ultraviolet (UV) light to crosslink the droplets and create a solid object. MJ printing produces solid objects at a faster pace than other forms of AM. Also, an added benefit of MJ method is that it allows for different materials to be printed in the same object. The MJ method does require objects to be printed with a support material, typically a wax that is printed simultaneously during the printing of the object. With the latest advances in MJ the support material can be removed from the printed structure with relative ease in the post processing state using standard solvents like acetone and isopropyl alcohol (IPA). MJ is one of the only types of AM technologies to offer printing with multi-material and full color printing. MJ offers the best surface finish of AM, MJ produces injection mold-like prototypes. MJ offers print resolution of 16 μm and surface roughness down to 10 μm RMS. A standard MJ 3D

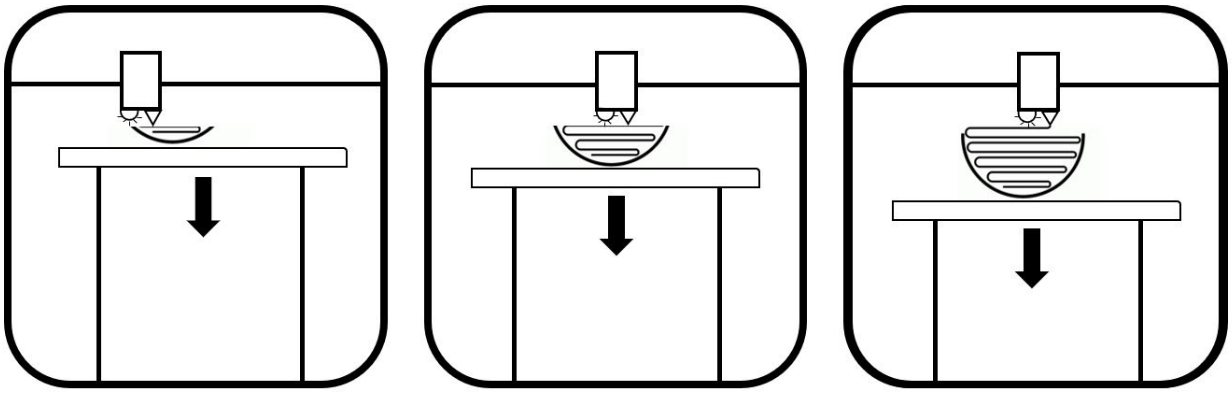

Figure 1.8: Drawing of the MJ.

printer is stratsys connex objet 350.

With MJ offering such a superior surface finish, it has been used for various RF components from microstrip circuits, waveguides, antennas, and dielectric lenses [17]. Recently techniques have been developed that utilize MJ to create microstrip structures and be able to selectively metalize using a damascene-like method [18]. While this method does not produce fine features to the same level as the industry standard of photolithography, it does allow creating fine featured microstrip structures without the use of chemicals, masks, and the need for precise alignment. Articles have been published that utilize MJ to print side-coupled filters and utilized the damascene-like method [18] to create the side-coupled filter structure. Horn antennas have been shown to work up into the W-Band frequency range utilizing MJ but dielectric probes have been fabricated using MJ up into the THz frequency range (300 GHz and above) [19]. From a RF standpoint the main disadvantage of MJ is typically the printed polymers have high dielectric losses (Tan-δ=0.04) which why it has been mainly used to make guided wave electronics that utilize air as the substrate and the AM components acts as a structure for the metal layer deposited on top of the plastic.

1.2.4 Inkjet/Aerosol Jet Printing (AJP)

Aerosol Jet Printing (AJP) and inkjet printing are very similar in nature, the principles of operation are, an ink which can be either dielectric or conductive is sent to the print head and printed and the object is created layer by layer. There are 3 major differences between these technologies. AJP offers a better print resolution almost 4 times better when compared to inkjet printing; AJP has a 5 μm print resolution where inkjet typically offers about 20 μm. The second main difference is the method of which AJP with using a sheath gas to columnize the ink where inkjet just does droplets as shown in Fig. 1.9; this allows AJP to have a greater variance in ink viscosity. Typically for AJP the ink can range from 0.5 to 2000 cP where inkjet is typically limited below 20 cP [20]. The third main difference is that AJP can have a larger variance in distance between the print head and the substrate; typically the distance for AJP can vary between 1 and 5 mm where for inkjet printing that distance is fixed typically around 1 mm. This allows AJP to print on non-flat objects where in some instances it may be impossible to do utilizing Inkjet. A standard AJP printer is the Optomec 5XJ.

The typical use for AJP and is to print fine featured conductive traces. Out of all the methods of AM; AJP offers the highest print resolution which makes it impractical to use for large 3D objects. AJP has been used to make very small microstrip lines or high frequency antennas, THz filters, and interconnects between substrates and bare-die IC components using conductive inks [20]. The conductive inks have been shown in recent publications to achieve conductivity as high as 70% of bulk silver (Ag) [21]. With this high conductivity , a recent publication showed AJP interconnects having a loss of 0.49 dB/mm for the entire structure including the trapezoidal transition. This same publication showed an AJP printed CPW on Rogers Ultralam 3850HT (LCP) exhibited 0.38 dB/mm at 110 GHz loss that is by far better than other AM techniques. AJP having such an extremely high resolution, it was recently used to create band-pass and band-stop filter at 250 GHz and 550 GHz [22]. This makes AJP highly attractive for fine featured microelectronics that otherwise would need to be fabricated in cleanroom (microfabrication facilities) using various harsh chemicals.

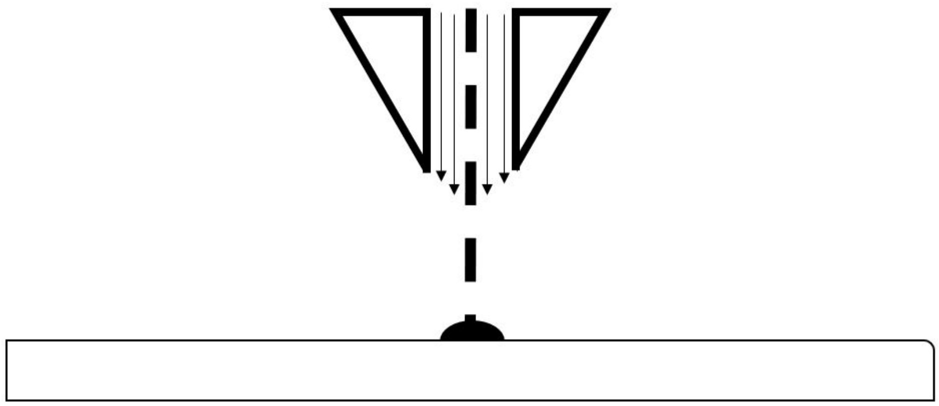

Figure 1.9: Drawing of Inkjet and AJP.

1.3 Limitations of Combining Standard Technology and Additive Manufacturing

Additive manufacturing has presented a new method in the evolution of RF passive component manufacturing. By providing a low cost means of rapidly producing prototype components necessary during design stages, as well as a method for fabricating components with minimal waste, these passive components can be easily designed and tested through out the design stages. While additive manufacturing has recently proven as an effective manufacturing method, and the standard manufacturing methods described have been utilized for a few years now, there has been very limited work that combines these different technologies together.

Each of the additive manufacturing methods offers distinct advantages over one an other. The limitations of these technologies are faced when trying to combining them with standard technologies. MJ and FDM printing offer a good solution to printing large structures but it becomes to incorporate the printed pieces with systems. The ability to easily fabricate large structures with MJ and FDM, limits this technology to incorporate it with standard and widely used active component packaging methods. With the high loss tangent material these printed components have to use external coupling methods like coaxial or waveguides to feed the signal. This greatly limits the ability to further increase the density.

Aerosol jet printing has recently proven to also provide a convenient means to deposit materials while achieving good print resolution. Fine featured structures in the several millimeters can be fabricated. Aerosol jet printing has been used to fabricate of a wide range of electrical circuits, including transmission lines operating in W-band [23], filters [24], and antennas [25]. Other passive components have been shown as well inductors, capacitors [26], and resistors [27]. Unlike the other forms of printing AJP offers a great method to fabricate fine structures and directly combine the standard forms of system integration. While this offers the best method to attaching standard packages to printed components, the disadvantage is the limitation in creating large thick structures. The thick structures will be needed for the traveling wave antennas.

In recent publications these various techniques have shown very effective. There have been no real work at combing additive manufacturing with standard packages to create a system. There needs to be a technique that combines various forms of additive manufacturing with standard component packages to create a system that maximizes the functional density of the entire system. This will minimize the cost and waste of manufacturing as well as allowing for the next generation of RF components through 100 GHz and beyond.

1.4 Rigid-Flex System On Antenna

The polyjet printing of these AM has been utilized to create antennas up into the V-band with high repeatability. AM can create large structures with resolutions up to 16 μm in a fast process with surface roughness below 100 μm Ref. [28]. AM techniques present a new manufacturing process in the evolution of RF component manufacturing by utilizing the Z-axis. By providing a low cost means of rapidly producing prototype components necessary during design stages, as well as a low cost method for fabricating components that can be integrated directly into modern systems. Some processes to package electronics utilizing additive manufacturing techniques have already been demonstrated. Packaged electronics have been embedded within printed objects, connected by wires or by traces formed from post-processing of the printed substrate [29]. By embedding devices in an object during the print process, blanket metallization has been utilized to create a resonator and antenna that can be tuned up to 7 GHz [30].

The objective of this thesis, is to investigate and demonstrate a fundamentally new approach to manufacture electronic systems. Here we exploit AM to realize high functional density systems by integrating planner circuits directly into a AM antenna to create a System on Antenna (SoA) as shown in Fig. 1.10. The process includes integrating active and passive elements, directly in a AM Vivaldi antenna. This allows the creation of a novel module that is fully enclosed inside of the unused portion of the antenna. This creates the smallest feed line for the system which inevitably leads to a higher signal-to-noise ratio (SNR). This thesis paves the way for AM components to be taken from a novelty of passive components to being utilized as a fundamental aspect of the entire system. This allows for the printed component to be utilized as the structure and foundation for the system to be created with in. The utilization of Aerosol printing further increases the functional density by allowing fine conductive traces to be created as well as finer VIAs to ground. This work creates a small form factor module that as almost entirely fabricated through A.M. This methodology allows for cost effective modules to be created which avoids the use of power splitters as well as the need for high power amplifiers due to the high efficiency of the individual modules. This work shows how a front end system can go from four antennas being fed from one power source to four individual modules being fed individually without the use of an inefficient high power amplifier. This achieves higher power transmission and better energy efficiency with out the need for a bulky heat dissipation metal plate. Each of these individual modules can be tuned to operate at the same frequency point through a simple phase lock loop (PLL) module which has the benefits of being very easy to implement and operates at a very low power level.

1.5 Dissertation Outline

The main objective of this work is to develop the methodology of combining RF circuits created on flexible substrates with AM components to create entirely packaged systems from the microwave frequency range into the W-band spectrum and pave the way for future work into the 500 GHz range. This work is organized as follows:

In chapter 2, this work will dive into better understanding of polyjet printing and understand-

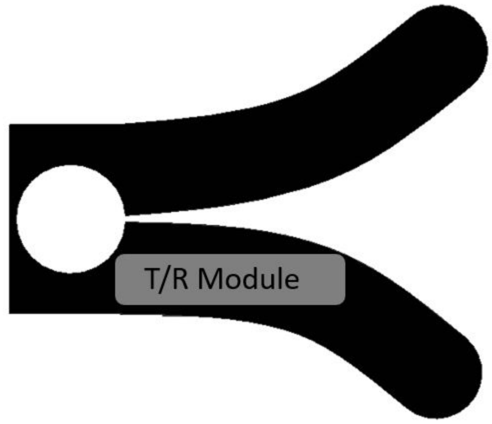

Figure 1.10: SoA Mock Up.

ing this technology. Components like transmission line, resonators, and antennas are studied to understand performance. Reduced height waveguides RHW are utilized to avoid using AM material as the substrate. Complex geometries are shown that can be fabricated with relative ease. The antennas presented have a efficiency above 80%.

In chapter 3, a combination of a flexible substrate and AM structures is presented. Beginning with Transmission lines, performance is studied through 67 GHz. Then This feed is utilized to create various antennas and antenna arrays that can be reconfigured at the 10-30 GHz frequency range. This chapter is then finished with a Vivaldi antenna directly embedded into a scaled down version of a automotive bumper.

In chapter 4, a combination of flexible LCP and AM is used to create a coax-like transmission line. This transmission line is utilized to create various RF components. This expands from very low-loss transmission lines, high Q-factor resonator, antennas, and antenna array. This approach shows a very effective way of creating small form factor RF components.

In chapter 5, this methodology is used to build a entirely 10-15 GHz packaged system inside of a AM antenna to create a receive SoA. This circuit that is fabricated through standard photolithography will be embedded inside of the unused space inside of the AM antenna. This system is compared to a standard gain horn antenna with the same circuit attached with edge mount connectors. Performance of this SoA is based on the received power compared to a standard gain horn an antenna with the same connectorized circuit..

in chapter 6, a transmitter SoA is built. With the high accuracy of the Aerosol Printer to put down conductive traces, the circuit traces for this system are printed directly onto the flexible substrate. The benefit of using the aerosol jet printer for the traces, it also allows to create VIAs to ground directly when printing the traces. This creates a high functional density SoA at 15 GHz that is within 1 dB of theoretical power transfer calculations.

CHAPTER 2

HIGH FREQUENCY APPLICATIONS OF POLYJET PRINTING

2.1 Introduction

Traditionally, fabrication of components utilizes various processes such as micromachining, and other lithographic techniques [31]. These processes require cleanroom facilities, multiple pieces of dedicated equipment, as well as highly skilled technicians to fabricate these components. The processes described above utilize various chemicals to layout a mask of a desired component pattern and then chemically etch the metal layer to only leave the desired pattern. While this method has been developed and become very good at fabricating components this method is very expensive and has a lot of material waste.

With advances in additive manufacturing (AM), prototype structures with precise dimensions and tolerances can readily be fabricated in a short turn around time. Now structures that would have been difficult, if not impossible, to produce using conventional micromachining techniques can readily be produced [32]. Recently, 3D printing has become a hot bed for research in the electromagnetic community and circuits operating well into the terahertz (THz) frequency range have been demonstrated [33]. The use of cleanroom facilities can be minimized to reduce overall labor and material costs. Due to these benefits and reduced material waste 3D printing has attracted significant interest in the design and fabrication of RF circuits and components [34].

Additive manufacturing (AM) has been studied as a potential replacement to traditional methods in the fabrication of RF components. Advantages of AM include fast prototyping, low material loss, and low hazardous waste generation. With AM, a single tabletop system is sufficient to fabricate a wide range of components, rather than requiring multiple machines, each dedicated to a specific fabrication task. Recently, a range of 3D printed RF components have been demonstrated using polyjet printing (MJ). This includes various structures like waveguide [35], coaxial cables [36] and antennas [34]. MJ has also been utilized to create components up in the THz [37], this work utilized MJ to create molds for the components.

The MJ process operates similar to the standard home printer. It jets droplets of photopolymer which after being exposed to a UV light crosslinks to become a solid. This process is repeated until the desired 3D geometry is completed. For complex geometries that have holes or overhangs, the 3D printer also jets a support material which is gel like. This material is sacrificial which is utilized to create a solid structure when pared with the photoplymer. Once the entire structure is printed the support material can be either mechanically removed or dissolved by solvents.

The goal of this chapter is to study the performance of AM components. In contrast to work presented in [34] & [36]; There have been several papers that have noted the dielectric properties of the printed material, a dielectric constant of 2.9 and a dielectric loss-tangent of 0.04 can be expected. To over come this realitivily high loss of the print material, this chapter will focus on Reduced Height Wave guides (RHW) which will utilize the print material as a support for copper and will allow air to be the dielectric. This work will focus on various RHW structures. RHW structures are investigated to test various complex geometries. These structures are AM then blanket metalized through sputter deposition and followed by a Damascene like process to achieve a desired metal pattern. This investigation will primarily focus on the 1- 30 GHz frequency range.

2.2 Design and Simulation

Several components have been fabricated to study the performance of the MJ components in the 1-30 GHz range. The components are printed using a commercially available Objet Connex 350 polyjet printer. VeroWhitePlus dielectric material, a UV-cured polymer, was used in the fabrication as it has the lowest loss among the different materials compatible with this printer. The printer has a 16 μm print resolution and can provide a smooth surface finish with surface roughness of <5 μm. After printing, the structures are metalized using sputter deposition with a 0.1 μm layer of Ti followed by 0.5 μm of Cu. The Ti layer is used to promote adhesion between Cu and the dielectric material. This is followed by electroplating of 6 μm of copper. The surface area around the copper was raised by 200 μm to use the Damascene-like process of mechanically polishing away excess copper [38]. Several constraints are considered in the design of each component to be fabricated. Due to the limitations of AM, no features smaller than 200 μm will be considered for fabrication.

2.2.1 Metallization

Most forms of AM the printing is limited to plastics (FDM, MJ, SLA) which requires blanket metalization of the AM object to be used for waveguide, microstrip, or antenna structures. One one of the most common methods for blanket metalization is Sputter Deposition, in which the objects are placed inside of a vacuum chamber and then a seed layer of Titanium (Ti) is coated (500 nm) around the structure, Ti acts as an adhesion layer for the the next layers of metal, Ti is typically followed by a layer of copper (Cu) which is coated on about 1 μm thick [38]. But other metals can be sputter coated aswell; the choice of metal is chosen based of desired conductivity and particular application. To avoid metallic losses caused by the skin-depth affect [39], which is defined by Egn. 2.1, the Cu coated pieces can either be electroplated or electrolysis with additional metal until the desired metal thickness is achieved. The main difference between electrolysis and electroplating is that electrolysis is the use of electrical current to drive a chemical reaction whereas electroplating is the use of electrical current to plate one metal on another metal. Sputter deposition is the most common method of blanket metallization due to its ability to produce a smooth metal layer on top of the AM object which helps with RF performance.

$$\delta = \frac{1}{\sqrt{\pi f \mu \sigma}} \tag{2.1}$$

2.2.2 Reduced Height Waveguide Transmission Line

Two waveguide based transition are designed to operate in the TE_{10} mode. The height of the waveguide was set to 1.52 mm such that a standard edge launch SMA connector can be used, see Fig. 2.1. This waveguide does not have the normal 50 Ω impedance, thus a transition section from microstrip to this waveguide is necessary so that standard edge launch SMA connectors can be

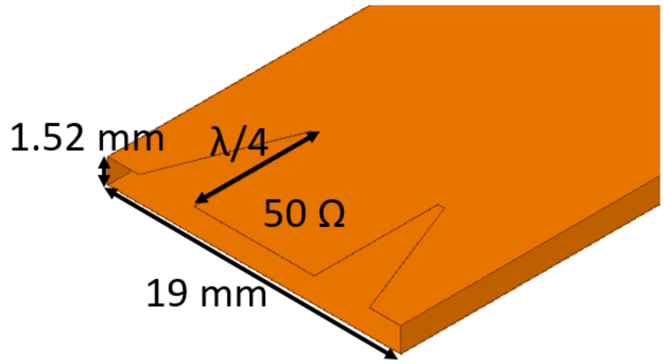

Figure 2.1: Designed inset for the RHW structure. λ is wavelength of the center frequency.

used. The inset of the 50 Ω microstrip line was set to be $\frac{\lambda}{4}$ at 20 GHz and the metal tapering from waveguide to the 50 Ω microstrip line was optimized to achieve low insertion loss.

$$f_{c_{10}} = \frac{1}{2a\sqrt{\mu\varepsilon}} \tag{2.2}$$

Two waveguides having the same transition but different lengths (40 and 60 mm) were designed and fabricated. Waveguide loss can be determined with higher accuracy from the difference in the insertion loss measurements of these waveguides. This approach removes any losses associated with the transition section. The two RHW structures are shown in Fig. 2.2. At 20 GHz the 40 mm and 60 mm waveguides have a simulated insertion loss of 0.0975 dB and 0.128 dB, respectively. The difference in insertion loss between the two structures was 0.0053 dB which is effectively the loss of a 20 mm long section. It also shows that the loss of these individual waveguides is dominated by the transition sections and can be further optimized to reduce loss. The simulated results can be seen in Fig. 2.3.

2.2.3 Reduced Height Waveguide Resonator Resonator

Typically when describing filters and resonators, the Q-factor is an important measure. Higher Q-factors denote a better performance and this is inversely proportional to the loss in the resonator. Standard microstrip resonators have a Q-factor between 10-100 whereas waveguide based T-line resonators have Q-factors > 1000. For this RHW resonator the 60 mm RHW through from above

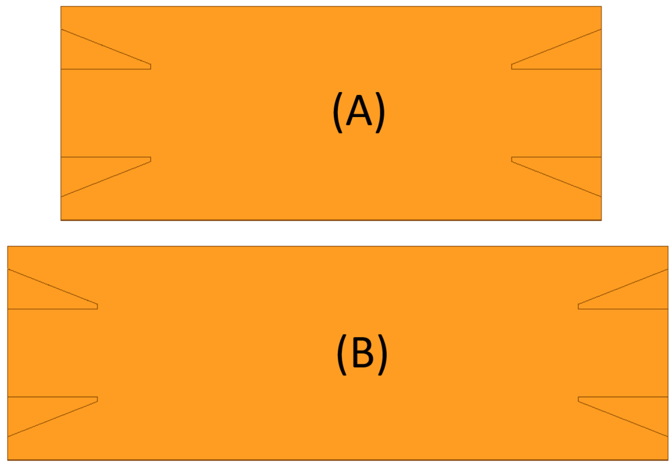

Figure 2.2: Designed RHW structure. (A) 40 mm length (B) 60 mm length.

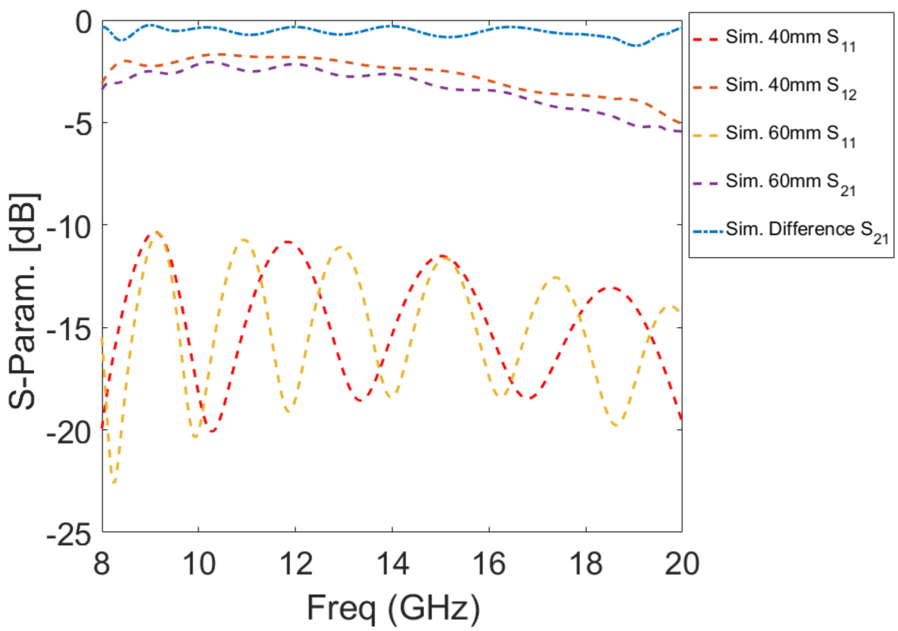

Figure 2.3: RHW Through simulated results.

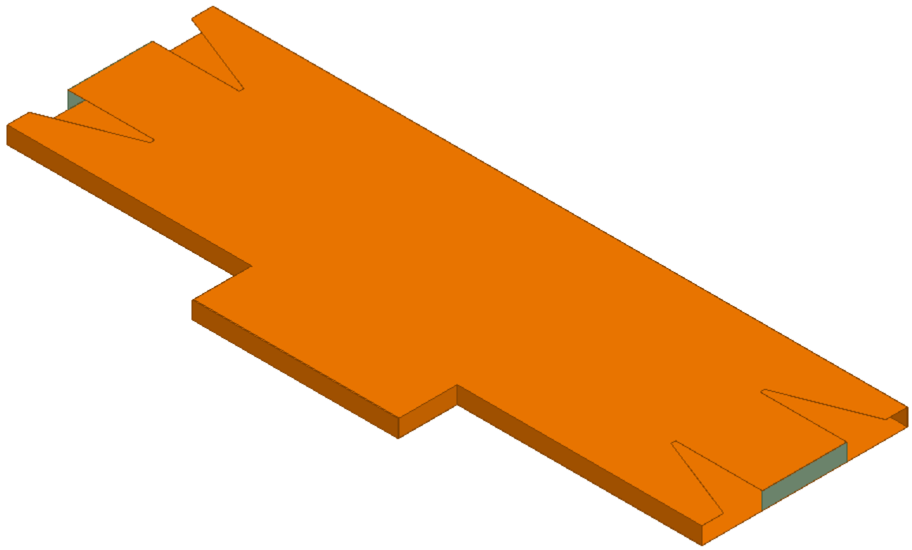

Figure 2.4: Designed RHW Resonator.

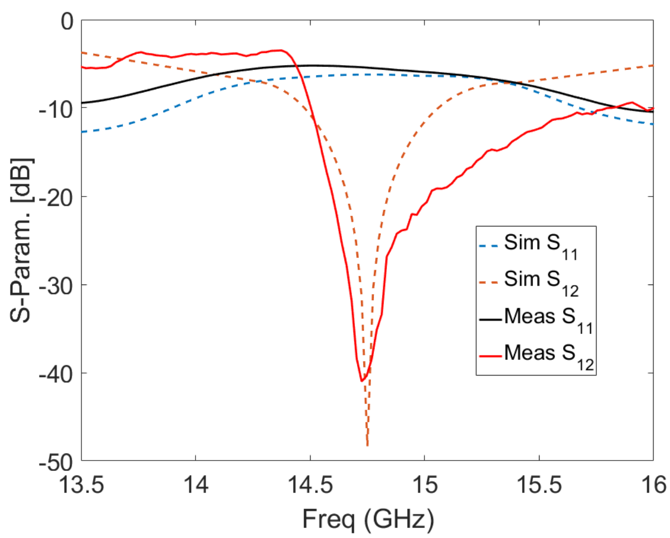

Figure 2.5: RHW Resonator simulated and measured results.

was modified with a $\frac{\lambda}{4}$ stub added to the structure. The RHW resonator is shown in Fig. 2.4. The frequency of operation was chosen to be 14.75 GHz as it is a common communication band. This resonator had a simulated insertion loss of 48.34 dB at 14.75 GHz, a simulated Q-factor of > 1500 was achieved.

$$Q = \frac{f_c}{\Delta_{3dBBandwidth}} \tag{2.3}$$

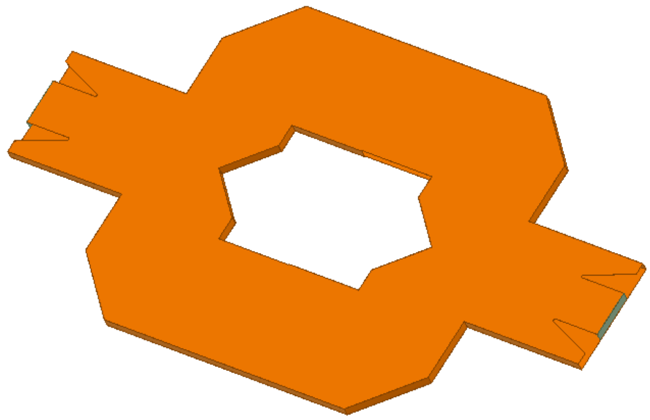

Figure 2.6: Designed power divider.

2.2.4 Reduced Height Waveguide Power Divider

In modern RF applications, power dividers and power splitters are a key component in the design of many circuits. Microstrip based power dividers (e.g., Wilkinson) have higher loss compared to metal waveguide based designs. Waveguide based power dividers offer low loss across the entire band of operation. The designed RHW power divider is shown in Fig. 2.6. As can be seen, the RHW inset was used in this section. A back-to-back structure was used to allow for easier measurement. The power divider was optimized to have a low insertion loss in the X-band. The simulated results can be seen in Fig. 2.7. The power divider exhibits low loss, with a maximum insertion loss of 3.85 dB. The fabrication follows the same process described above.

2.2.5 Reduced Height Waveguide Leaky-Wave Antenna

A leaky-wave antenna is a waveguide based antenna that radiates along the cut slit. A half-width microstrip leaky wave antenna (HWLWA) has been commonly studied and is attractive due to its compact size [40]. It uses a half-width microstrip transmission line, with one edge grounded using either a via wall or copper tape. Recently, a 3D printed leaky wave antenna was demonstrated [41]. This work showed that leaky wave antennas can readily be prototyped using 3D printing; however, the efficiency was low due to the high loss of the 3D printed dielectric material used. In this work, a RHW structure which avoids the use of solid dielectric substrates is used to design the antenna.

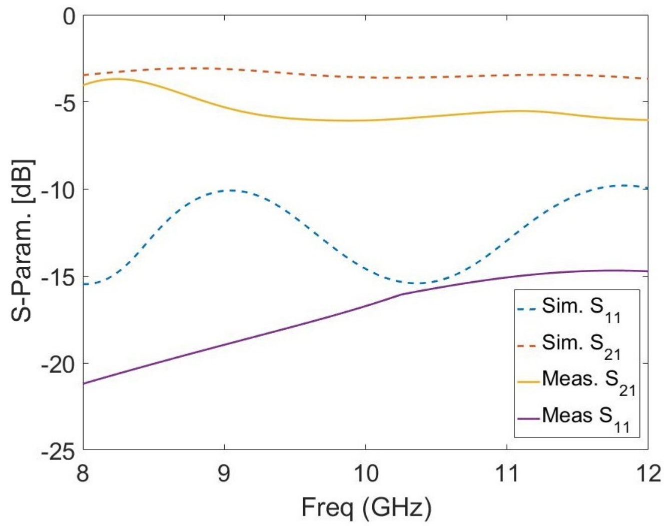

Figure 2.7: RHW power divider simulated and measured results.

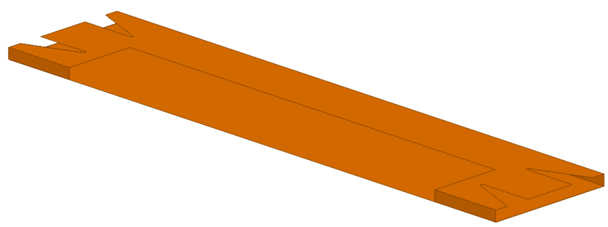

Figure 2.8: Designed RHW leaky-wave antenna.

The RHW-based leaky wave antenna structure is shown in Fig. 2.8. It is designed to operate at 10 GHz where the top width of the waveguide is made to be equal to one quarter of a wavelength. The simulated return loss for the antenna is shown in Fig. 2.9. It has a simulated gain of 9.42 dBi at 10 GHz, as shown in Fig. 2.10, which is about a 2 dB improvement in gain over the work that has been demonstrated using a solid 3D printed substrate [41].

2.2.6 Reduced Height Waveguide Vivaldi Antenna

The Vivaldi antenna is an ultra-wide band antenna that offers high gain due to the high directivity. Unlike previous work that showed 3D printed Vivaldi antennas [42] this work does not require a coaxial cable to feed the antenna. The Vivaldi antennas smallest spacing between the two flares dictates the highest frequency the Vivaldi antenna will operate at and the largest spacing dictates the lowest frequency which the antenna will operate. To achieve constant beam-width the flare rate

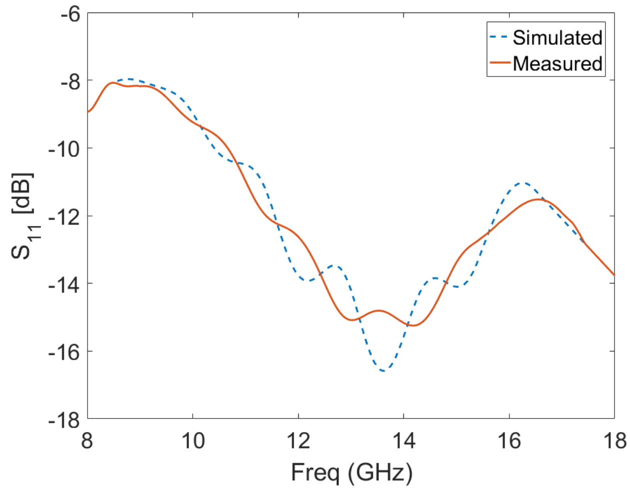

Figure 2.9: RHW leaky-wave antenna simulated and measured S_{11}results.

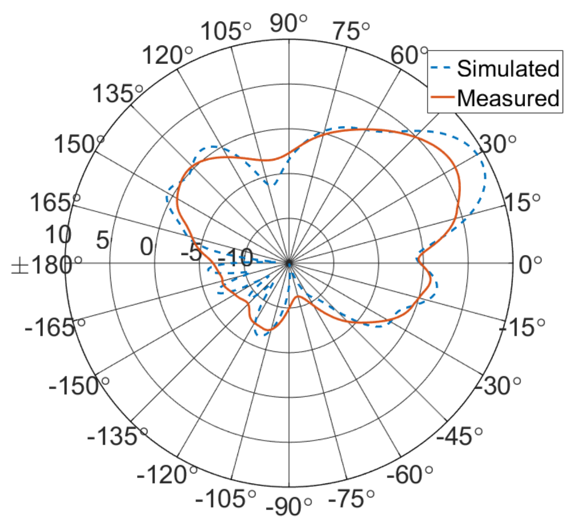

Figure 2.10: RHW leaky-wave antenna simulated and measured gain results.

change should be proportional to the wavelength. The design of the rate of separation can be seen in Fig 2.11. One of the design issues that was encountered when using a waveguide was that both legs of the Vivaldi antenna would be at separate elevations, but due to the enhanced capabilities of 3D printing it was feasible to design the Vivaldi antenna where the legs would start at two elevations and be able to meet at one elevation which would reduce cross-polarization as shown in Fig 2.11.

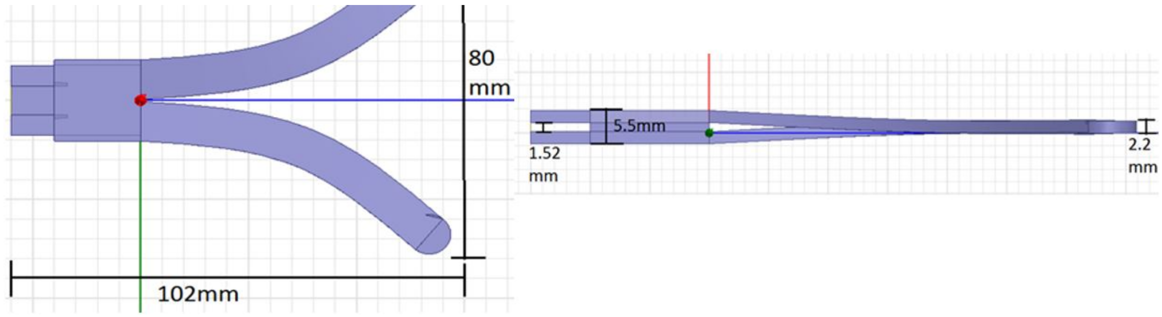

Figure 2.11: Designed Vivaldi antenna with dimensions.

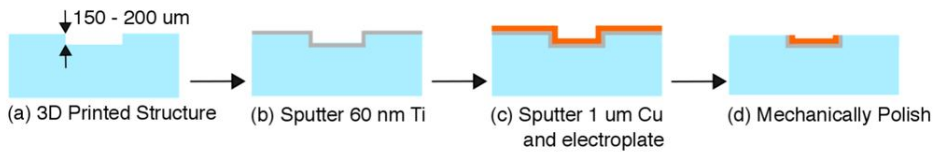

Figure 2.12: Damascene process.

2.3 Fabrication and Measurement

These sections are printed on a Stratsys Connex350 3D printed using plastic material. Print resolution as high as 16 μm and surface roughness <6 μm can be achieved using this printer. The components come out of the printer with a relativity smooth layer which can make it difficult for proper adhesion between the plastic and the metal. To promote better adhesion some mechanical polishing was done after printing to prepare the surface for metalization.

For metalization, the printed peaces are metalized utilizing a Denton desktop pro sputtering system, first 60 nm of titanium (Ti) followed by 1 μm of copper are sputter deposited. Using this Cu as a seed layer, a total of 6 μm of copper is electroplated. To pattern the copper, a Damascene-like process was used, as described in [38]. This process can be seen in Fig. 2.12

The performance of the components for return loss and insertion loss is measured utilizing an Agilent N52227A PNA. The far field components of the antennas are measured utilizing a SATIMO Starlab® near field measurement system which extrapolates fair field data by utilizing calibration horn antennas.

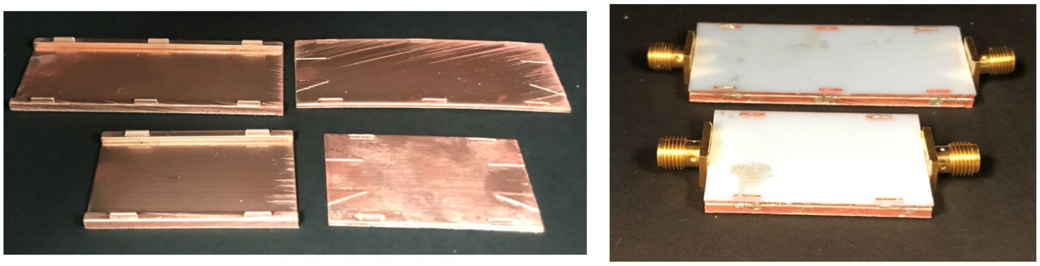

Figure 2.13: RHW Through before (left) and after (right) assembly.

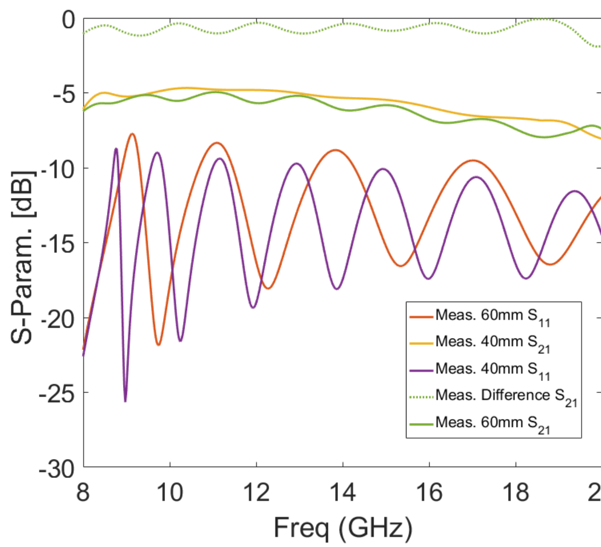

Figure 2.14: RHW Through measured results.

2.3.1 Reduced Waveguide Transmission line

The reduced waveguide transmission line were printed in two half sections and then blanket metalized, The two printed pieces followed the damascene process to process the desired pattern. After patterning, the two sections are assembled using a "Lego-like" process. During this assembly, an 18 GHz SMA connector is attached between the two pieces. The pieces and SMA connector are held together with conductive silver epoxy. Waveguides after assembly are shown in Fig. 2.13. The measured results for these two RHW structures are shown in Fig. 2.14. These structures have about 2 dB greater loss than the simulated results. However, the difference in transmitted signal is small, which indicates low loss characteristics of these waveguides. The measured higher loss is largely due to the transition section.

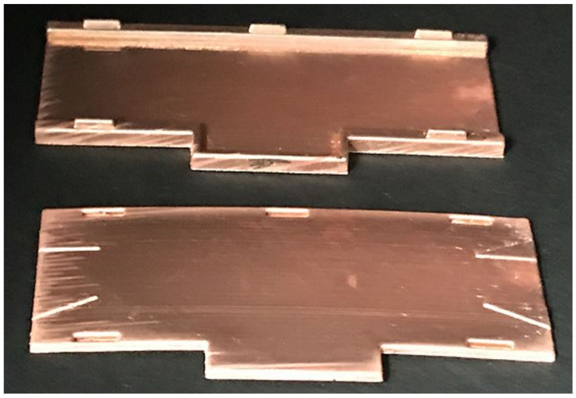
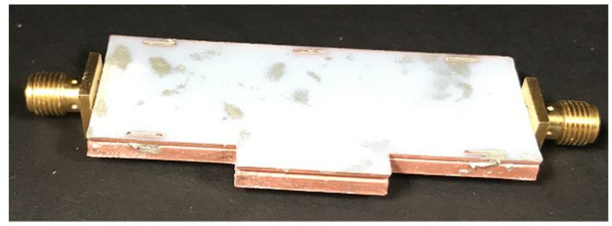

Figure 2.15: RHW Resonator before (left) and after right blanket metalization.

2.3.2 Reduced Height Waveguide Resonator

The RHW resonator followed the same fabrication process discussed above, the 3D printed pieces after blanket metalization are shown in Fig. 2.15 and the fully assembled resonator is shown in Fig. 2.15. The measured results for the RHW resonator can be seen in Fig. 2.5. As shown, there is good correlation between the simulation and measured results. The resonator has a measured Q-factor of 245. surface roughness of the print material and the dimensional accuracy of the printer is believed to be the main cause of Q-factor reduction when compared to simulation. In simulation perfect dimensional accuracy and no surface roughness was simulated.

2.3.3 Reduced Height Waveguide Power Divider

The AM RHW power divider shell is shown in Fig. 2.16, and fully assembled RHW power divider with SMA connectors is shown in Fig. 2.16. The measured results can be seen in Fig. 2.7. The measured results deviated slightly from simulation, as a maximum insertion loss of 5.64 dB (including power divider loss) was measured, the higher loss was believed to be mainly due to the loss added by the conductive epoxy as it has poor conductivity at higher frequencies as well as the dimensional accuracy of the printer.

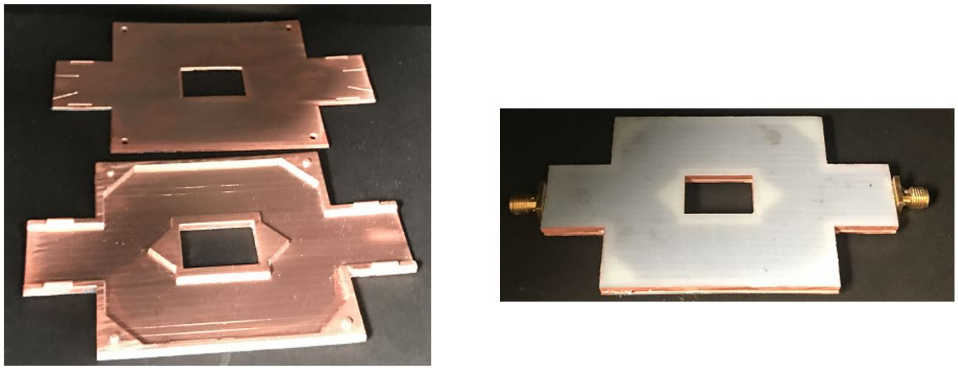

Figure 2.16: RHW power divider before (left) and after assembly (right).

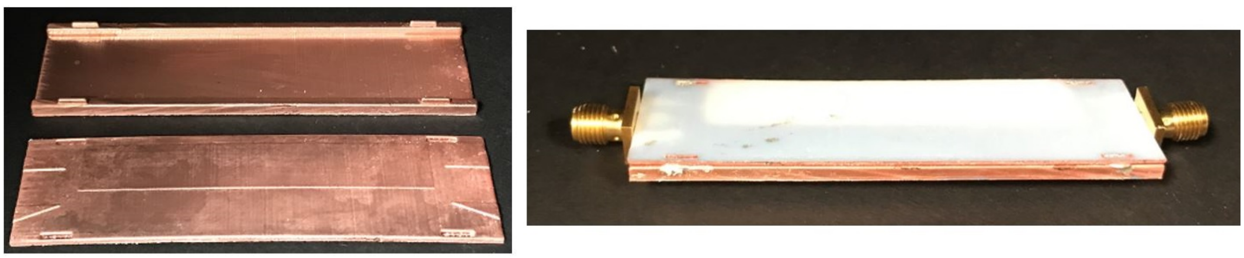

Figure 2.17: Fabricated RHW leaky wave antenna prior to assembly (left) and after assembly (right).

2.3.4 Reduced Height waveguide Leaky-wave antenna

The fabrication process of the RHW leaky-wave antenna was done similarly as described above, the 3D printed pieces after blanket metalization are shown in Fig. 2.17 and the fully assembled antenna is shown in Fig. 2.17. The measured results in comparison to simulation can be seen in Fig. 2.9. There is good correlation between simulation and measured results. The RHW leaky wave antenna has a measured gain of 8 dBi as shown in Fig. 2.10. Again, the simulation and measured results match closely. The difference is largely due to the losses associated with the connectors and conductive epoxy which are missing from the simulation results.

2.3.5 Reduced Height waveguide Vivaldi antenna

Similar to the other components the Vivaldi antenna was fabricated in two pieces for uniform metalization, Both pieces of the antenna are joined together using a Lego-like assembly, using

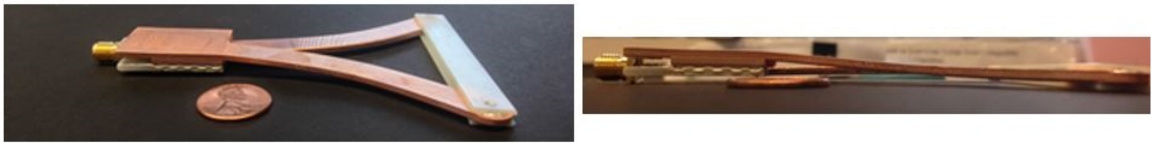

Figure 2.18: Angled (left) and side (right) view of fabricated Vivaldi antenna.

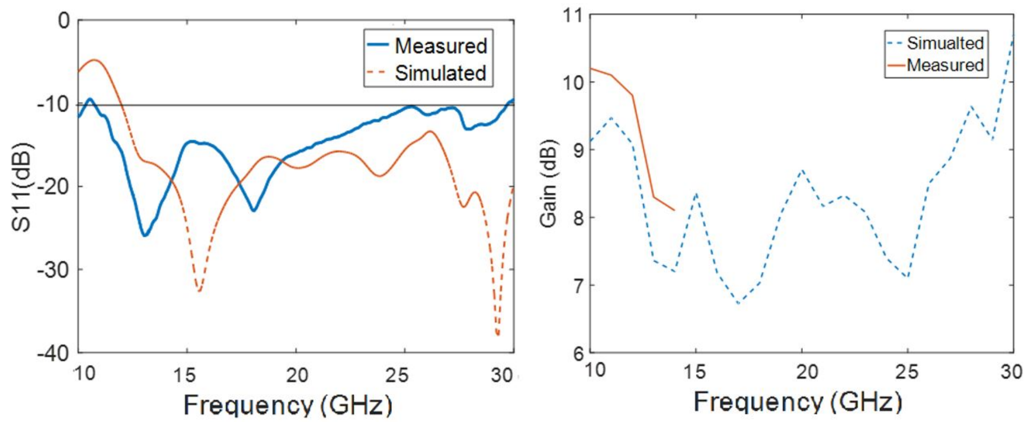

Figure 2.19: Measured and simulated return loss (left) and gain (right).

conductive silver epoxy (MG Chemicals 8331S). Between the two half sections is an SMA edge-mount connector. Fig 2.18 also shows the picture of the assembled antenna from its side. A slow tapper in the flare section can be seen in Fig 2.18. The simulated reflection coefficient as well as maximum gain are shown in Fig 2.19. Simulation results show that the entire substrate integrated waveguide Vivaldi antenna has high return loss and high gain across the entire bandwidth. A maximum gain of 10.2 dB is shown a return loss entirely above 10 dB across the entire bandwidth.

2.4 Summary

In this chapter, a few components were studied. Unlike previous publications, a reduced height waveguide was utilized that allowed for the usage of a standard SMA connector for connections instead of coaxial cables or waveguides. This reduced height waveguide allowed for the usage of air as the substrate which gave a low loss design. The transmission line showed 0.13 dB/mm as well as a wideband Vivaldi antenna which showed over 10 dBi gain.

CHAPTER 3

RIGID-FLEX COUPLED ANTENNA

3.1 Introduction

Typical printable dielectrics currently available have ε_r = 2.9, tan-δ = 0.04 [41]. Such high dielectric losses lead to antennas and other components with inefficiencies. To overcome the loss of the printed materials, air substrate designs can be implemented using 3D printing [43, 44]. However, due to material limitations, 3D printed polymer structures are rigid, brittle and do not lend themselves for printing of free standing thin film form. Thus, flexible circuits are difficult to fabricate using current print technology.

On the other end, photolithography is the main technique of the semiconductor and electronics industry to fabricate circuits with fine line resolution [45]. Photolithography is a subtractive fabrication method that utilizes a mask to transfer a pattern. Photolithography is the highest resolution standard fabrication method with feature sizes as small as 10s of nm. Using electron beam lithography, features smaller then 5nm can be achieved [45]. Photolithography is the clear choice to fabricate planar structures since it offers extensive material options with a wide range of electrical characteristics. These material choices offer the benefits of lower losses and flexibility. However, thick or high aspect ratio structures are difficult to produce using this technique.

A.M. has been gaining interest from the automotive industry as a possible manufacturing technique to manufacturing of various automotive body parts. Interest has gained for direct printing of fascias (bumper) on the assembly line. The automotive market is very price competitive in nature and thus new and innovative methods of integrating antennas are needed. Here we present a novel technique to make antennas an integral part of the 3D printed or molded plastic automotive parts.

This chapter combines the 3D printed rigid structures with flex circuits to fabricate novel RF components that would be difficult to fabricate otherwise. This technique will couple transmission lines directly into antennas. An aperture-coupled 2x2 element patch antenna array designed to operate at 15.2 GHz is presented. Patch elements with air substrate are fabricated using 3D printing and the slots and power divider circuit are fabricated using conventional lithography on a flex substrate (Rogers 3850, LCP). As well as a couple Vivaldi antenna printed directly into a scaled down automotive fascia (Bumper) that operates in the V-band (30-67 GHz).

3.2 Apperature Coupled Patch Antenna

An aperture-coupled antenna consists of two dielectric and three metal layers. The middle metal layer is used as the common ground plane to the microstrip transmission line and the patch element. The microstrip power divider is fabricated on the bottom metal layer and the patch antenna elements are fabricated on the top layer. The coupling between the transmission line and the patch resonant cavity occurs through a slot in the ground plane [46].

The structure was designed following the design procedure in [47]. Here, the microstrip and the slots were fabricated onto a flexible LCP film. The patch was fabricated onto a 3D printed plastic structure. With 3D printing, the spacing between the slot and the patch can be customized unlike traditional board methods where it is limited by the available substrate thicknesses. Also, an air substrate can be designed using 3D printing. For this work, an air spacing of 250 μm between the slot and patch was used.

All simulations were carried out using ANSYS HFSS. A return loss of 19 dB at 15.2 GHz was simulated as can be seen in Fig. 3.1. The radiation pattern at 15.2 GHz is shown in Fig. 3.1 and a maximum gain of 8.4 dBi is achieved. The fabricated patch can be seen in Fig. 3.2 and the entire antenna structure is shown in Fig. 3.3. The antenna had a measured return loss of 18 dB (see Fig. 3.1). The measured radiation pattern is shown in Fig. 3.1, and a gain of 7.5 dBi was measured. This slight deviation between simulation and measurement was mainly due to the loss contributed by the SMA connector and slight misalignment of the patch. The return loss and radiation pattern matches closely with the simulation results. To fabricate the patch, a table like structure is 3D printed, metalized and patterned, see Fig. 3.2. The 3D printed patch structure was attached to the LCP using an adhesive paste at the outer edges of the structure.

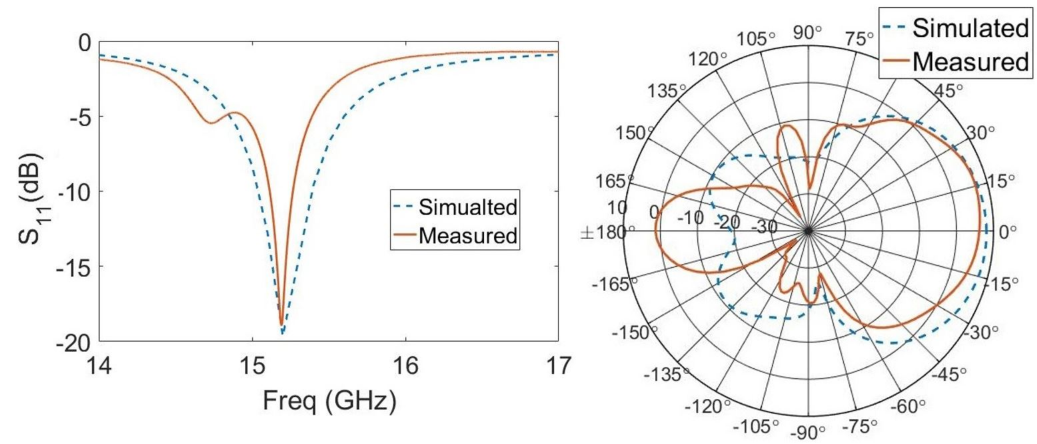

Figure 3.1: Simulated and measured return loss (left) and gain (right) shown for the patch antenna.

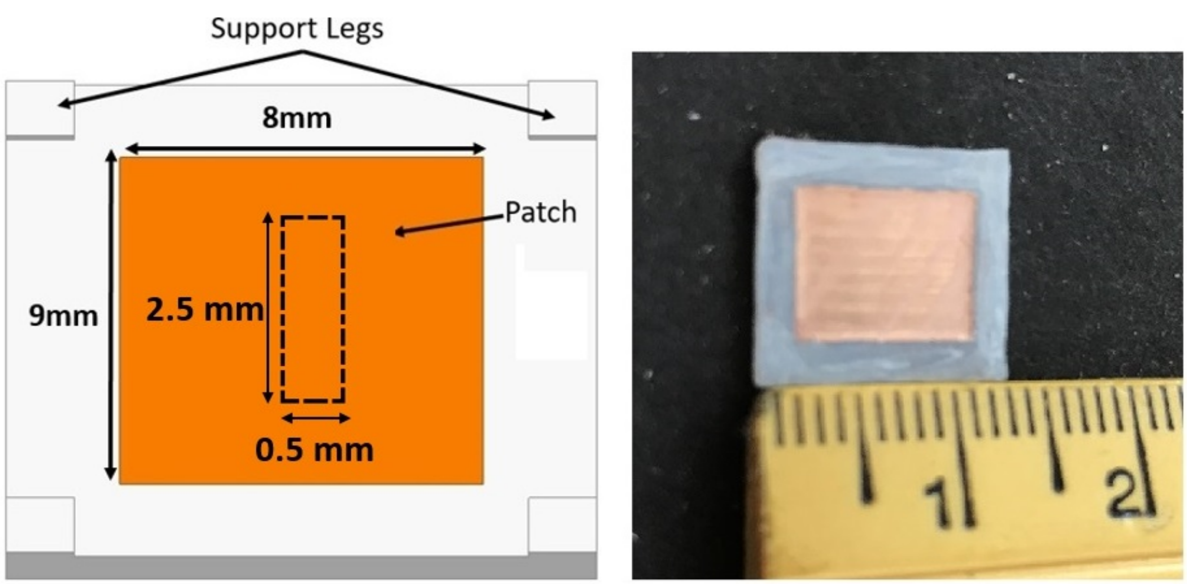

Figure 3.2: The schematic design (left) of the antenna and a the fabricated patch (right) are shown. The dashed box denotes slot size.

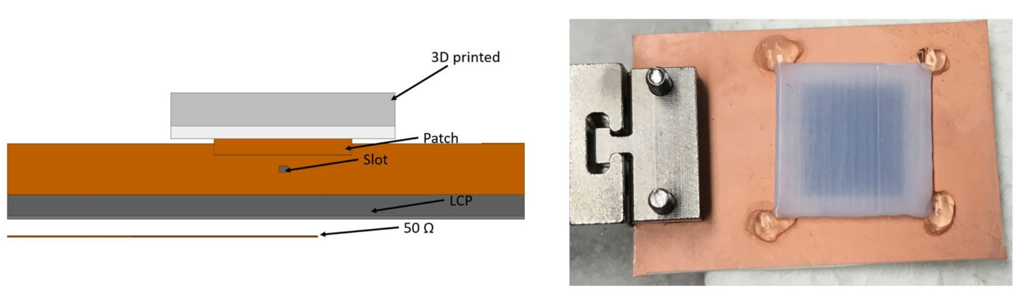

Figure 3.3: Designed Patch (left) and fabricated patch (right).

3.3 Rigid-Flex Patch array

To enhance gain, a 2x2 antenna array was designed and fabricated. Similar to the single element, a flexible LCP substrate was combined with the 3D printed rigid structure that supports the patch array. The pitch between each patch was $\frac{\lambda}{2}$ at 15.2 GHz, and for the power splitter a simple quarter-wave step impedance transformer was used. In simulation, a return loss of 31 dB was achieved as is shown in Fig.3.5. The array also had a simulated gain of 13.4 dBi at 15.2 GHz (see Fig. 3.6). The fabrication of this array was similar to the single element patch, and the fabricated structure is shown in Fig. 3.7 while the layout of the power splitter is shown in Fig. 3.4. Here, a manual alignment of the patch to the slots was carried out, and a slight misalignment led to the difference in the return loss between simulated and measured results as can be seen in Fig. 3.5. A gain of 10.8 dBi was measured as seen in Fig. 3.6 which is slightly lower than simulated; this was mainly due to the misalignment of patch antennas to the slots and the losses contributed by the connector.

One of the major benefits of this hybrid technology is the ability to fabricate antennas that can be mounted on curved or bent surfaces. As demonstrated in Fig. 3.7, the patch array was bent around the corner of a foam material. Fig. 3.5 shows the simulated and measured return loss, and shows good agreement. The simulated radiation pattern is shown in Fig. 3.6; for which a gain of 7.4 dBi was achieved. The drop in gain, as compared to its flat counterpart, is due to the decrease in the array factor. A half power beamwidth of 200^o was obtained in simulation. For the bent array a gain of 7.2 dBi was measured as shown in Fig. 3.6. These results correlate well with simulations.

3.4 Apperature Coupled Vivaldi Antenna in Large structure

The number of sensors used in an automobile is growing at a rapid rate over the past decade. Sensors include radars, cameras, Lidars, ultrasonic parking aid, etc. There are many antennas operating in different frequency bands used in a typical automobile. This includes antennas for radios (analog, digital, satellite), GPS, cell phones, radars, Bluetooth, etc. With rapid advances in wireless

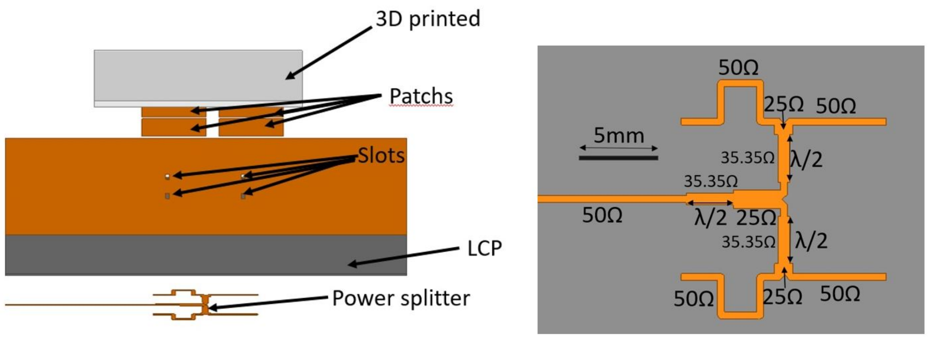

Figure 3.4: The Rigid-Flex patch array design (left) and power divider dimensions (right).

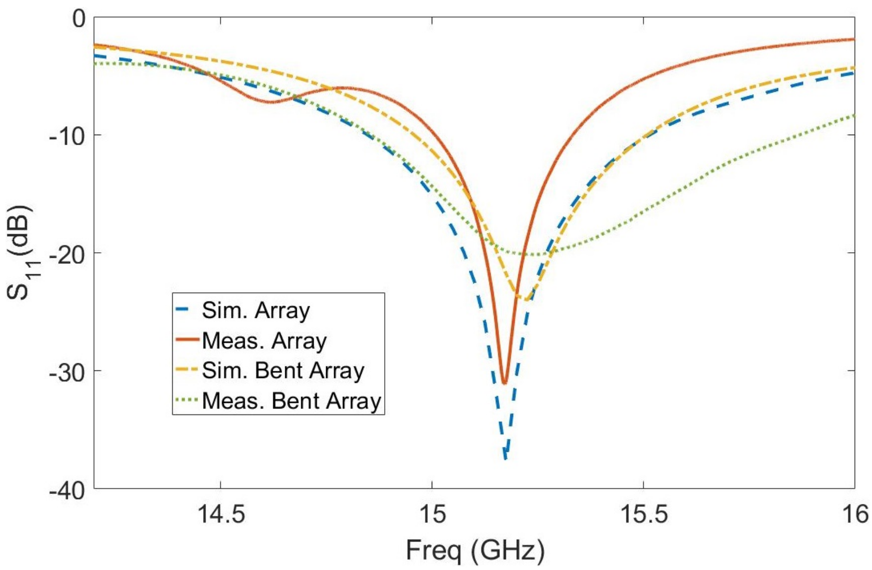

Figure 3.5: The measured and simulated return losses for planer and bent arrays.

communication, 5G for example, the number of antennas in a car is expected to grow significantly over the next decade. Mounting of sensors and integration of antennas is labor-intensive, and in most instances, integration of antennas is an afterthought.

Allowing the packaging of RF components that are fabricated and patterned directly onto large printed structures will lead to substantial cost savings and allow for further customization of electronics within automobiles. For the integration of electronic components, esp. antennas, patterning of conductive traces with fine resolution on large area non-planar surfaces is a major challenge. Conventionally, conductive ink (silver) is patterned using aerosol printing [22], inkjet printing [48], and screen or stencil [49]. However, these techniques are slow and difficult to implement for printing on large non-planar surfaces. Here we propose the use of two techniques to pattern conductive

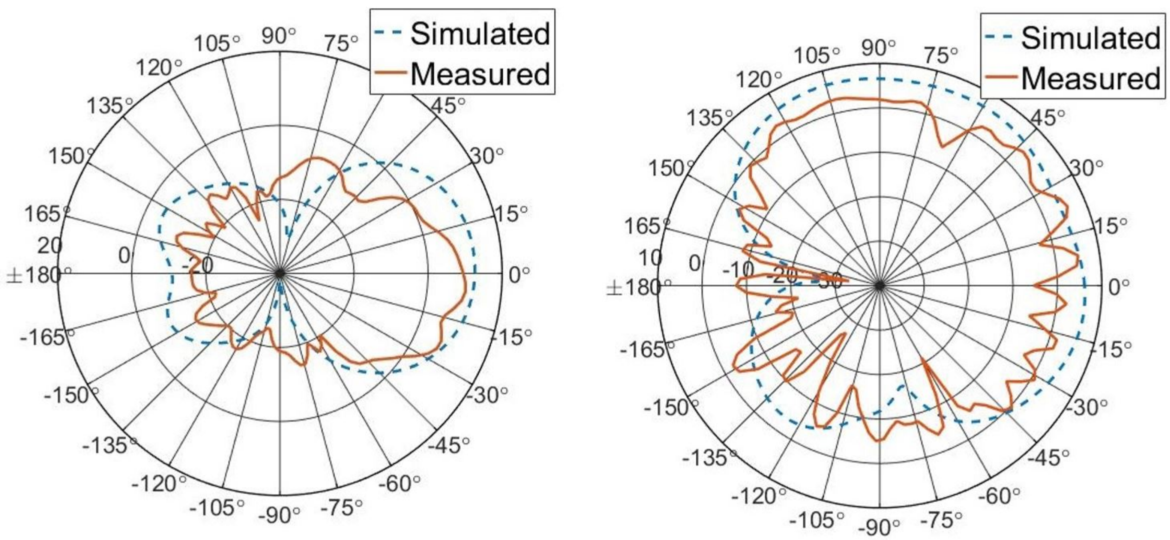

Figure 3.6: Measured and simulated array radiation pattern at 15.2 GHz for flat (left) and bent (right).

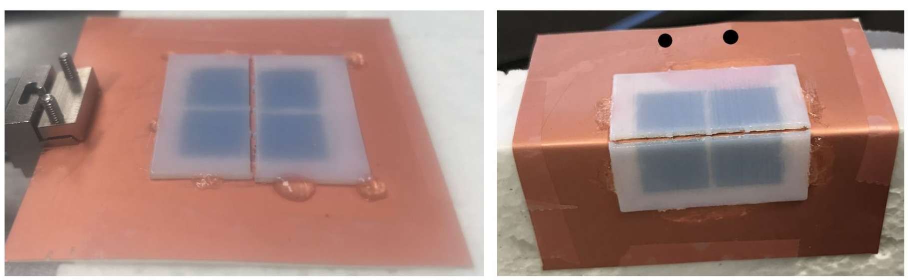

Figure 3.7: Fabricated Rigid-Flex patch array (left) and after bending (right) around a + 90^o angle is shown.

layer: (1) insitu printed stencil layer and (2) damascene-like patterning.

This method has huge benefits to be utilized in industries where additive manufacturing is being studied for component manufacturing. This section studies the fabrication of a scaled-down car bumper manufacturing with Vivaldi antennas directly printed with the bumper. The V-band (30-67 Ghz) frequency range chosen as this can be used for parking and driving sensors as well as vehicle-to-vehicle communication.

3.5 Characterization of Conductive Film Coatings

Off the shelf (OTS) aerosol paint from MG Chemicals is used here. Conductive paints are available in both liquid and aerosol spray form. To demonstrate this concept, the use of an aerosol spray of silver particles is used as it has a very high conductivity, and provides a smoother surface finish. Traditionally, conductive spray paints have been used for RF and electromagnetic interference (EMI) protection or FCC compliance on plastics and mobile electronics packaging. Due to the relatively high conductivity of the silver paint, the material coating on plastics is well suited for direct electroplating of copper. Other spray paints were also tried, however, the conductivity achieved was low and had a rough surface finish. The aerosol paint is used as a method to avoid the use of vacuum chambers since it becomes difficult as the size of components increase. This becomes impractical as the size of components increase so will the size of the vacuum chamber which will lead to longer metalization times.

The conductivity of the as-deposited silver ink and after plating was measured. A four-point probe and source measurement process was used with 10 mm square conductive structures to measure the DC conductivity. For the measurements, conductive structures were fabricated on glass substrates using 3 mil polyimide stencils purchased from OshStencils to pattern the structures for four-point probing and thickness measurements. Fig. 3.8 shows the patterned structures for four-point probe measurements. The DC measurement was done using a Lucas Labs 4-Probe conductivity probe and the Keithley source measurement unit. It is difficult to achieve controlled thickness using spray coating; therefore, several samples were made in order to determine the average conductivity of the paint.

For the measurements, after deposition, the coating was air-dried 10 minutes for handling before baking at 65^{o}C for 10 minutes to remove any moisture before measurement. Thickness was measured using an AEP Technology NanoMap-500LS advanced stylus contact surface profiler to determine step height and average RMS surface roughness of the films on glass.

The provided datasheet lists the conductivity as 1.5 %, while our measurements show the conductivity to be 1.3% of bulk silver. This conductivity is low for the design of RF circuits. Thus, to further increase the conductivity of these samples they were electroplated with an additional 5 μm of copper. Leads were attached to the patterned silver structures for copper electroplating. The same process for drying and measurement was then taken on the copper-plated structures to de-

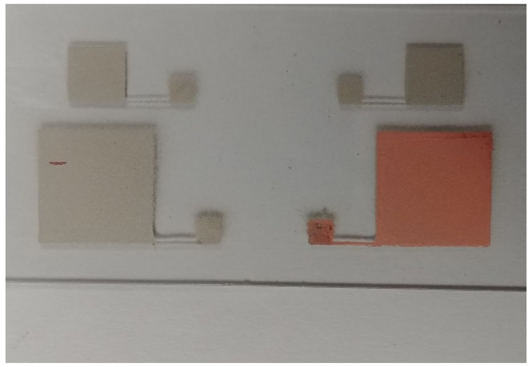

Figure 3.8: Painted silver and electroplated copper silver paint.

termine a before and after conductivity value for this process. This yielded an effective 20% bulk conductivity of copper. Several thicknesses of the paint were studied to see how it might affect performance.

Fabrication of the Vivaldi antenna on 3D printed plastic used the same process as discussed above. Patterning of the conductive layer was done using a shadow mask. Once dried and plated, the Vivaldi antenna was measured and compared to a traditional fabricated Vivaldi using DC sputtered copper. Details of design, fabrication, and measurement are discussed below.

3.6 Antenna Design and Measurement

A process called rigid-flex is utilized in this paper to demonstrate a Vivaldi antenna fabricated on a 3D printed part using silver ink. This process bridges the gap between standard PCB technologies (planar) and probing of 3D printed structures. This was recently presented and it showed promising results [50]. Here, instead of a coax to feed the 3D printed Vivaldi, the feed network is fabricated on Panasonic Felios R-F705 LCP (Liquid Crystal Polymer, ε_r=3 tan_δ=0.004) and is capacitively coupled to the Vivaldi structure. This feed is commonly utilized in planner Vivaldi antennas designs. Here, instead of Vivaldi structure on a planar substrate, the Vivaldi structure is 3D printed and is coupled to the feed network fabricated on the LCP substrate (flexible substrate).

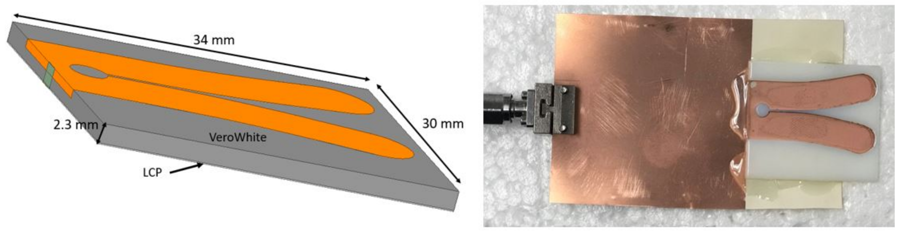

Figure 3.9: Designed (left) and fabricated (right) printed Vivaldi with coupled feed.

3.6.1 Vivaldi Antenna Design

Numerous papers have demonstrated 3D printed Vivaldi antennas [51, 52, 53]. The 3D Vivaldi antenna has the benefit of thickness that can be utilized to achieve good impedance matching and to enhance gain. This section starts a new design to a printed Vivaldi antenna. The new design is shown in Fig. 3.9. Here, 100 μm LCP is stacked below the 2.2mm thick VeroWhite Plus polymer structure to provide the feed network. The LCP has the microstrip coupler which couples to the Vivaldi which is embedded into the VeroWhite layer. The Vivaldi structure is depressed 0.8 mm into the VeroWhite layer. The design was optimized for this stack up. The simulated return loss is shown in Fig. 3.10. The return loss is greater than 10 dBi over a frequency range of 40 - 67 GHz. The simulated gain is shown in Fig. 3.10, and gain as high as 10 dBi can be attained.

The Vivaldi structure was printed on Stratsys Connex 350 SLA printer which has a 16 μm print resolution in the z-direction. To metalized the printed Vivaldi structure, a stencil is utilized which aligns with the Vivaldi depression formed in the 3D printed material. Fig. 3.11 shows the fabrication and assembly of the Vivaldi antenna. The metalization of this Vivaldi followed the same process as described above with one crucial difference. This method utilized a condutive aerolsol paint to initiate the seed layer for the electroplate process. The process started with a shadow mask (or stencil) on top of the Vivaldi. Approximately 10 μm of silver paint is spray-coated and the stencil is then peeled off. Any over-spray on the edge is removed using the damascene-like process discussed earlier. The paint is then allowed to dry at 65^{o}C for 10 minutes. It is then electroplated with an additional 5 μm of copper in a sodium persulfate solution. The entire fabricated Vivaldi is shown in Fig. 3.9.

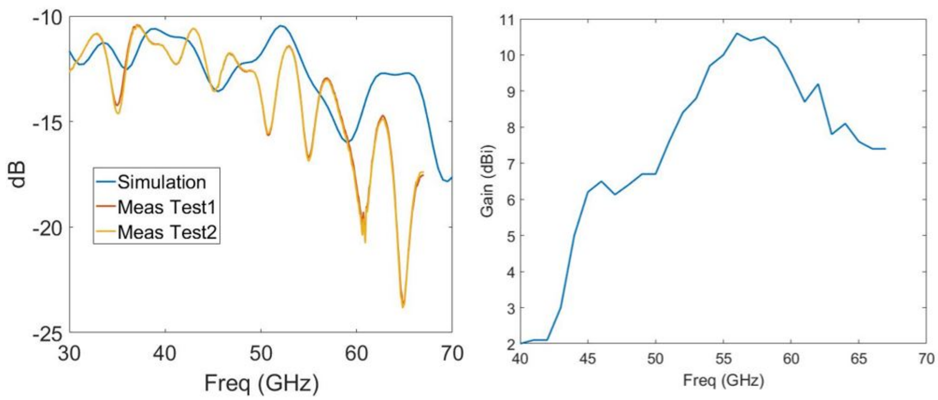

Figure 3.10: Planner Vivaldi returnloss (left) and gain (right).

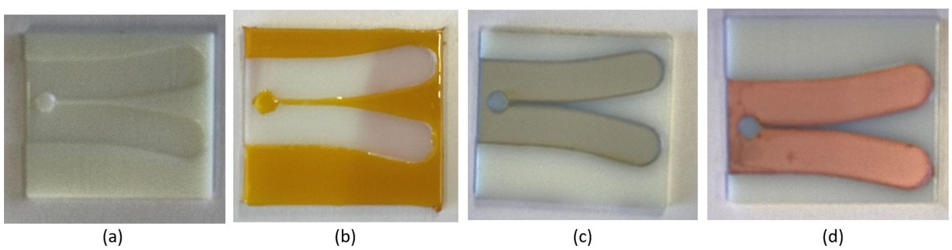

Figure 3.11: (a) Planner Vivaldi printed (b) Vivaldi antenna coated in Silver paint (c) Vivaldi antenna after electroplating copper. (d) Fully fabricated Vivaldi Antenna.

The antenna was measured using Agilent N5221A PNA with 1.85 mm southwest edge mount connectors added to the transmission line on the LCP substrate. The measured results are shown in Fig. 3.10. There is good correlation between the simulation and measured results. The slight difference can be attributed to any misalignment between the Vivaldi structure and the coupler LCP, alignment was done manually.

3.7 Antenna on Structure

The main aim behind this paper is to demonstrate antennas on large 3D printed (or molded) structures. To demonstrate the applicability of the proposed process, the above antenna design was incorporated into edges of the scaled-down bumper as shown in Fig. 3.12. Note, here two antennas are incorporated into the structure. The Vivaldi structures are bent to match the curvature of the bumper. Stratsys Connex 350 SLA printer (16 μm resolution) was again used in the printing of this new design. It took approximately 12 hours to print the bumper model, with print resolution set at

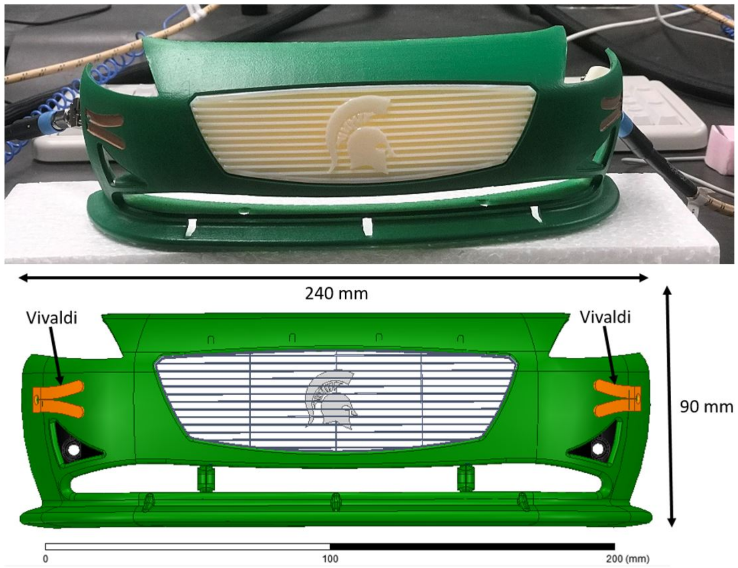

Figure 3.12: Automobile bumper design with Vivaldi antennas embedded in corners (Bottom). Fully fabricated with metalized Vivaldis (top).

32 μm. The print resolution can be reduced to increase print speed. The whole structure, as shown in Fig. 3.12, was printed in one piece.

The antenna structure was metalized as described earlier, and the coupled fabricated on LCP substrate was utilized. The bumper measured results are shown in Fig. 3.13. The two antennas have similar performance and show good return loss. The difference in performance can be attributed to the alignment tolerance of the coupler to the Vivaldi structure. Also, shown in the graph is the measured isolation between the antenna elements which is greater than 30dB over the measured frequency range. In other words, the Vivaldi antennas are highly directive and this is beneficial for distance ranging, parking aid, and anti-collision. To demonstrate the antenna in transmit and receive mode, a copper sheet was placed approximately 15 cm in front of the antennas and the insertion loss between the antennas was measured. This measured transmit and reflection results are shown in Fig. 3.13. This demonstrates that antenna designs can directly be incorporated in the plastic structures of the car, and can be used in radar and parking aid applications. The antenna was mounted on the exterior of the bumper to show the method being studied. The antenna can be mounted on the interior of the bumper with no noticeable degradation to the antenna. This would allow for a slick undisturbed look to the bumper which is desired in the next generation automotive

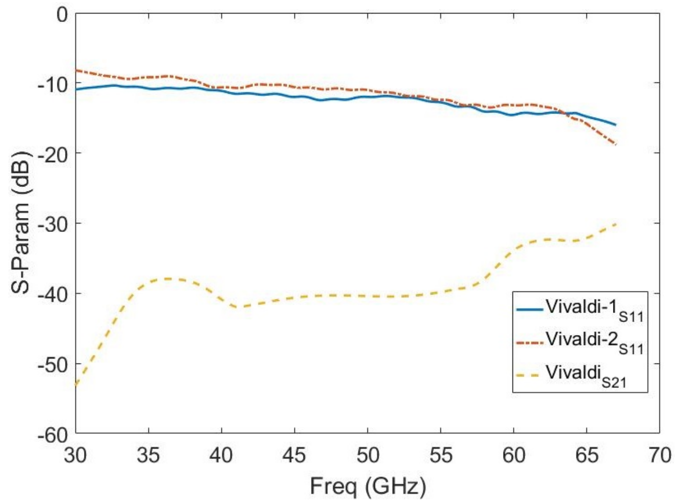

Figure 3.13: Measured transmit and reflected signal of the Vivaldi antennas on the bumper.

design.

3.8 Summary

This chapter covers creating two versions of coupled antennas. The patch coupled antenna showed an effective method to achieve high gain antennas as well as achieving a 200 degree 3dB beamwidth. The Vivaldi antenna which was directly printed with a scaled down bumper showed an effective way that the automotive industry can start incorporating antennas and sensors directly into printed bumpers. This method studied using conductive aerosol paints and shadow masks to create the desired pattern. This method proved effective in the V-band frequency range and allows for a method of metalization which can be directly used in the assembly line.

CHAPTER 4

RIGID-FLEX COAX TRANSMISSION LINE

While it has A.M. has been proven to be efficient at rapid component prototyping, which this leads to significantly reducing component production time and cost. As seen in the precious chapter, the fabrication of components that would be difficult to fabrication could be easily create through A.M. With the ability to deposit material in a wide range of geometries it has been used for wide verities of RF geometries [34, 54, 55]. This allowed for optimized RF performance geometries to be created.

This chapter demonstrates, for the first time a new hybrid structure that is coaxial like. This structure will be referred to as rigid-flex as it will contain both flexible substrate material and rigid AM structures. This flex-rigid structure is similar to higher cost air dielectric coax cables with being low loss, but has far greater system integration capabilities. This unique structure bridges the gap between standard PCB technologies and 3D printed structures. For the first time a combination of LCP and 3D printing are combined to create new coaxial like structures. In this paper rigid-flex coax, rigid-flex coax filter, flex UWB power dividers, and rigid-flex antenna feeds for both single and multiple element arrays are shown.

4.1 Rigid-Flex Coax Structure Simulation and Fabrication

Recently, a 3D printed Coaxial transmission line was demonstrated having low loss (≈ 0.1 dB/mm at 20 GHz) [36]. The advantage of such a structure is that it allows for fabrication of 3D geometries while avoiding the use of conventional planar substrates. However, in [36], the fabrication required complex assembly which does not make it practical for most applications..

4.1.1 Rigid-Flex Coax Transmission Lines

Current A.M. materials are typically lossy and are not designed for RF applications. For this reason another material was chosen that could be used as a substrate. The material chosen was 7

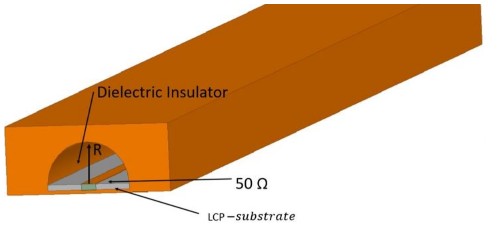

Figure 4.1: Flex-Rigid coax design (left) and fabricated (right).

mil Liquid Crystal Polymer (LCP)(180 μm) Rogers ULTRALAM 3850HT (εr = 2.9, tanδ = .001) that has very low loss and is flexible [56]. The flex-rigid coax design can be seen in Fig 4.1. The rigid-flex coaxial structure unlike traditional coaxial cables, only requires a half circle for the air gap. This is beneficial as it shrinks the overall size of the structure. The radius R, which is the radius of the interior coax shell, as shown in Fig. 4.1 is calculated using the formula shown in 4.1. For this structure air was used as the dielectric so ε_r is 1. This formula was initially described for a shielded microstrip in [57] with a rectangular opening and was modified for a circular opening. The fully fabricated Rigid-Flex coax can be seen in Fig. 4.1.

Looking at the S-parameters, the simulation results for this coaxial transmission line are shown in Fig. 4.2. This structure has an insertion loss less than 2 dB over the 10 - 40 GHz frequency range. At 40 GHz, the insertion loss is 0.024 dB/mm, which is significantly low compared to results reported in literature for microfabricated coax structures. The measured S-parameters of this transmission line which includes the loss of two connectors and the extended 50 Ω line. At 40 GHz this Rigid-Flex coax showed a measured insertion loss of 0.04 dB/mm.

$$R \geq \frac{\lambda}{20 * \sqrt{\varepsilon_r}} \tag{4.1}$$

4.1.2 Rigid-Flex Coax Resonator

The design of high-selectivity, narrow-band resonators with tailored transmission zeros presents important challenges [58]. The main advantage of using coaxial lines for filters is that they typically have higher quality (Q) factors resulting in lower losses. The difficulty in manufacturing

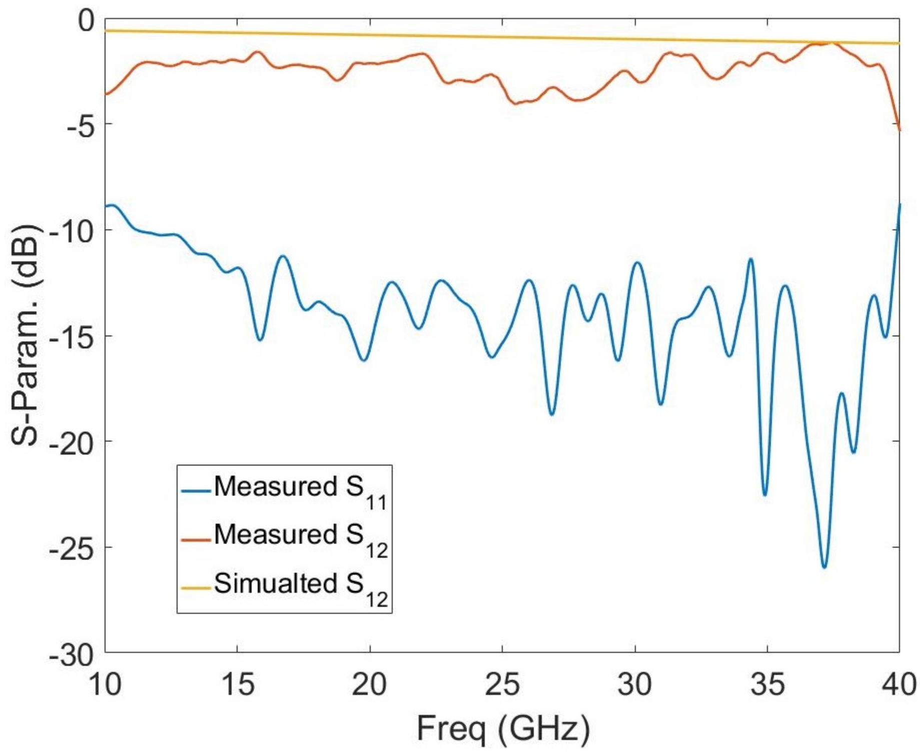

Figure 4.2: Simulated vs Measured insertion loss of printed Rigid-Flex Coax.

coaxial filters can be substantially decreased by using this rigid-flex technology which uses AM to augment fabrication.

This filter design followed the same approach for the design as the flex-rigid coax described above and it was fabricated in 3 parts and assembled using conductive epoxy. The designed filter can be seen in Fig. 4.3. The performance of the resonator is judged by the increase in Q factor(which was evaluated as in [59]). which compares favorably to traditional microstrip T-line resonator Q factors of 10-20 and demonstrates the possibilities for increased performance by combining these fabrication methods.

The simulated results for the flex-rigid resonator are shown in Fig. 4.4. The fabricated resonator can be seen in Fig. 4.3. Similar to that shown in Fig. 4.3, the 50 Ω feed line was extended by a microstrip 50 Ω line, like the coax line, to allow for edge mount SMA connectors to be attached. The measured results are plotted in Fig. 4.4; a Q factor of 113 was measured using the center frequency over a 3 dB bandwidth as described in [60]. When compared to the other work on AM

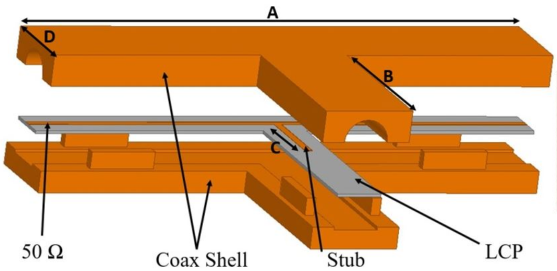

Figure 4.3: Rigid-Flex T-line resonator structure, exploded view (left) and fabricated (right).

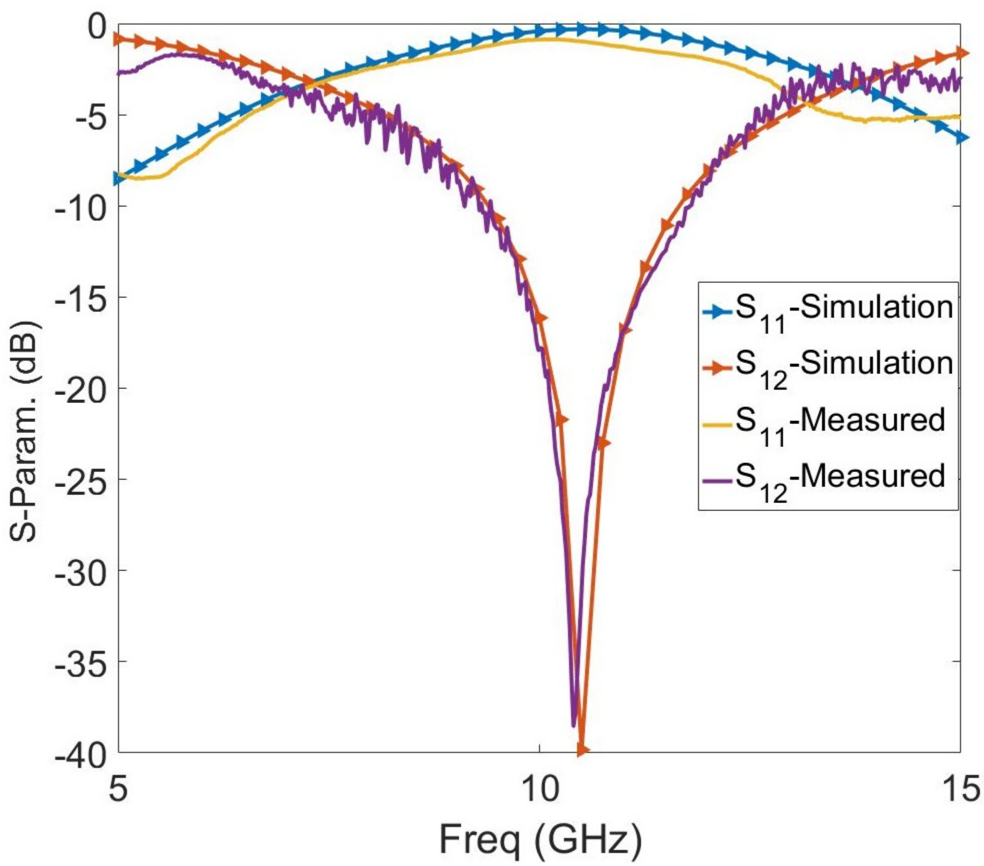

Figure 4.4: Resonator simulated and measured results.

resonators [61], this work showed a slightly increased Q, but with a significant reduction in size and weight. Other work had a measured weight of 60 grams [61] where this work had a weight of 5.1 grams (an order of magnitude improvement).

4.1.3 Rigid-Flex Coax Transmission line With Substrate steps

To demonstrate the advantage of the proposed rigid-flex design, the structure above is further optimized varying geometry along the transmission line is first demonstrated, Fig. 4.5. This design while having various line widths and trench depths is a simple continuous 50 Ω line. The top portion of this coax shell was a half cylinder with a radius of 1.3 mm and the bottom section is flat. As shown in Fig. 4.1(c), 2 trench depths were used for demonstration (0.3 mm and 0.6 mm deep). A slope of 45° between the trench transition was used. Similarly, a 45° transition angle was used for the center conductor, see Fig. 4.5.

The simulation results for this coaxial transmission line are shown in Fig. 4.6. This structure has an insertion loss less than 1 dB over the 10 - 40 GHz frequency range. At 40 GHz, the insertion loss is 0.013 dB/mm, which is significantly low compared to results reported in literature for microfabricated coax structures. The fabricated Rigid-Flex coax can be seen in Fig. 4.5, the 50 Ω was fabricated on LCP using standard photolitography process, and the coaxial shells was 3D printed and blanket metalized using the same process described in [41]. To allow for a standard SMA connector to be attached, a standard microstrip 50 Ω line was extended out of the structure. The three pieces (top, bottom and LCP layer) were snapped together using a Lego-like self assembly process. Silver epoxy was used to permanently join the pieces together. Fig. 4.5 shows the measured S-parameters of this transmission line which includes the loss of two connectors and the extended 50 Ω line. Below 20 GHz, the simulation and measured results match closely. Overall, it shows that low-loss rigid-flex coax-like transmission line can readily be designed using the proposed process.

4.1.4 Rigid-Flex Hemispherical Coax Resonator

Some of the best benefits of A.M. is the ability to produce spherical geometries with ease. Here, a hemisphere design was chosen over a rectangular structure for the fact that spheres will have less parasitic capacitance since there are no corners. The inner diameter of the sphere was designed to be 3 mm to achieve a resonance frequency near 44 GHz. To be able to easily couple to a planar

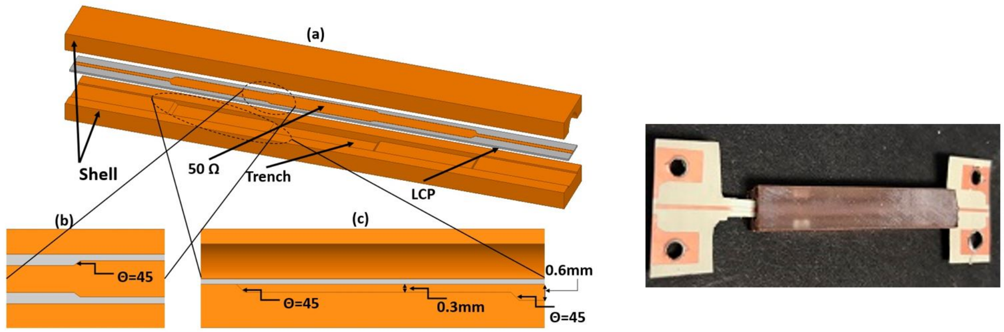

Figure 4.5: Exploded view of the Rigid-Flex coax design with varying trenches (left) and fabricated (right).

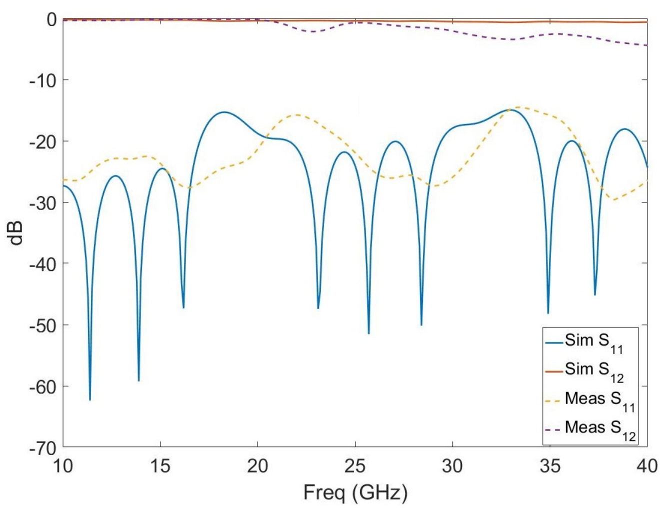

Figure 4.6: Simulated and measured return loss of the Rigid-Flex coax with varying depths.

transmission line, a semi-hemispherical design was chosen, at the expense of slight degradation in performance over a fully spherical design.

For the RF signal to couple into the air-filled semi-hemisphere, a small slot was created in the ground plane of the transmission line which directly covers the cavity. With a slot in the ground plane to the resonator, a higher Q can be achieved by optimizing both the structure simultaneously. The optimized slot can be seen in Fig. 4.7, and Fig. 4.7 shows the assembly of the pieces. The fully fabricated resonator can be seen in Fig. 4.8.

The simulated and measured results are shown in Fig. 4.9. The simulation results for this assembled structure shows a return loss of 28 dB at 44.04 GHz with a 4.15 MHz 3dB bandwidth. Using Eq. 1, this yields a Q-factor of 10600. The fabricated resonator has a resonance frequency

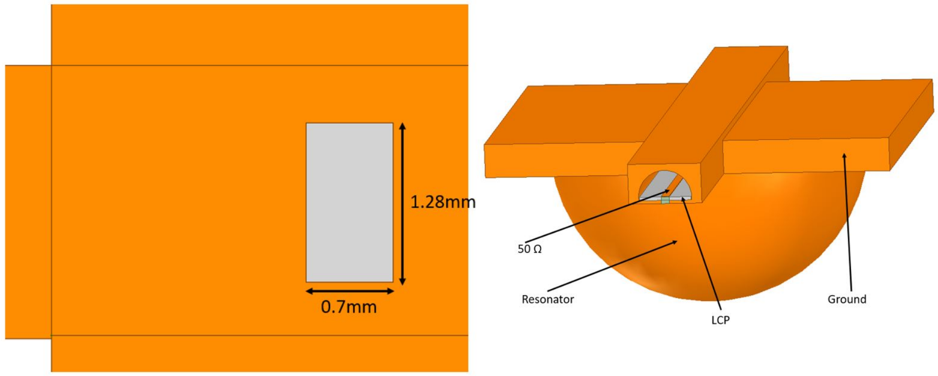

Figure 4.7: Close up view of the slot in the ground plane (left) and blown out view (right).

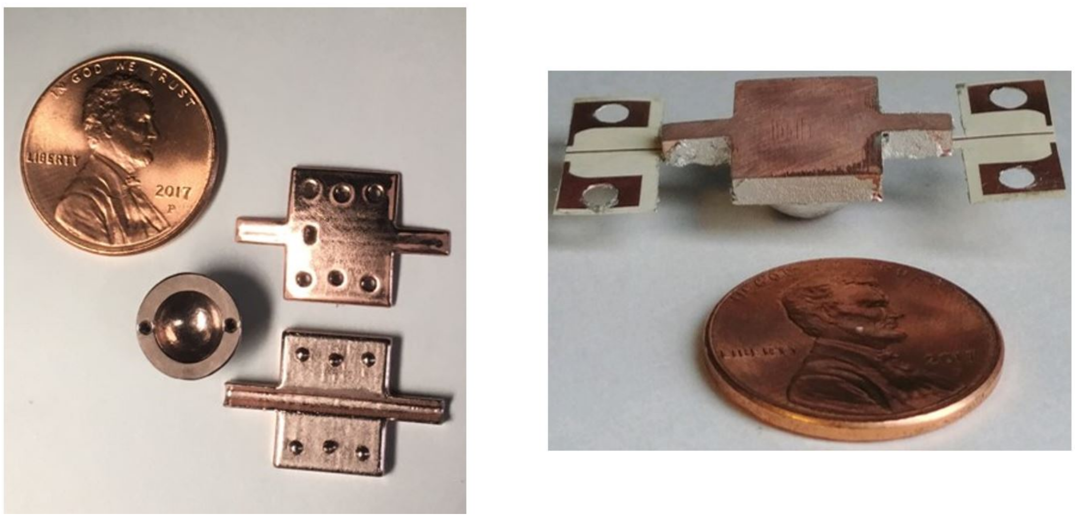

Figure 4.8: Printed and meatallized resonator pieces (left) and fully assembled (right).

at 44.23 GHz with 5 MHz 3 dB bandwidth. Utilizing Eq. (1), the Q-factor was calculated to be approximately 8800.

4.1.4.1 Rigid-Flex Resonator error analysis

The resonant frequency of the fabricated structure is 220 MHz higher than the simulation results. In the simulations, it was assumed that the semi-hemisphere has perfect dimensions (radius), whereas the fabricated structure is slightly elongated. Also, the feed line which was fabricated through photolithography was off by 15 μm which showed no major difference in simulations. The biggest difference, between simulated vs fabricated, is noted in the slot dimensions. Fig. 4.10 shows the

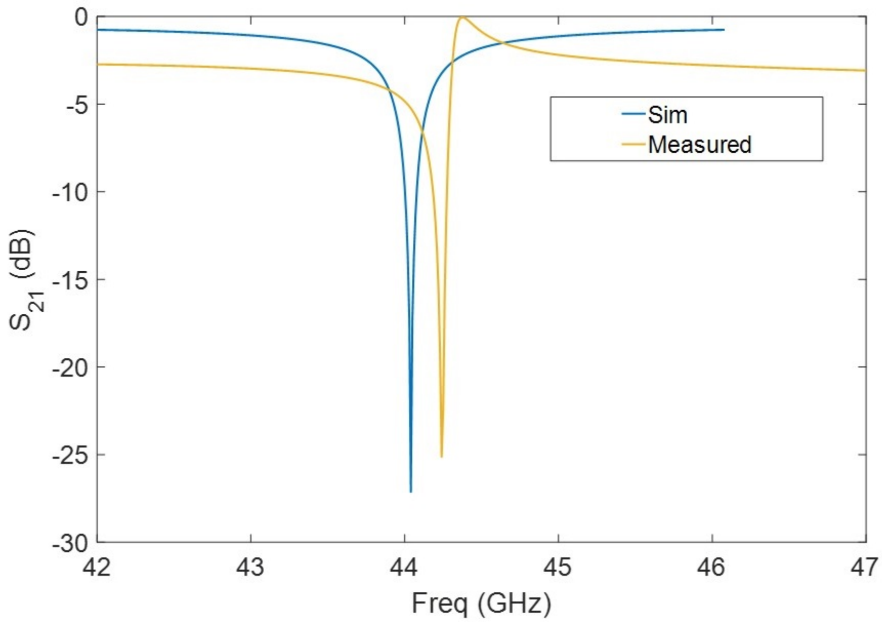

Figure 4.9: Simulated and Measured results for the Hemispherical resonator.

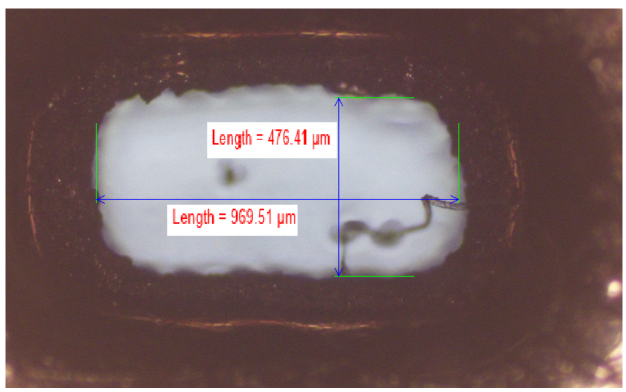

Figure 4.10: Fabricated Slot dimensions.

measured dimensions of the slot, in comparison to the simulated structure, Fig. 4.7, a considerable difference can be noted. The difference in the slot dimension is approximately 225 μm in one direction and 250 μm in the other direction. This dimensional inaccuracy is due to the Connex 350 printer adding a wax-like support material which slightly changed the structure dimensions during print. Also, as specified in the datasheet, the printer has a dimensional accuracy of 100 μm [62] in the x- and y-direction. Fig. 4.11 compares the simulated S21 against measured results after the as-fabricated slot dimensions are included in the simulations. A good match between the measured and simulation results is achieved.

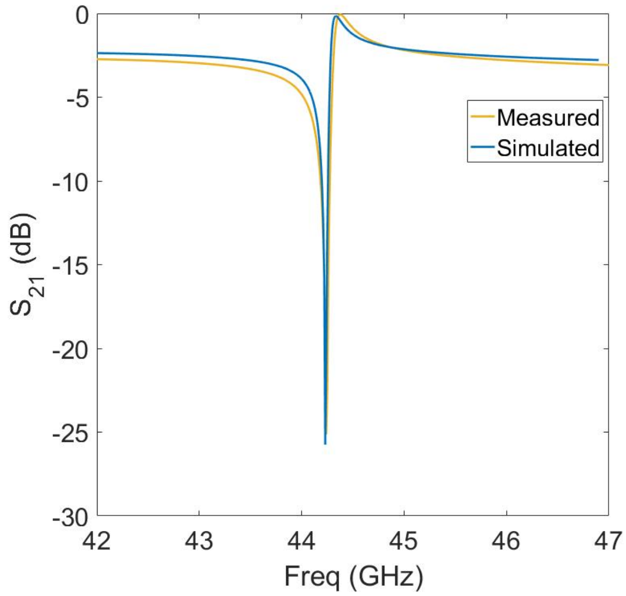

Figure 4.11: Measured and simulation results after correction for slot dimensions.

4.2 Rigid-Flex Coax Antenna Feed

Vivaldi antennas have been fabricated using AM with good results, but that work required the antenna to be fed using an expensive semi-rigid coax cable [63]. Using this method degraded the quality of the fabricated antenna due to the semi-rigid coax cable adding a series resistance which contributed to achieving only about 9 dBi gain and 60% radiation efficiency (the semi-rigid coax cable also increases the cost of the structure). In the previous chapter a A.M. Vivaldi antenna used substrate integrated waveguides (SIW) to feed the Vivaldi which further increased the radiation efficiency up to 81% . But this method really limits the ability to create an array of antennas that are wideband.

4.2.1 Rigid-Flex Coax Antenna

The Vivaldi antenna presented here will be similar to the one published in [63]. This antenna will be designed to work between 10 GHz and 25 GHz. The antenna feed network was first optimized in a back to back fashion as shown in Fig. 4.12; the cavity in the back of the structure was set to have a radius of $\frac{\lambda}{4}$ for the center frequency which was 3.75 mm. On top of the cavity, plates were

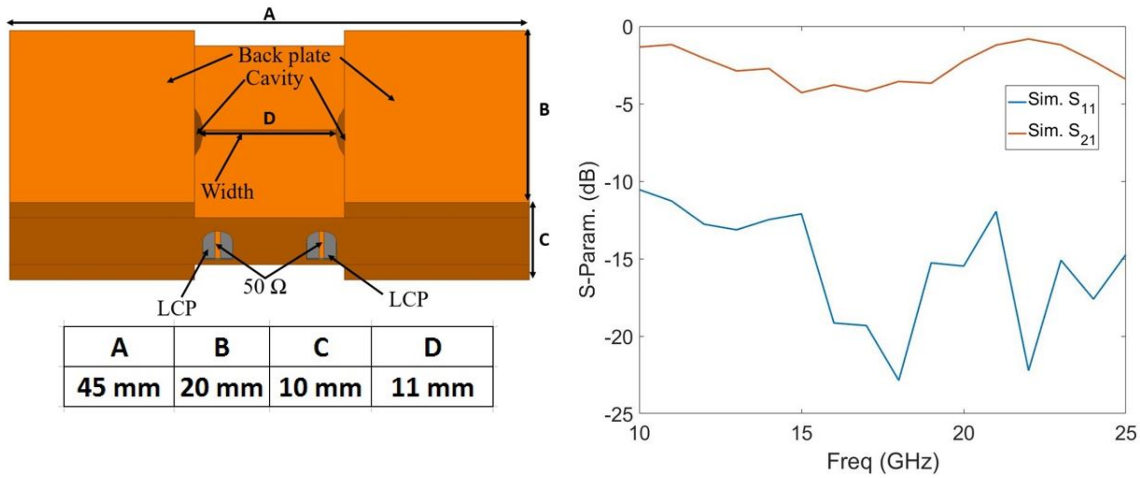

Figure 4.12: Designed front-to-back cavity (Left) and Cavity S-parameters (Right).

added which would help with impedance matching and reducing the radiated signal. The width of the gap of the structure was set to be smaller than $\frac{\lambda}{4}$ of the highest frequency. The structure was optimized to have the lowest insertion loss between both ports. The structure had a a max insertion loss of 3.8 dB, as can be seen in Fig. 4.12.

With this optimized configuration half of the structure was removed and then the Vivaldi legs were attached as shown in Fig. 4.13 and the table of dimensions. To optimize the Vivaldi antenna further the rate at which the Vivaldi legs flared up was changed until a return loss of > 10 for the entire bandwidth was achieved, as shown in Fig. 4.14. The antenna simulated a gain of greater than 9 dBi for the entire bandwidth with a maximum gain of ≈ 13 dBi. The fabricated antenna after blanket metalization and assembly can be seen in Fig. 4.13. The Vivaldi measured return loss can be seen in Fig. 4.14; as can be seen there is good correlation between simulated and measured results. The 50 Ω line attached to the Vivaldi was attached with MG Chemicals® 8331 conductive epoxy. The measured gain is shown in Fig. 4.14. this measurement showed good results when compared to simulation. The antenna was measured up to 18 GHz as that is the maximum frequency the SATIMO can measure. The effects of the conductive epoxy is apparent; as we saw about 1 dB of difference which is expected as it is not designed for RF applications. The simulation

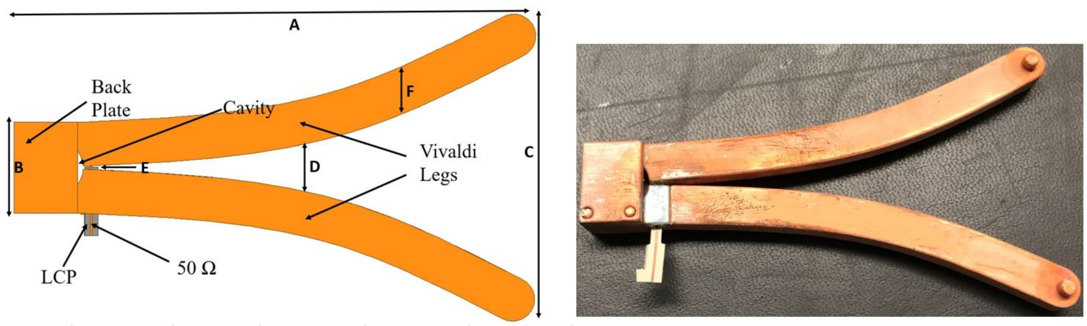

A	B	C	D	E	F
95 mm	16.5 mm	55 mm	7 mm	0.5 mm	10 mm

Figure 4.13: Designed Vivaldi (left) Fabricated Vivaldi (Right).

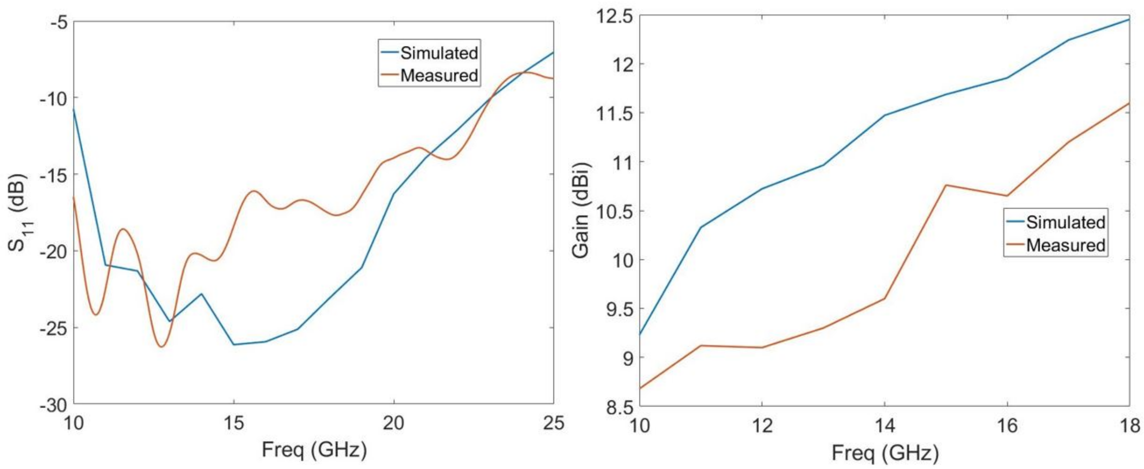

Figure 4.14: Vivaldi simulated and measured S-parameters (left) Vivaldi simulated and measured gain (Right).

4.2.2 Rigid-Flex Coax Antenna Array

This chapter presents a major advantage that the coax structure uses a standard substrate material; with this advantage a power divider can be made fairly easy and can be used for various circuits incorporated with the flex-rigid coax. The power divider being chosen to be studied is a Wilkinson divider because of its ability to work for UWB applications [64] and its low insertion loss. The center frequency was chosen to be 20 GHz which allows the Wilkinson power divider to operate between 10-30 GHz[60]. The designed Wilkinson power divider can be seen in Fig. 4.15. The 100 Ω resistor was modeled as a 0603 resistor since it was easily accessible to get physical 0603 resistors that operate up to 57 GHz. The fabricated Wilkinson divider can be seen in Fig. 4.15. It

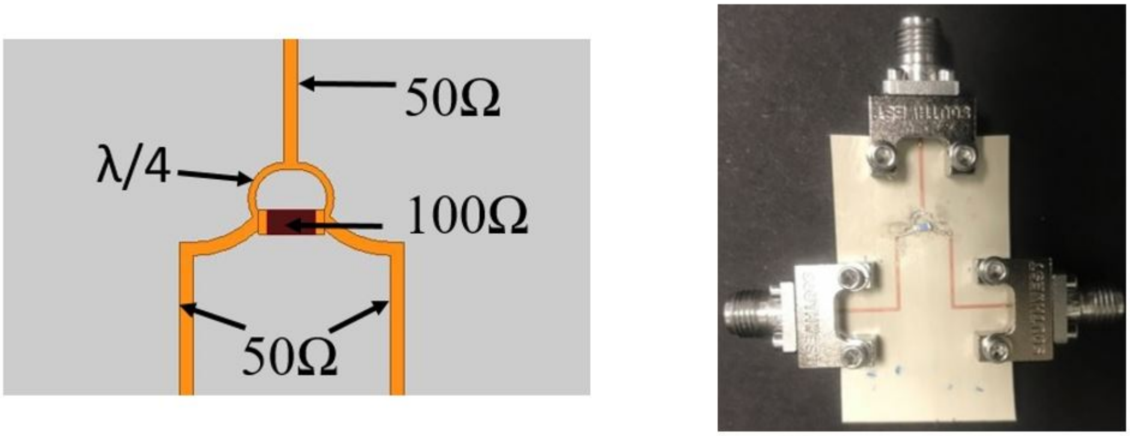

Figure 4.15: Wilkinson Power divider design (left) and fabricated (right).

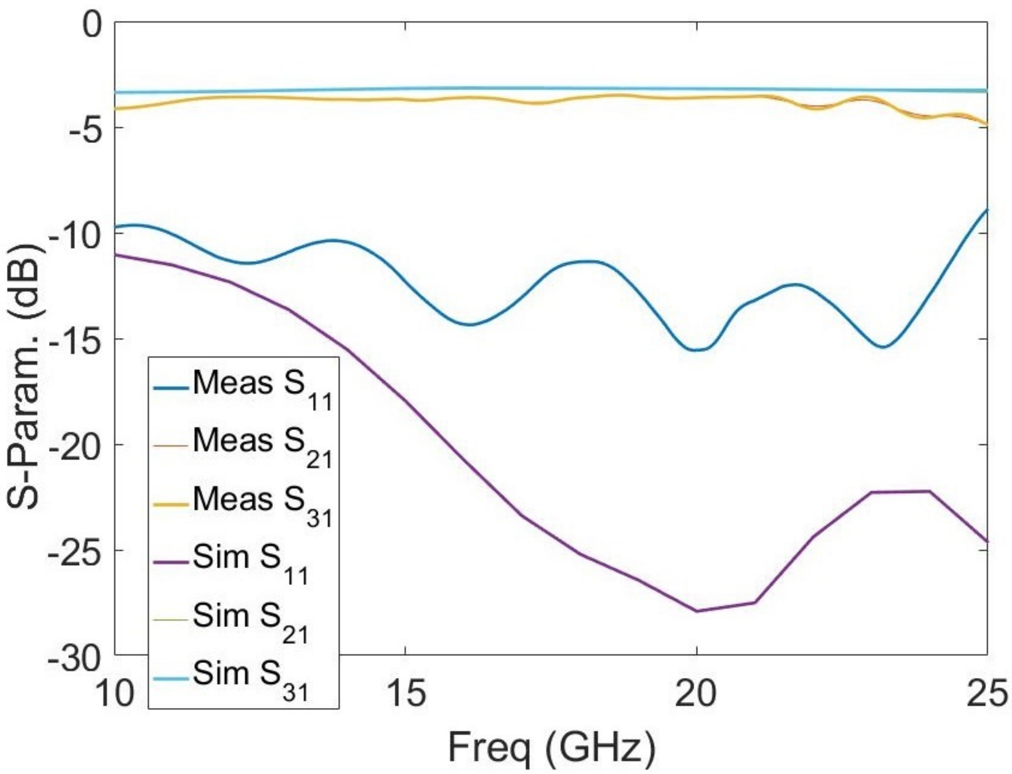

Figure 4.16: Wilkinson Power divider simulated and measured S-Parameters.

was fabricated using standard photolithography and the resistor was hand soldered to the board. As seen in Fig. 4.21, the power divider had about 1 dB of insertion loss up to 23 GHz. These results include the loss of the two SMA connectors.

This part of the chapter combines the UWB Vivaldi and Wilkinson power divider described

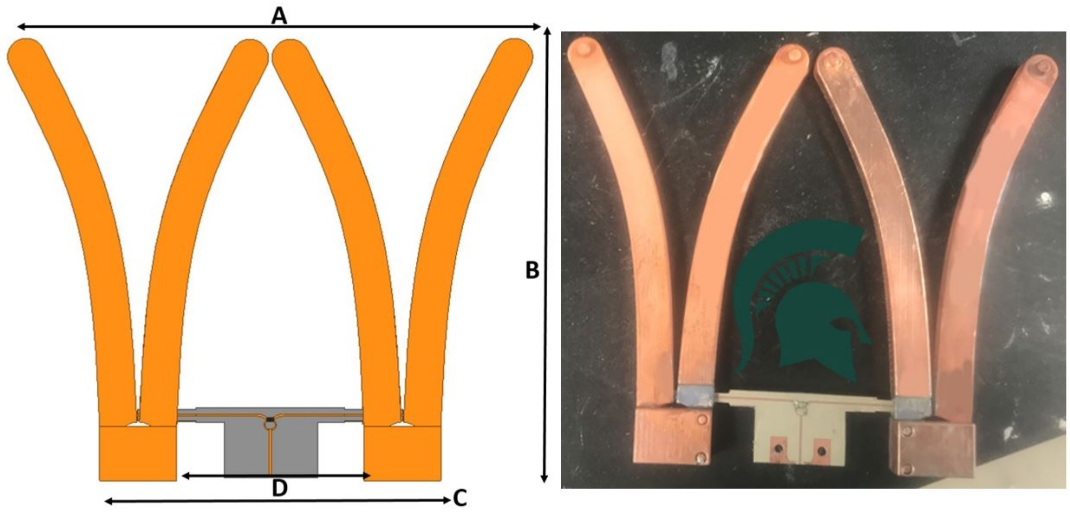

A	B	C	D
114 mm	95 mm	73 mm	40 mm

Figure 4.17: Vivaldi array design (left) and fabricated (right).

above to create a 1x2 Vivaldi array. The designed 1x2 Vivaldi array can be seen in Fig. 4.17. For the array spacing, due to the geometry, it was impossible to get $\frac{\lambda}{2}$ spacing between each antenna element; so the spacing was minimized as much as possible to about 56 mm. As can be seen in Fig. 4.18 the array had a return loss larger than 10 dB for the entire desired bandwidth. The simulated realized gain for the structure was larger than 12 dBi for the entire bandwidth as is shown in Fig. 4.20. Since further optimization was not possible in this orientation the array was fabricated. The fabricated array can be seen in Fig. 4.17, The antennas were 3D printed and blanket metalized up to 6 μm of copper, and the power divider was fabricated using standard photolithography process. The elements were attached to the power divider in a similar way as the 50 Ω line in the Vivaldi antenna described above. The measured return loss in comparison to simulation can be seen in Fig. 4.18. These measured results show very good correlation to simulation results. The fabricated array did maintain a return loss $>$ 10 dB. Between 16-18 GHz a resonance that does not correlate to simulation was seen and this was due to the 0603 resistor being a 3D dimensional component with larger parasitic effects than simulated. The measured gain can be seen in Fig. 4.18. Between 10-17 GHz the array had a measured gain $>$ 9 dBi.

The main disadvantage of using Vivaldi antennas is the physical size of the antennas that limits

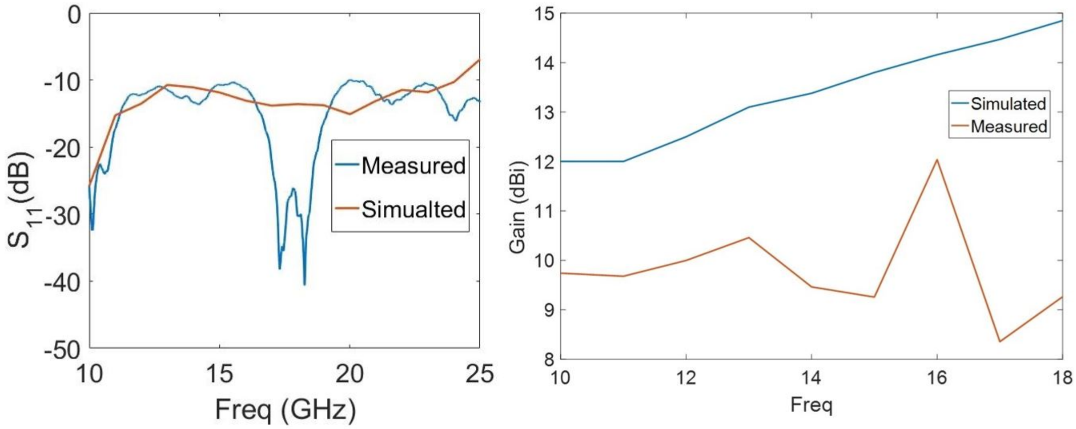

Figure 4.18: Vivaldi array S-parameters results (left) and gain (right).

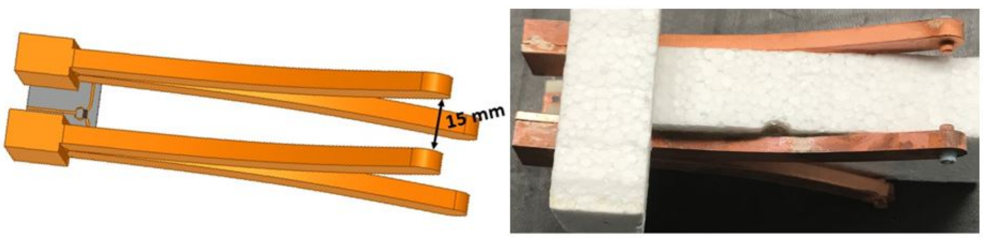

Figure 4.19: Vivaldi vertical array design (left) and fabricated (right).

the $\frac{\lambda}{2}$ spacing of the antennas in array applications. Shown above the array spacing was set to be $\frac{\lambda}{2}$ for 3 GHz due to the Vivaldi leg size. The benefit of this flex-rigid coaxial structure being used for the feed lines for the antenna, is that the Vivaldi antennas can be in vertical orientation to allow for better $\frac{\lambda}{2}$ spacing. This can be seen in Fig. 4.19, this allowed for better array spacing, as shown in Fig. 4.18 a $\frac{\lambda}{2}$ for 10 GHz was used. The returnloss as shown in Fig. 4.20 showed a good improvement. The simulated gain shown in Fig. 4.20; shows a good improvement across the the entire bandwidth. A maximum gain of 16.25 dBi was achieved. The fabricated Vivaldi array was simply bent around Styrofoam that was 15 mm thick as shown in Fig. 4.19. Styrofoam was used as it has characteristics similar to air, so no loading effects should be seen by the antennas and the spacing will be maintained at 15 mm. The measured return loss can be seen in Fig. 4.20; an overall 1.3 dB increase in return loss was seen when compared to the horizontal case. The measured gain can be seen in Fig. 4.20.

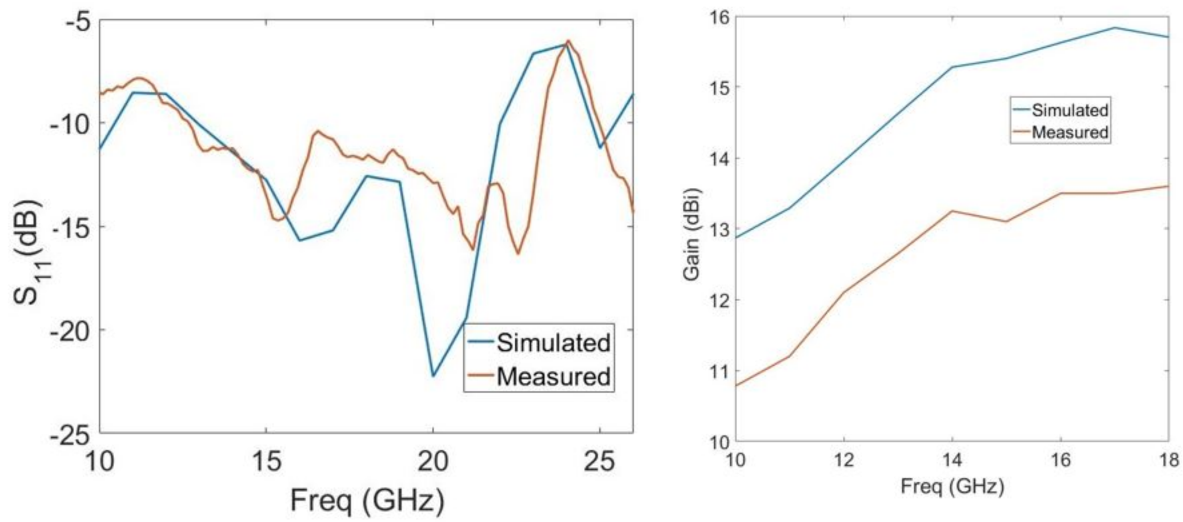

Figure 4.20: Vertical Vivaldi array S-parameters results (left) and gain (right).

4.3 Rigid-Flex Vivaldi Array with Printed Resistor

With surface mount components, there are physical and electrical limitations that could potentially be improved by using additive manufacturing (AM). Previous work has been done with static (DC) circuits to fabricate passive components such as resistors, capacitors, and inductors using injet printing techniques [65, 66, 67, 68]. However, to the best of our knowledge, resistors for microwave applications. By fabricating the passive elements directly onto a circuit there is a potential for reducing undesired parasitics. There are many materials available for AM that can be used individually or in combination to fabricate novel passive components. A common material used often in the fabrication of flexible circuits and solar cells for electrode connection is conductive polymers. For the purpose of replacing a chip-resistor with an aerosol printed thin-film resistor, we chose to use of PEDOT:PSS (Poly(3,4-ethylenedioxythiophene)-poly(styrenesulfonate)). PEDOT:PSS is a conjugated polymer [69] whose conductivity is low compared to copper and can readily be used in the design of a resistor. The geometry of the printed resistor can be used to achieve desired resistance values.

In order to replace the 100 Ω chip-resistor with a printed thin-film conductive polymer resistor, the same footprint was used. By using the same footprint for the resistor, a one-to-one comparison can be made between the commercially available and the customized aerosol-jet printed resistor. Using an Optomec 5X aerosol-jet printer with ultrasonic atomizer, to deposit thin-film conductive polymers onto a liquid crystal polymer (LCP) substrate with direct contact to etched copper pads and traces. Since PEDOT:PSS is a low viscosity material, it can easily be aerosolized and deposited. The area taken up by the chip-resistor was used as the pattern area of the printed thin-film resistor, with feature sizes as small as 40μm. By adjusting the amount of material deposited and successive layers of PEDOT:PSS, the resistance of the film can be precisely controlled. Aerosol jet printing allows for successive layering of material and overcomes many geometrical challenges. If a printed component such as a thin-film resistor is not within a margin of error, then additional geometric structures can be added to increase or reduce the resistivity. This is a major improvement over the current processes of laser trimmed chip-resistors.

An identical Wilkinson power divider was fabricated using the same process as discussed above and instead of utilizing a high frequency surface mount resistor the resistor was printed utilizing PEDOT:PSS and was printed in layers until the 100 Ω resistance was achieve. The measured results for the Wilkinson power divider with the printed resistor compared to the Wilkinson power divider that utilizes a standard surface-mount resistor are shown in Fig. 4.21. As can be seen, the results for both Wilkinson power dividers matches closely, and shows that the printed resistor can provide similar performance to a commercially available high frequency resistor.

The Wilkinson power divider described is combined with the 3D printed Vivaldi to create a 1x2 element antenna array. The Wilkinson power dividers from above will have their connectors removed and used with the printed Vivaldi structure. The array S_{11} results are shown in Fig. 4.23a. There is good correlation between simulation and measured results for the arrays. As shown in Fig. 4.23a, the array that utilized a 0603 surface mount resistor had a resonance between 16-19 GHz; through simulation it was found that the resonance was caused from the parasitic inductance and capacitance of the 0603 package and soldering to the board. The PEDOT:PSS based resistor did not show any resonance over the measured frequency band. Fig. 4.23b shows the gain of the array. The array had a simulated gain of 12 dBi at 10 GHz and a max gain of 15 dBi at 18 GHz.

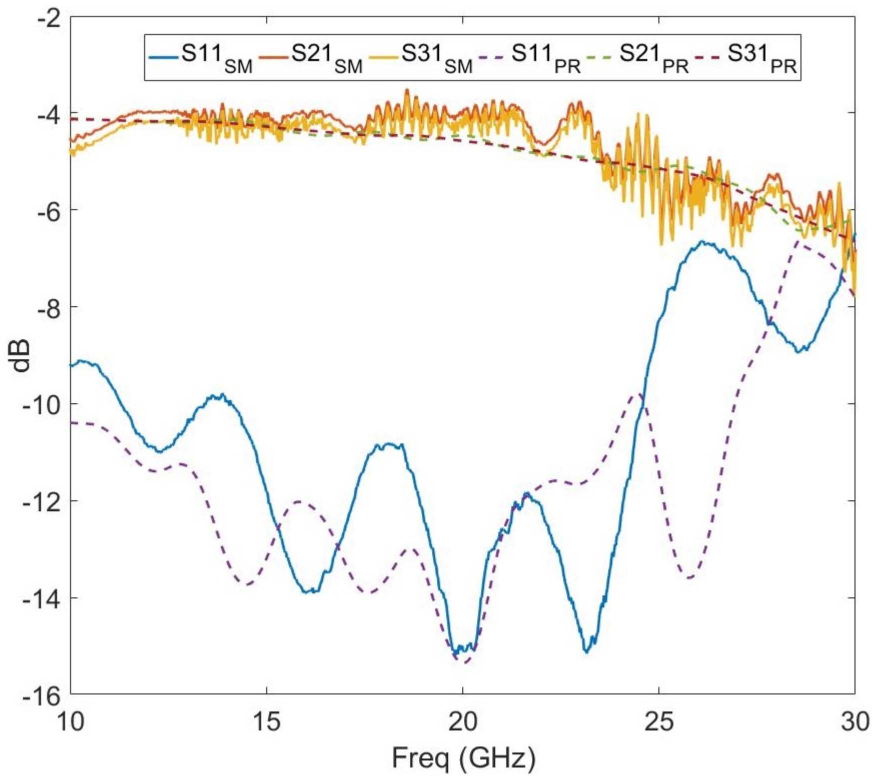

Figure 4.21: Measured results of the Wilkinson power divider. PR- Printed Resistor, SM- Surface Mount.

The measured gain for the surface mount resistor array was approximately 10 dBi at 10 GHz with a maximum gain of approximately 11.75 dBi at 16 GHz; however, the gain begins to drop where the resonance occurred. For the printed resistor array the gain started at approximately 10 dBi and with a maximum gain of 12.5 dBi at 17 GHz.

4.4 Summery

This chapter showed the an effective way of creating coaxial like transmission line. This approach utilized standard substrates to create the fine features through photolithography and additive manufacturing to create the larger features. This approach created the lowest loss transmission line in recent publications. This work achieved a resonator with a Q-factor over 10000. This transmission line design also allowed us to create a Vivaldi antenna and for the first time in publication a UWB Vivaldi antenna array. This approach shows an effective and an easy way to create compact transmission lines, resonators, and antennas in a small form factor.

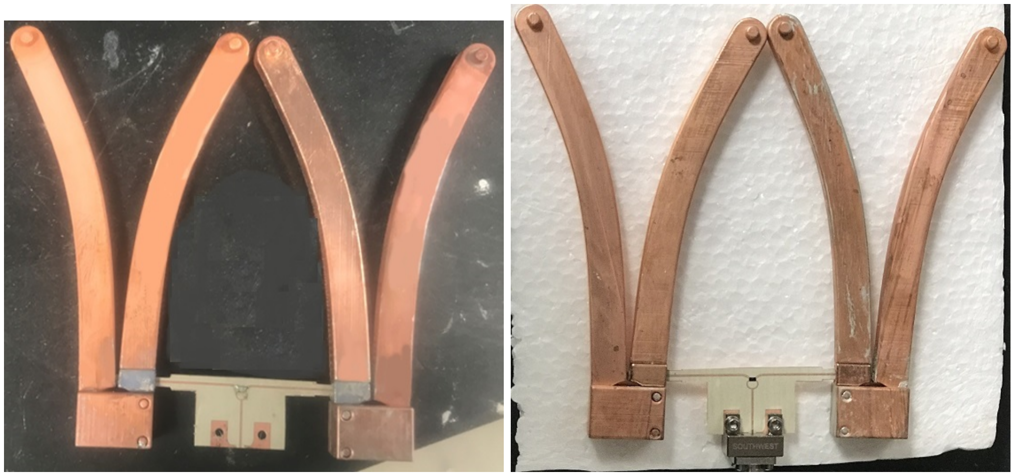

(a) (b)

Figure 4.22: (a) 1x2 Vivaldi array with surface mount resistor. (b) 1x2 Vivaldi array with printed resistor.

This also showed for the first time utilizes PEDOT:PSS as a high frequency resistor for the Wilkinson power divider and shows measured results up to 25 GHz. This chapter showed an effective way of creating RF resistors through additive manufacturing.

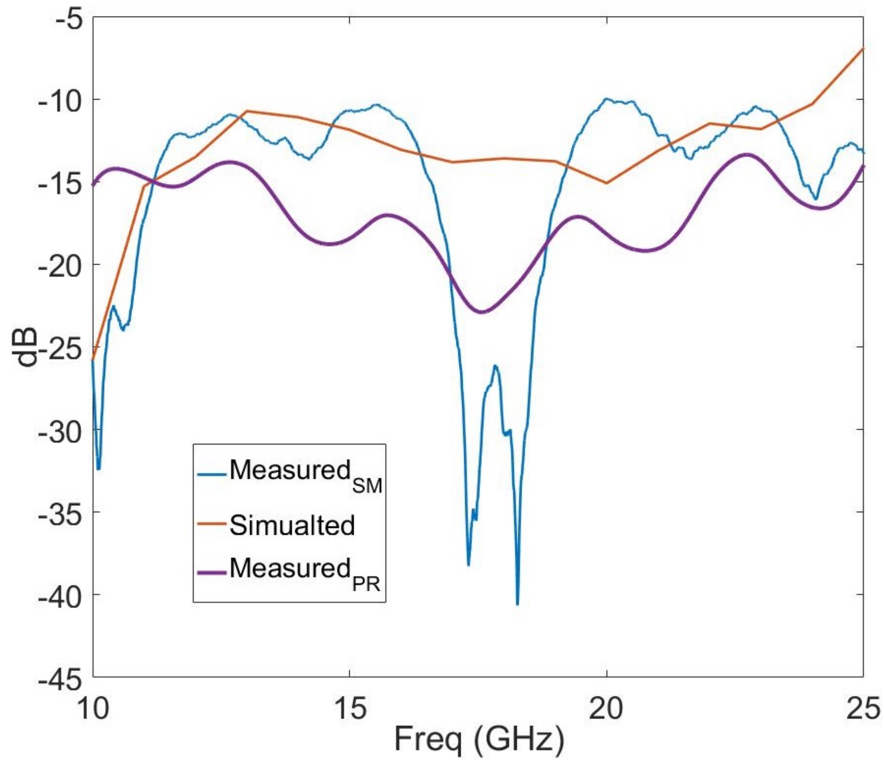

(a)

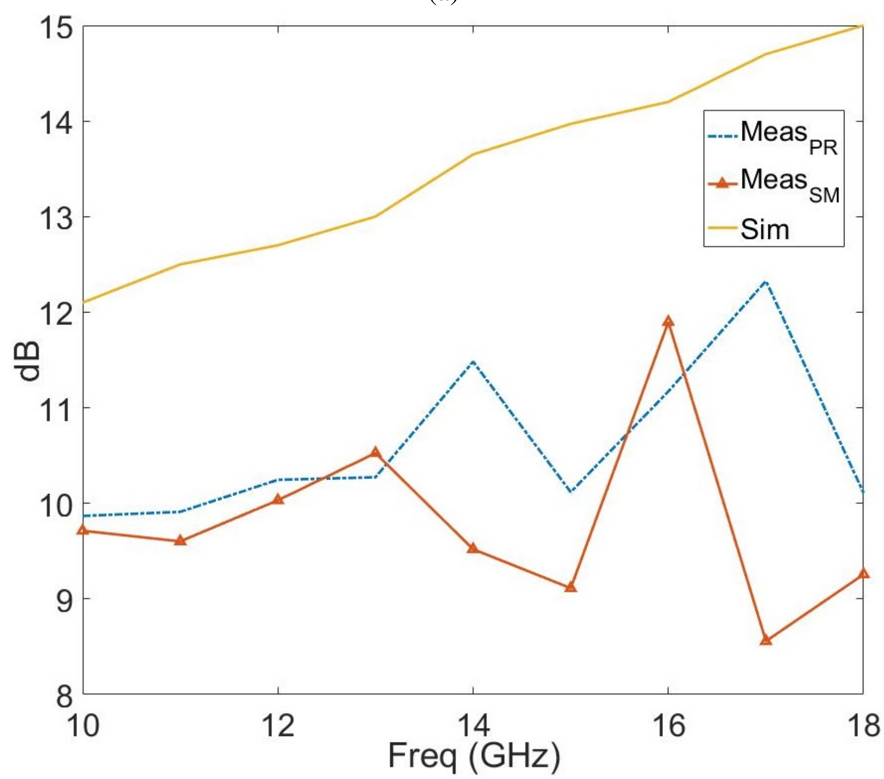

(b)

Figure 4.23: (a) Simulated and Measured S_{11} . (b) Simulated and Measured gain results. PR- Printed Resistor, SM- Surface Mount.

CHAPTER 5

RIGID-FLEX SOA

Microwave and mm-wave systems are important for many automotive, communications, and military applications. In the electronic front-end of radar systems, the transmit and receive (T/R) modules are of critical importance [70]. T/R modules play a critical role in determining the overall cost and performance of radar systems. The T/R module needs to be compact and light-weight, and have low-loss and low-distortion characteristics [71]. On the receiver end, it is of utmost importance to achieve high signal-to-noise ratio. Apart from using low-noise components, it is critical to also reduce integration losses. One approach to meet this goal is to integrate the receive module in close proximity to the antenna element.

Many system design approaches are commonly employed in the design of compact T/R modules, including System-on-Chip (SoC), System-in-Package (SiP) and System-on-Package (SoP). SoC offers the promise for the most compact, light-weight system that can be mass-produced. This has been and continues to be the road map for the wireless RF industry. SoC seeks to integrate numerous system functions on one silicon (or other semiconductor) platform horizontally, typically a chip [4]. SoC is a very attractive solution to achieve high levels of integration in a small package. Some of the challenges associated with the SoC concept are long design times due to integration complexities, high wafer fabrication costs, and incompatibility with heterogeneous integration [4]. Another challenge faced is degraded antenna performance due to lossy silicon substrates when designed in CMOS and SiGE-BiCMOS, which is the optimal technology for modern SoC integration [72, 73, 74].

This chapter shows, building upon the concept of SoP, a compact front-end module that utilizes a section of the antenna element to embed the receive circuit elements. The antenna and active circuits can be co-designed and combined to achieve small form factor while enhancing system performance. This co-design between the antenna and the circuit can help solve the major issue faced with developing SoP, which is how to efficiently integrate an antenna, including active feed structures [75]. A receive module is shown that is compatible with system designs for unmanned aerial vehicles, automotive anti-collision, and other constrained installations that will need to be compact and lightweight [76]. In the future, RF modules will be embedded in wings, bumpers or other sections of a platform. 3D printing is becoming the key enabling technology for these higher levels of integration and conformality.

The Rigid-Flex fabrication technique demonstrated in the previous chapter is adopted here to design a complete receive module. This technique utilizes Rogers® 3850HT (Liquid Crystal Polymer, LCP) flex and 3D printed rigid structures to fabricate antennas and antenna arrays. In this chapter, the fabrication technique is applied more broadly to include active elements as integral parts of the antenna structure, and a compact receive module is demonstrated.

5.1 System Design and Fabrication

Figure 5.1a shows the schematic diagram of the receive module design chosen for demonstration. It is comprised of an amplifier and a mixer integrated circuit. The integrated mixer down-converts the RF to an IF band. This was done as a practical concern, since in a real application the IF frequency will be used to for the signal processing rather than the RF signal itself. The amplifier used in this design was a Mini Circuits® AVA-24+ surface mounted amplifier, which has 12.3 dB of gain[77]. The mixer used was a surface mount Mini Circuits® SIM-153+ ceramic mixer [78].

The receive module housing the active and passive components (resistors and capacitors) was fabricated on Rogers® 3850HT (LCP). The circuit was patterned using a standard positive photolithography process. The vias to the ground for the mixer and the amplifier were formed using a high speed 200 μm diameter drill bit. The vias were filled by MG Chemicals® 8331 conductive epoxy to complete the electrical connections. The conductive epoxy was cured at 60^oc for one hour at atmospheric pressure. The surface mount components were reflow-soldered using hot air. Fig. 5.1b shows the fabricated circuit. To verify the circuit was operating as intended, it was first tested on a spectrum analyzer using a signal generator as the RF-input.

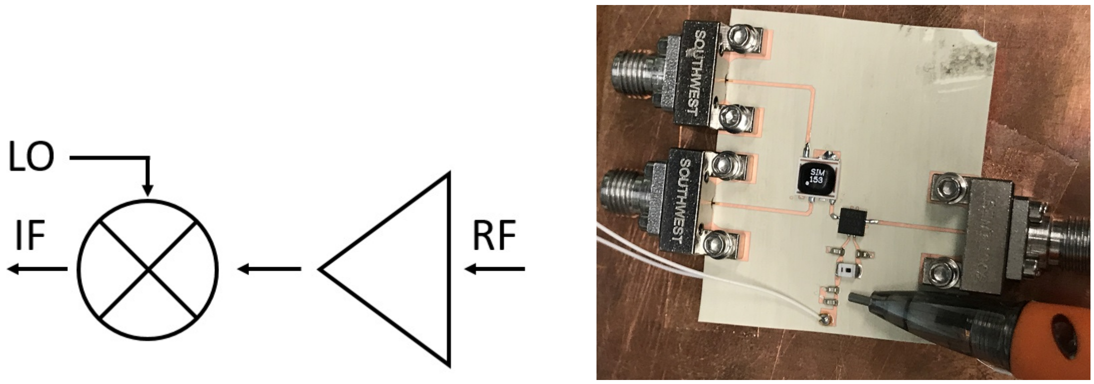

(a) (b)

Figure 5.1: (a) System schematic of receive circuit. (b) Fabricated circuit.

5.2 Package Design and Fabrication

Previously, as shown in Fig. 5.2, a 3D printed Vivaldi antenna fed by a Rigid-Flex transmission line was developed [79] and is the basis for this design. The 3D printed Vivaldi antenna had a gain greater then 9 dBi over 10 - 25 GHz with a maximum gain of 13 dBi at 25 GHz. For the Vivaldi antenna, the inside volume of the legs is important for maintaining the radiation characteristics but the rest of the Vivaldi leg volume is electrically unused space. Here, the exterior of the Vivaldi leg was used as a cavity to package the receive system circuit. The cavity was slightly larger than the Vivaldi leg in order to accommodate the surface-mounted mixer, which is shown in Fig. 5.2.

To fabricate the Vivaldi antenna, a similar approach as described in [79] was followed. To create the SoP, we removed the RF input connector and excess substrate material from the receive circuit and placed it into the cavity as shown in Fig. 5.2. The ground plane of the receive circuit was adhered to the Vivaldi antenna package using MG Chemicals® 8331 conductive epoxy. Following that, the 3D printed cavity cover was placed onto the antenna as shown in Fig. 5.2 to complete the SoP. This package also has the added benefit of providing isolation for the receive circuit.

5.3 Measurement

To measure the performance of this 3D printed SoP, a duplicate receive circuit was fabricated and attached to a Cobham H-1498 horn antenna with a SMA male to male through as shown in Fig.

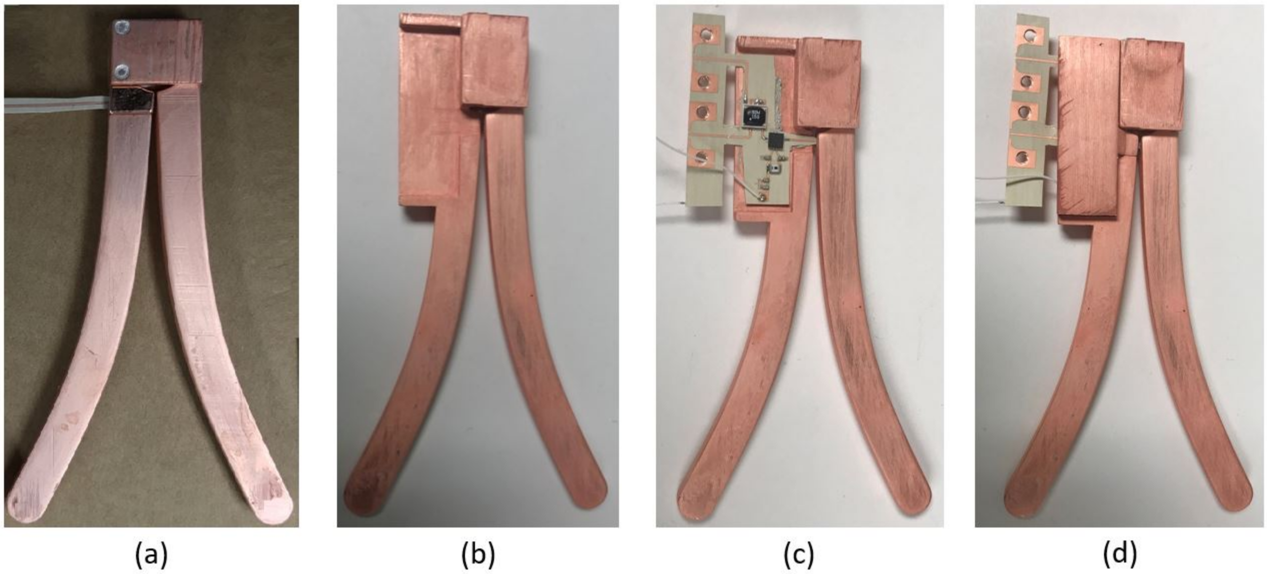

Figure 5.2: (a) Rigid-Flex Vivaldi antenna. (b) Modified Rigid-Flex Vivaldi for SoP receive circuit. (c) Vivaldi with circuit embedded in the cavity. (d) Final package with cap covering the cavity.

5.3a. This horn antenna with receive circuit is compared directly to the 3D printed SoP Vivaldi with identical measurement conditions. The measurement conditions for both setups consist of a Cobham H-1498 transmitting horn antenna driven by an HP 83592A signal generator as the RF input. A HP 83731A signal generator was the LO drive for the receive circuit. The IF power from the receive circuit was measured using an HP 8562A spectrum analyzer. Both front-end modules were measured inside of an anechoic chamber.

The transmitter was set to 10 dBm for each of the frequency points. The LO drive was 11 GHz with 7 dBm output power and held constant throughout the measurement. As can be seen in Fig. 5.4, the 3D printed SoP front-end module at 12 GHz collects 1 dB more power than the reference horn and linearly increases to approximately 5 dB more at 15 GHz. This directly corresponds to the Vivaldi antenna gain, which starts at 9 dBi and increases to 12 dBi with increasing frequency over this range whereas the Cobham H-1498 horn maintains 11 dBi gain across the band [35]. Also, the loss from the SMA male-to-male adapter and the SMA connector used to connect the horn to the receive circuit contributes to the lower received power. As can be seen in Figs. 5.5a-5.5d the radiation characteristics of the carrier frequency match closely to the theoretical end-fire radiation

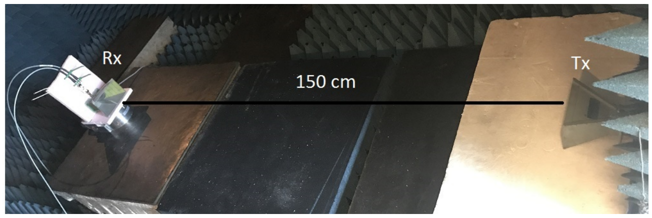

(a)

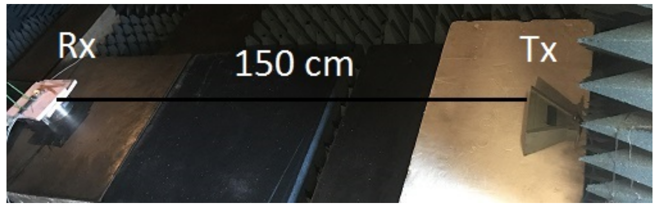

(b)

Figure 5.3: (a) Horn antenna with receive circuit. (B) 3D printed SoP receive module.

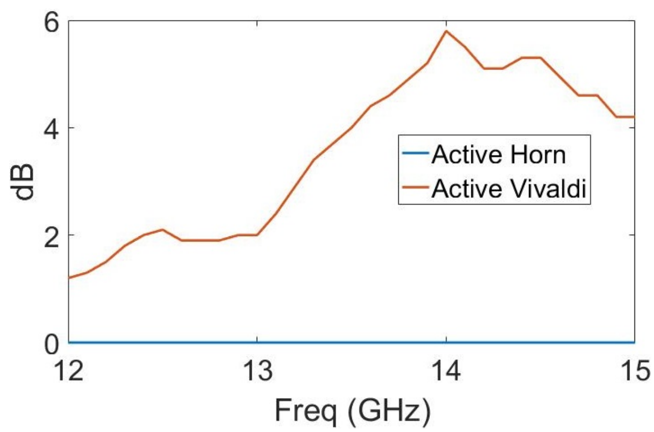

Figure 5.4: Receive power difference between the active horn and Vivaldi antenna (normalized to the horn).

pattern for both the horn and 3D printed Vivaldi antennas.

5.4 Summery

A demonstration of a hybrid additive manufacturing approach for the fabrication of high functional-density packages has been presented. Building on previous work with passive-structures, the hybrid Rigid-Flex transmission lines, an active receive circuit embedded in a 3D printed Vivaldi antenna has been measured. When compared directly to a standard rigid horn antenna the 3D printed Vivaldi antenna showed 5 dB improvement on receive. This work demonstrates a low-cost, light-weight, and high-density package with improved performance through 3D printing.

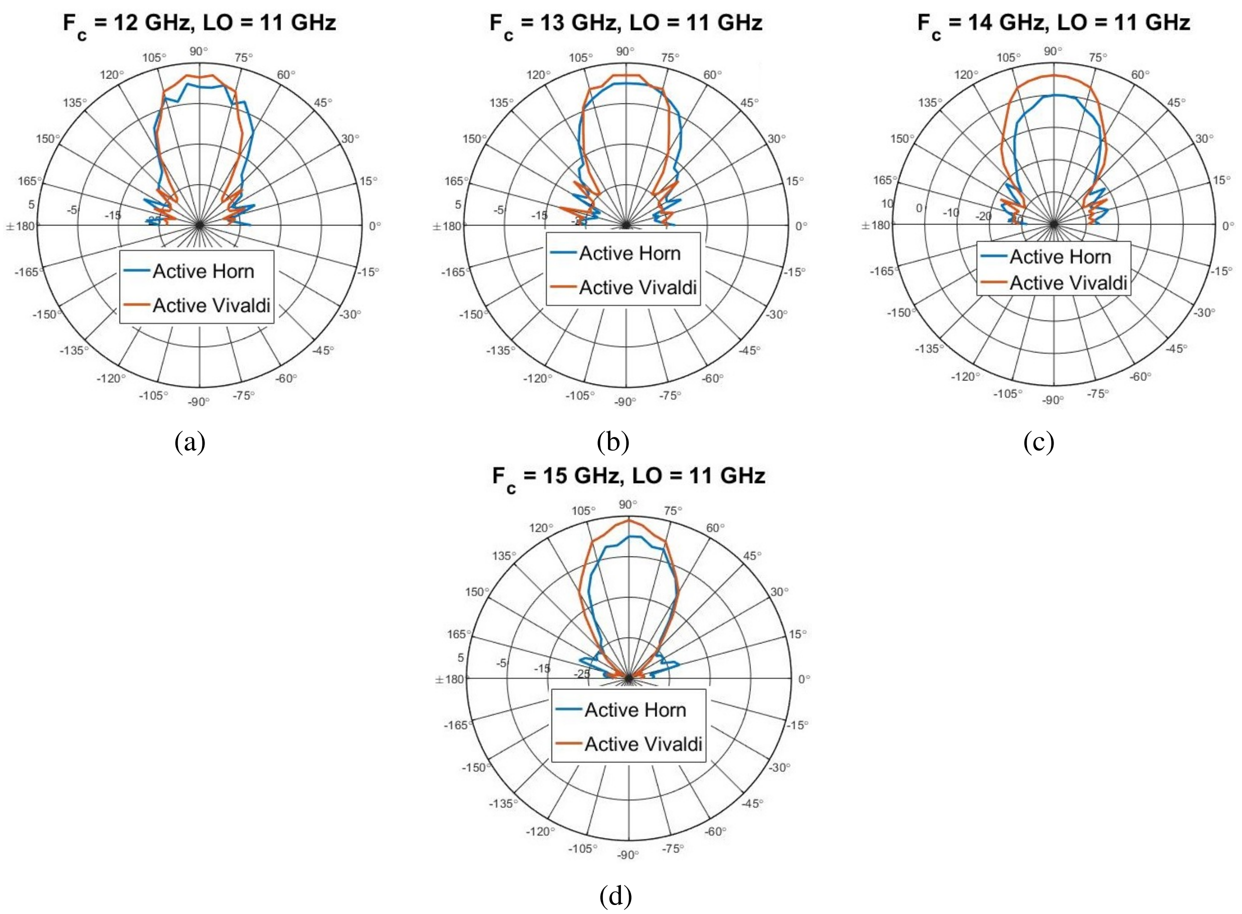

Figure 5.5: (a) Measured radiation pattern at 12 GHz. (b) Measured radiation pattern at 13 GHz. (c) Measured radiation pattern at 14 GHz. (d) Measured radiation pattern at 15 GHz.

CHAPTER 6

RIGID-FLEX PRINTED VIA SOA

This chapter covers new approach to packaging of RF front-ends u sing a combination of polyjet printing and aerosol jet printing (AJP) techniques. The transmit system demonstrated consists of a Vivaldi antenna having a pocket for packaging as an integral part of the design and a transmit circuit fabricated on LCP using AJP that is placed in this pocket. The transmit circuit consists of a VCO, PA and the bias network. The radiated power was measured using a horn antenna and a spectrum analyzer. The effective power loss in the circuit is approximately 0.5 dB. The proposed process avoids the use of conventional photolithography or machining techniques. This work shows that high functional density complex RF systems can readily be fabricated using additive manufacturing.

Aerosol jet printing technologies present a new technique for rapid production of RF circuits and systems. Aerosol jet printing offers a ability to put down a wide range of conductive materials. With the large standoff distance of aerosol jet printing, complete metallization of out-of-plane features can be achieved, enabling complete circuit fabrication without the use of clean room facilities and chemicals. By reducing the time and cost associated with prototyping, designs can quickly be iterated to converge on an optimal solution.

Building upon the work in the previous chapter, the aim of this chapter is to demonstrate a truly compact and light weight transmit system fabricated using Additive Manufacturing . Fig. 6.1 highlights the aim of this paper where the antenna and the transmit (Tx) module are combined as a single platform.

AJP has shown promising results for the fabrication of passive components working over a wide frequency range, DC to THZ applications [69, 80, 81, 82, 83]. AJP shows a method that can be utilized as a cost-efficient technology for various applications like internet of things (IOT), radio frequency identification (RFID), and wireless sensors. Recent publications have been looking into the fabrication of VIAs in circuits with AJP. VIAs are one of the most critical factors for the

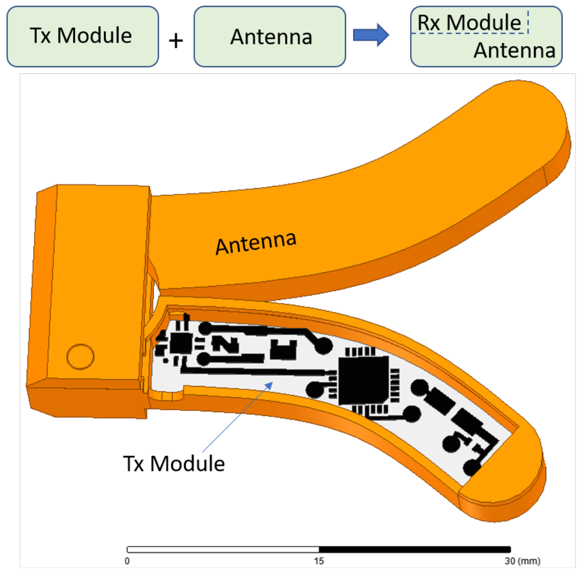

Figure 6.1: An ultra compact receive front-end.

realization of highly integrated systems, packages, and multilayered structures[9]. This paper studies and shows the results of VIAs created with AJP in holes created utilizing a standard rotary tool.The issue faced in [41] was the VIAs were drilled in the substrate and manually filled with a conductive epoxy which really increased the dimensional size of the circuit so much so that the Vivaldi had to be slightly increased to fit the circuit. This work utilizes a combination of SLA and AJP to create a SOA transmitter all inside a small form factor Vivaldi antenna. A recent publication showed results of VIAs created with AJP in holes that were created with femtosecond lasers [84] and this work shows similar results. This works studies utilizing these AJP VIAs to create a high functional density circuit which is utilized to create a system. The circuit is fabricated on standard liquid crystal polymer dielectric (LCP, Rogers Ultralam 3850HT) with AJP completely cutting out the need to utilize photolithography to create the circuit for the components. Utilizing AJP for fabrication of the circuit is far superior in creating circuits when compared to other additive manufacturing methods. This AJP circuit is then housed inside of printed antenna to create the packaged system.

This chapter shows a VCO and an amplifier inside of the Vivaldi antenna to create a transmitter which is within $\pm$ 1 dB of the theoretical calculation. For this entire fabrication process no standard fabrication processes were utilized.

6.1 Aerosol Jet Printing

With Additive Manufacturing (AM) as the main goal for this design, an Optomec 5x Aerosol Jet Printer (AJP) was used to pattern and fabricate the conductive traces for the PCB. Using an AJP process expands the abilities for small flexible circuits requiring design rules that traditional photolithography fabrication may not easy to produce. With a contactless fabrication process, planar and nonplanar substrates may be used, as well as the elimination of chemicals traditionally used for the patterning of copper.

6.1.1 Circuit Fabrication

The conductive ink deposited by the printer is Clariant Prelect TPS 50G2 50 wt% loaded silver (Ag) nanoparticle ink. This ink has good RF characteristics with thermal sintering below 200C, where the substrate begins to warp and lose its structural properties. The fine features of the AJP allow for precise resolution down to 10um, and the control over thickness of the deposited material. This design included 10um thickness (z axis) of Ag traces and pads, with 40um feature size (x,y axis) using the Fine Feature setup on the Optomec 5x. Connections to the surface mount components and leads for DC connection were made using Epotek H2OE-FC conductive epoxy with a low temperature cure of 150C on a hotplate. This conductive epoxy works well with the printed Ag ink on both pads and ground planes. The printed circuit can be seen in Fig. 6.2 before being populated with components.

6.1.2 VIA Fabrication

Vias are commonly used in electronics for connections between physical layers to connect electrical pathways of two or more layers. For multi-layer PCBs (printed circuit boards), Vias can be used to connect signal paths, bias voltages, and ground planes between various layers for easy routing around or under components such as ICs (integrated circuits). For single-layer or two-sided

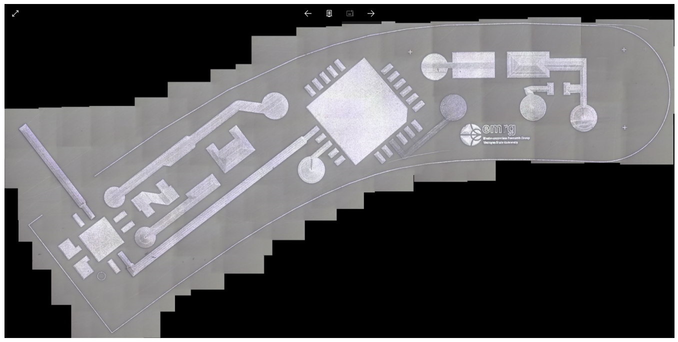

Figure 6.2: AJP printed transmitter circuit.

PCBs, the most common use of VIAs are to make connections to ground without routing traces on both sides. This technique is very common, where a simple through-hole VIA is used to connect components to ground through the substrate. A few fabrication methods include laser drilling, photolithographic masking and chemical etching, and mechanical drilling. If fine precision of laser drilling is not required, and chemical processes need to be avoided, mechanical drilling is the simplest and least costly choice. Mechanical drilling is also material-agnostic, as it does not require particular chemicals or specific wavelengths and power to penetrate through various material types.

While there are many different techniques for fabricating VIAs, the authors chose to use mechanical drilling due to the low cost and availability of tools for the process. Two types of VIAs were created with this method: through-hole and blind VIAs. Mechanical drilling allows for ease of use in prototyping and allows for a material-agnostic process usable on most rigid and flexible laminated substrates. This method works well for LCP, leaving smooth tapered VIA wells. Blind VIAs were created with various diameters ranging from 100 μm to 600 μm using a high-speed drill press and CNC drills. The drill was used to create a well in the LCP that bottoms out at the copper cladding on the backside of the substrate. This type of well is best suited for the fabrication of plugged or plated VIAs, as there is a large conductive area at the bottom to build upon. Through-hole VIAs were created using the same technique as the blind VIAs, except the drilled well continued through the copper cladding at the bottom. By drilling through the cladding by a small amount, a tapered hole was formed allowing for metallization of the VIA walls to be formed.Plating of VIAs requires chemicals as well as leaving behind a lot of unused waste. Additive Manufacturing avoids the unnecessary waste caused by chemical plating solutions which use a large volume of material for plating of small areas in VIAs. Selective VIA plating is also time consuming and difficult, so AM was chosen as a method to create plug-like VIAs in the LCP substrate. By printing in the tapered VIA well using conductive silver ink, a conductive path was formed from the bottom copper to the LCP sidewalls and upward onto the surface of the LCP where pads of conductive silver were printed previously. Once the ink was dried and sintered into a solid conductor, a plugged VIA had been created.

With the use of a Optomec 5x AJP (aerosol jet printer), many traditional methods can be supplemented or supplaced by depositing aerosolized particles layer at a time in selective areas and geometries. Many features can be created with the use of AJP, including ones which may have been previously impractical. Because AJP does not require contact with the substrate or conductors like plating processes do, conductive or dielectric materials can be used as fill agents for VIAs easily. The tapered well created by mechanical drilling is perfect to print on from the vertical position of the AJP without any special setup to print on a vertical surface. A simple spiral pattern starting at the bottom or top surface was used to connect the silver pads at the LCP surface to the copper cladding on the backside of the substrate. Some close up of the VIAs can be seen in Fig. 6.3. High vertical aspect rations were realized by decreasing the speed of the printer tool path. Applying 2-3 layers as needed, 100-200 μm deep wells were plugged on both test coupons as well as the final SOA circuit board. Test coupons were created in order to measure contact resistance between the ground plane and the printed VIAs and pads on 4 mil and 9 mil LCP laminates. The measurement of the VIAs was done with a 4-point conductivity probe. The measured resistance for both 4 mil and 9 mil LCP was less then 0.01 Ω.

6.2 Transmitter Circuit Package

This portion covers the design of a 3D printed ultra wide band (UWB) Vivaldi antenna which is blanket metalized and fed directly with a simple 50 Ω transmission line on LCP. This technique of Rigid-Flex yields great performance with out the need of utilizing coaxial feeds or complex

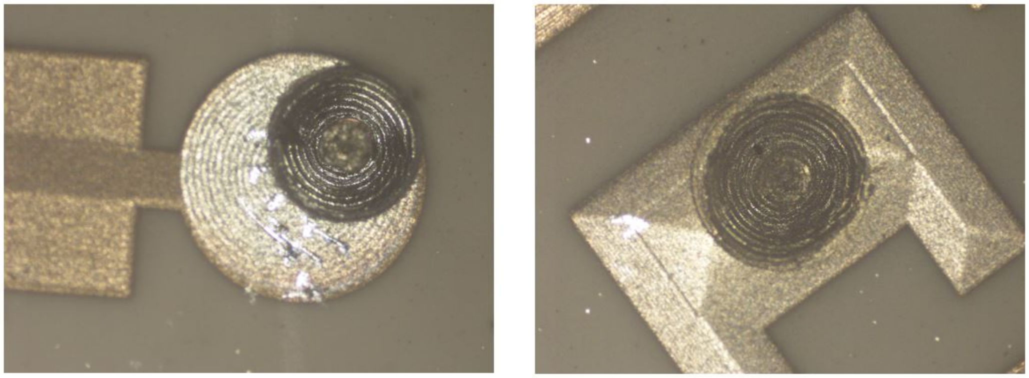

Figure 6.3: VIA close ups.

complex coupling feeds. This process of design and fabrication was described in great detail in the previous chapter.

6.2.1 Vivaldi Design and Measurement

The same process is utilized in this paper but the length of the antenna is shortened which yields to a smaller gain of the antenna. The designed antenna can be seen in Fig. 6.4. The total length of this antenna is approximately 40 mm and the total with is 16.5 mm. The legs of the Vivaldi are 8 mm in width with a gap of 500 μm between the legs. With the Vivaldi antenna being rather short for the frequency range, impedance matching can difficult, an advantage of 3D printing the antenna the thickness of the antenna can be changed to the get good impedance matching. For this antenna to get a good impedance match (return loss $>$ 10 dB) the Vivaldi leg was designed to be 4 mm. The 50 Ω transmission line is modeled for 7 mil ($\approx$150 μm) LCP where the ground plane is connected to one of the Vivaldi legs. The center conductor of the 50 Ω line continues to the opposite Vivaldi leg without a ground plane beneath it. The simulated returnloss can be seen in Fig. 6.5. The simulation was done in Ansys HFSS (version 18.2). The antenna has a S_{11} below -10 dB for the frequency range 12-17 GHz. The antenna showed a simulated gain between 9 - 11 dBi for the frequency range as can be seen in Fig. 6.5. With these results the antenna was fabricated.

The fabricated Vivaldi antenna can be seen in Fig. 6.4b. The antenna was blanket metalized with 0.50 μm of Titanium (Ti) followed by 1 μm of Copper (Cu). The layer of Ti acts an adhesion

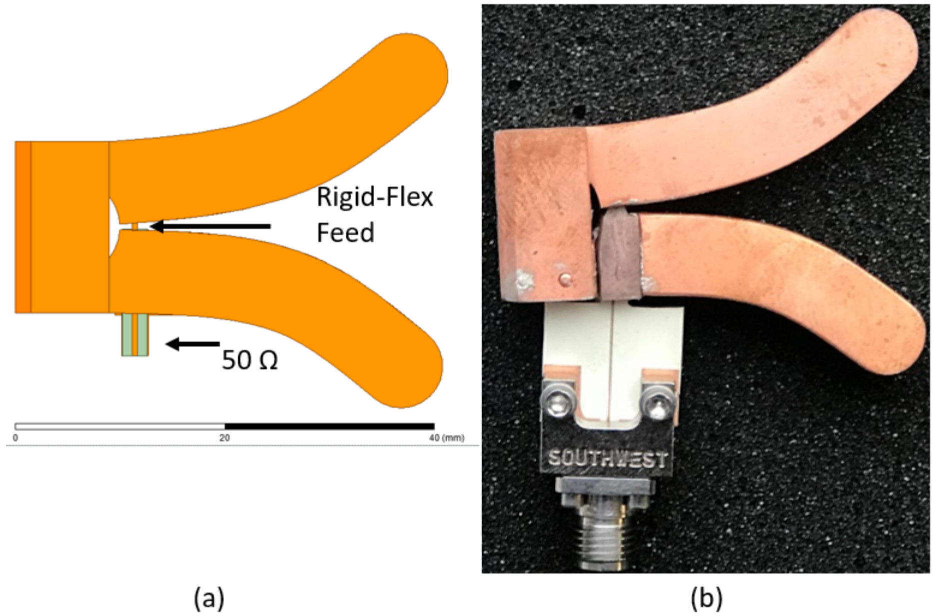

Figure 6.4: 3D Printed Vivaldi Design (left) 3D Printed Vivaldi Fabricated(right).

layer between the copper and 3D printed plastic material. The copper layer was thickened to a total Cu thickness of 6 μm with electroplating. The antenna was fabricated in two pieces to ensure proper Cu coating in all the crevasses and the two pieces where combined together using a MG Chemicals 8331 conductive epoxy. The Rigid-Flex feed was fabricated on 7 Mil LCP utilizing standard photolithography to. The antenna was fed with a 3.5 mm edge-mount connector. The measured S_{11} of the antenna can be seen in Fig. 6.5. The measurement Slight discrepancies can be seen, This was due to the longer 50 Ω to account for the edge-mount connector causing a standing wave. The gain of the antenna is as can be seen in Fig. 6.5 matches simulation within 1 dB.

6.2.2 SOA Fabrication and Measurement

The outside portions of the Vivaldi leg is essentially unused space. A cavity was created in the Vivaldi leg and the transmitter circuit was set inside of it as can be seen in Fig. 6.6. Following the same fabrication steps as above a new 3D printed Vivaldi was created with the cavity for the circuit. The transmitter circuit was placed inside of it and the ground plane was epoxied to the antenna with the MG chemicals epoxy. This created a DC ground for the entire antenna and the

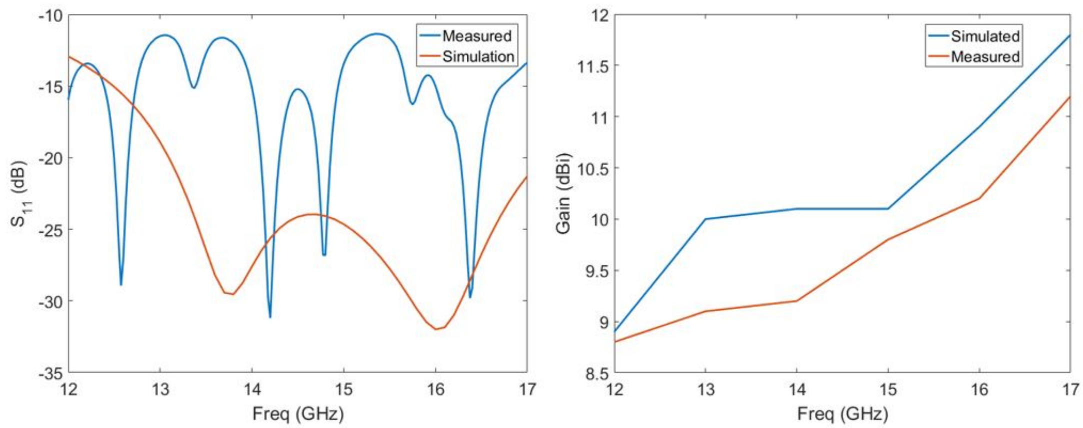

Figure 6.5: Simulated and Measured S_{11} (left) and Gain (right).

Vivaldi leg with the cavity became a RF ground. The RF-out of the amplifier is connected to the opposite Vivaldi leg with the Rigid-Flex feed to create the transmitter circuit.
Looking at the Fig. 6.7, with the VCO outputting 5 dBm and we can account for 3 dB of loss between the VCO and amplifier due to the loss contributed by the silver printed transmission line, the amplifier amplifies the signal by 11.8 dB into a 8.8 dB antenna. Calculating the free space loss Egn. 6.1 for a distance of 10 cm gives approximately 30 dB of attenuation. That signal goes into a 10 dB standard horn antenna which is connected to the spectrum analyzer through a SMA coaxial cable which measures 1.7 dB of attenuation. The theoretical received power at the spectrum analyzer is calculated to be -0.01 dBm, as can be seen in Fig. 6.8, for the measurement set up shown in Fig. 6.7 this SOA is within 0.7 dB of theoretical value. This small derivation from the theoretical can be easily accredited to contact resistance between the VCO and AMP to the circuit due to the conductive epoxy.

$$L_{air} = 20Log_{10}(\frac{4\pi df}{c}) \tag{6.1}$$

6.3 Summary

This chapter shows a new approach to the packaging of RF front-end is demonstrated using a combination of polyjet printing and aerosol jet printing (AJP) techniques. The transmit system

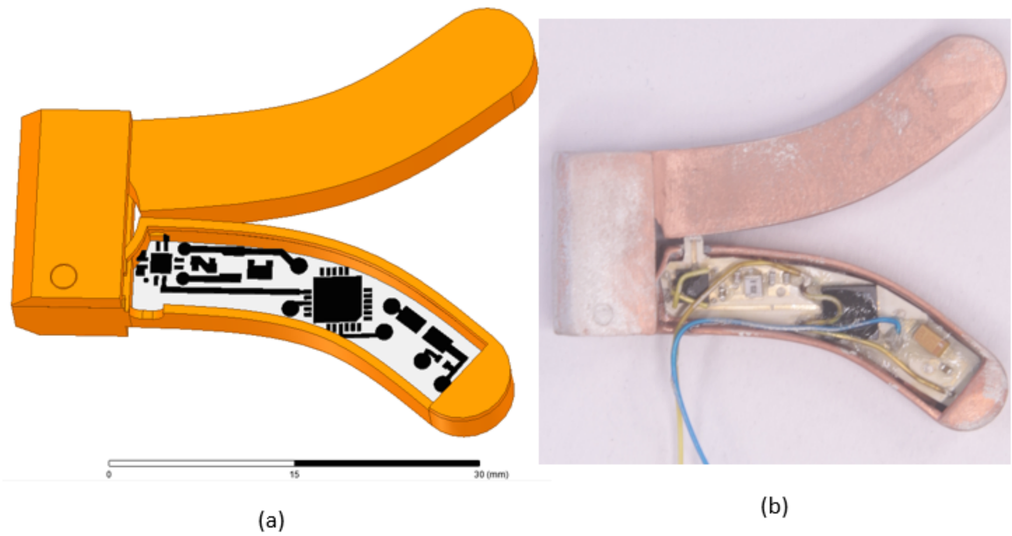

Figure 6.6: Designed SOA (left) Fabricated SOA (right).

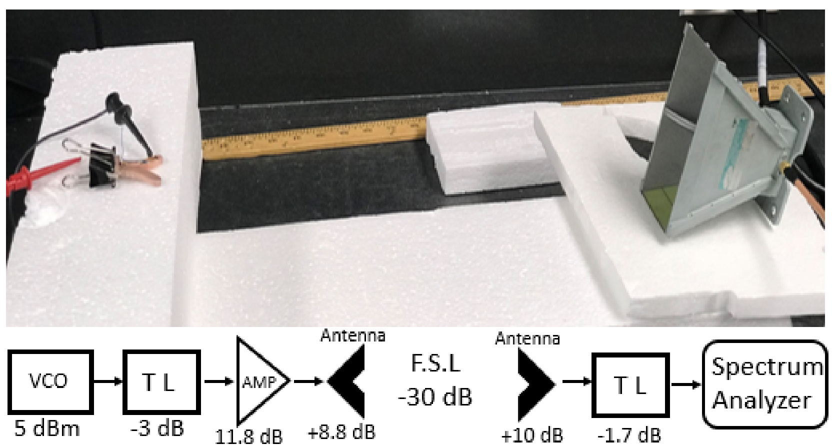

Figure 6.7: Measurement Set-Up.

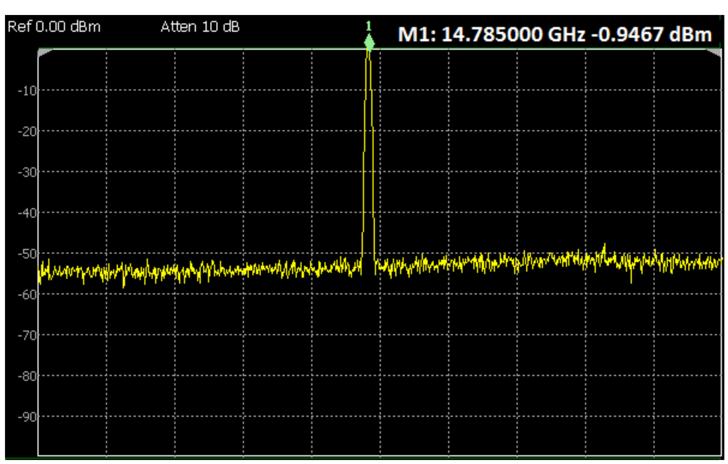

Figure 6.8: Spectrum Analyzer results.

demonstrated consists of a Vivaldi antenna having a pocket for packaging as an integral part of the design and a transmit circuit fabricated on LCP using AJP that is placed in this pocket. The transmit circuit consists of a VCO, PA and the bias network. The radiated power was measured using a horn antenna and a spectrum analyzer. The effective power loss in the circuit is approximately 0.5 dB. The proposed process avoids the use of conventional photolithography or machining techniques. This work shows that high functional density complex RF systems can readily be fabricated using additive manufacturing.

CHAPTER 7

CONCLUSIONS

7.1 Conclusion

In this dissertation, various processes have been shown and developed to combine additive manufacturing with subtractive manufacturing techniques to create high frequency Rf electronics that can be created into a small package which can be capable of operating in the 5G/mm-wave frequency range. This technique began by leveraging photolithography to create fine featured circuits and 3D printing to create the packages to create a System-On-Antenna package. This was further developed to utilize aerosol jet printing to remove the need for photolithography, this reduced the time and cost to create the fine featured circuits which removed the need for specialized equipment and facilities which are typically used to create high frequency systems.

In chapter 2, Polyjet printing was demonstrated to create various passive circuits. This work demonstrated an alternative method to subtractive methods and A.M. methods to create passive components. This showed how Reduced Wave Guide components can be could be made to avoid the use of the printed material as a substrate and allowed for the use of standard edge mount connectors. This chapter demonstrated transmission lines, power divider, a resonator, and various antennas up to 30 GHz. This work demonstrated waveguide like performance in a compact design.

In chapter 3, A.M. components were combined with a flexible substrate LCP to create two antenna versions. The first was a slot coupled patch antenna where the patch was mounted above the ground plane with an A.M. table that supported the patch with air as the substrate. This showed both a single patch and a patch array. High gain was able to be achieved for both the single patch aswell as the 2x2 array. The flexible substrate allowed the array to be bent around a 90 degree bend which yielded a wide 3 dB beamwidth. A scaled down automotive bumper was also demonstrated which had Vivaldi antennas directly embedded within the structure. This work showed how the use of vacuum chambers can be eliminated with the use of aerosol conductive paints which can be incorporated in the assembly for ease of manufacturing. This bumper with embedded antennas operated in the V-band. This demonstrated a promising technique to directly embedding components can be achieved in large structures.

In chapter 4, This built upon the method described in chapter 3. This work utilized a combination of flexible substrates and rigid printed components to fabricate a Rigid-Flex coax-like transmission line. The center conductor of the Rigid-Flex coax was fabricated on the flexible substrate through photolithography and the rigid shell was 3D printed. The Rigid-Flex coax transmission line showed very low loss characteristics. This technique was then utilized to create a high Q-factor resonator as well as a Vivaldi antenna. This technique can be fed with a microstrip 50 Ω line which then allows for the use of a Wilkinson UWB power divider, this allowed for the creation of an A.M. UWB antenna array. This technique allows for a method of achieving 3D printed antenna arrays without the need for coax cables or waveguide structures. This chapter also demonstrated combing aerosol jet printing with the Rigid-Flex Vivaldi array to 3D print the RF resistor for the power divider. This chapter showed a method of achieving high Q resonators as well as 3D printed antenna arrays. With the combination of Aerosol jet printing this technique showed how RF resistors can be printed and fine tuned to achieve the desired resistance.

In chapter 5, a demonstration of a hybrid additive manufacturing approach for the fabrication of high functional-density package was demonstrated. Building on previous chapter work with the hybrid Rigid-Flex transmission lines and Vivaldi, an active receive circuit embedded in a 3D printed Vivaldi antenna was shown. This work allowed for the unused portion of the Vivaldi antenna to be the package for the active circuit. This technique allows to create high-functional density System-On-Antennas that can deliver better performance then traditional methods that utilize connectors and other components to connect directly to horn antennas. This is a promising method to further decreasing the size of the feed between the circuit and the antenna.

in chapter 6, this chapter combines aerosol jet printing and polyjet printing to create a high-functional density package. This technique printed the circuit which has been previously created through photolithography. Using the aerosol jet printer allowed for the creation of the circuit as well as the VIAs to ground to further increase the density of the circuit. The antenna package was printed with the polyjet printer. This technique allows for an extremely cost effective method of producing Systems-On-Antennas with the ability to go into the THz range since the fed size is further decreased.

This work showed the advantages of utilizing two forms of additive manufacturing and commercially available low loss substrates to create high functional density systems. This technique allows for systems to be created without the need for sterile enivroments and wasteful and harmful chemicals. This work shows methods for very fats turn around time at a low cost.

7.2 Additive Manufacturing Limitations

Post printing cleaning of the polyjet printed components poses a significant challenge for metallization. The support material has to be either chemical removed with solvents or mechanically removed, the challenge of this is with any remaining support material the metal comes off. This poses a challenge of needing multiple attempts to metalize if the object is not entirely cleaned. This can be minimized with support material removal optimization.

The metalized layers are when exposed to the environment begin oxidizing over time. This degrades the performance of the components and system. While traditional methods of plating additional metals like gold can help mitigate the issue of oxidation. The issue faced with this is the needing of extra steps to achieve the additional layer. This requires equipment and additional personal. Another method that can be utilized is the use of dielectrics to encapsulate the metal but the dielectric loading effect will need to be taken into account in the design.

The printed metal out of the aerosol jet printer presents a few challenges, it needs to be sintered at temperatures that are not compatible with printed dielectrics. This ink also has relativity low adhesion to polymers which has issues with soldering components or perform rework. The printed metal also has low conductivity limits its ability to preform in high power applications. This can cause the metal to self-heat which can lead to metal degradation and substrate destruction.

APPENDIX

A.1 Future Work

Additive manufacturing has a promising future for creating passive components, with advances in metal printing, components can come off the print bed ready to be used without the need of metallization. With direct metal printing allows for avoidance of utilizing vacuum chambers or chemicals to metalize the structure which will further speed up the process of fabrication and allows for stronger metal.

With the variety of printable polymer materials with the aerosol jet printed, low-loss substrate materials can be deposited, this provides the added benefit of not needing to utilize commercially available substrates. Using these materials, the System-On-Antenna can be fabricated directly. This reduces the cost and time necessary to fabricate package. This would allow for an entirely printed System-On-Antenna with virtually no material waste.

The fine print resolution of the aerosol jet printer can be utilized to create the package directly inside of the polyjet printed antennas. Bare die components can be placed directly inside the cavity of the printed antennas and low-loss materials can be printed to create a specific substrate pattern. Following this the aerosol printer can be utilized to create connections between the die bonding pads and the antennas to create System-On-Antennas well into the THz frequency range. Reducing the number of connections between devices allows for an increase in functional density.

BIBLIOGRAPHY

BIBLIOGRAPHY

[1] J. S. Kilby. Miniaturized electronic circuits, February 06 1959. US Patent 3,138,743.

[2] T. K. Sarkar and M. Salazar Palma. A history of the evolution of radar. In *2014 44th European Microwave Conference*, pages 734–737, 2014.

[3] N. Karim, Y. Zou, and S. Wen. Enhancing overall system functionality and performance with the right packaging solutions. In *2012 13th International Conference on Electronic Packaging Technology High Density Packaging*, pages 19–24, Aug 2012.

[4] R. R. Tummala. Packaging: past, present and future. In *2005 6th International Conference on Electronic Packaging Technology*, pages 3–7, Aug 2005.

[5] M. Shimada. Low cost mcm package for mobile telecommunication. In *Proceedings. 1998 International Conference on Multichip Modules and High Density Packaging (Cat. No.98EX154)*, pages 124–128, April 1998.

[6] T. Datta-Chaudhuri, E. Smela, and P. A. Abshire. System-on-chip considerations for heterogeneous integration of cmos and fluidic bio-interfaces. *IEEE Transactions on Biomedical Circuits and Systems*, 10(6):1129–1142, Dec 2016.

[7] R. R. TUMMALA and J. LASKAR. Gigabit wireless: system-on-a-package technology. *Proceedings of the IEEE*, 92(2):376–387, Feb 2004.

[8] V. Sundaram, R. Tummala, G. White, K. Lim, Lixi Wan, D. Guidotti, Fuhan Liu, S. Bhattacharya, R. M. Pulugurtha, I. R. Abothu, R. Doraiswami, R. V. Pucha, J. Laskar, M. Tentzeris, G. K. Chang, and M. Swaminathan. System-on-a-package (sop) substrate and module with digital, rf and optical integration. In *2004 Proceedings. 54th Electronic Components and Technology Conference (IEEE Cat. No.04CH37546)*, volume 1, pages 17–23 Vol.1, June 2004.

[9] S. Kim, A. Shamim, A. Georgiadis, H. Aubert, and M. M. Tentzeris. Fabrication of fully inkjet-printed vias and SIW structures on thick polymer substrates. *IEEE Transactions on Components, Packaging and Manufacturing Technology*, 6(3):486–496, March 2016.

[10] ASTM International. ASTM Standards . https://www.astm.org/industry/additive-manufacturing-overview.html/, 2015. [Online; accessed 28-July-20019].

[11] M. Liang, J. Wu, X. Yu, and H. Xin. 3d printing technology for rf and thz antennas. In *2016 International Symposium on Antennas and Propagation (ISAP)*, pages 536–537, Oct 2016.

[12] H. Saghlatoon, R. Mirzavand, P. Mousavi, and M. M. Honari. Investigation on the effect of roughness of 3d printed structure on performance of microwave devices. In *2018 18th International Symposium on Antenna Technology and Applied Electromagnetics (ANTEM)*, pages 1–2, Aug 2018.

[13] 3D Systems. 3D Systems . https://www.3dsystems.com/sites/default/files/downloads/3D-Systems-Charles-W-Hull-Executive-Bio.pdf/, 2015. [Online; accessed 28-July-20019].

[14] Formlabs. Formlabs Material. https://formlabs.com/materials/, 2015. [Online; accessed 28-July-20019].

[15] E. Macdonald, R. Salas, D. Espalin, M. Perez, E. Aguilera, D. Muse, and R. B. Wicker. 3d printing for the rapid prototyping of structural electronics. *IEEE Access*, 2:234–242, Dec 2014.

[16] T. Tiedje, S. Lüngen, M. Schubert, M. Luniak, K. Nieweglowski, and K. Bock. Will low-cost 3d additive manufactured packaging replace the fan-out wafer level packages? In *2017 IEEE 67th Electronic Components and Technology Conference (ECTC)*, pages 1065–1070, May 2017.

[17] J. A. Byford and P. Chahal. Ultra-wideband hybrid substrate integrated ribbon waveguides using 3d printing. In *2016 IEEE MTT-S International Microwave Symposium (IMS)*, pages 1–4, May 2016.

[18] J. A. Byford, M. I. M. Ghazali, S. Karuppuswami, B. L. Wright, and P. Chahal. Demonstration of rf and microwave passive circuits through 3-d printing and selective metalization. *IEEE Transactions on Components, Packaging and Manufacturing Technology*, 7(3):463–471, March 2017.

[19] P. Chahal, J. A. Hejase, S. Shane, K. Y. Park, A. Kaur, and J. Byford. Millimeter wave and terahertz dielectric probe microfluidic sensors. In *2014 39th International Conference on Infrared, Millimeter, and Terahertz waves (IRMMW-THz)*, pages 1–2, Sep. 2014.

[20] A. Delage, N. Delhote, S. Verdeyme, B. Bonnet, L. Carpentier, C. Schick, T. Chartier, and C. Chaput. Aerosol jet printing of millimeter wave transmission lines on 3d ceramic substrates made by additive manufacturing. In *2018 IEEE/MTT-S International Microwave Symposium - IMS*, pages 1557–1560, June 2018.

[21] M. Abt, A. Roch, J. A. Qayyum, S. Pestotnik, L. Stepien, A. Abu-Ageel, B. Wright, A. C. Ulusoy, J. Albrecht, L. Harle, J. Papapolymerou, and T. Schuelke. Aerosol-printed highly conductive ag transmission lines for flexible electronic devices. *IEEE Transactions on Components, Packaging and Manufacturing Technology*, 8(10):1838–1844, Oct 2018.

[22] C. Oakley, A. Kaur, J. A. Byford, and P. Chahal. Aerosol-Jet Printed Quasi-Optical Terahertz Filters. In *2017 IEEE 67th Electronic Components and Technology Conference (ECTC)*, pages 248–253, May 2017.

[23] F. Cai, Y. H. Chang, K. Wang, W. T. Khan, S. Pavlidis, and J. Papapolymerou. High resolution aerosol jet printing of D-band printed transmission lines on flexible LCP substrate. In *2014 IEEE MTT-S International Microwave Symposium (IMS2014)*, pages 1–3. IEEE, 2014.

[24] M. T. Craton, J. Sorocki, I. Piekarz, S. Gruszczynski, K. Wincza, and J. Papapolymerou. Realization of Fully 3D Printed W-Band Bandpass Filters Using Aerosol Jet Printing Technology. In *2018 48th European Microwave Conference (EuMC)*, pages 1013–1016, Sep. 2018.

[25] Y. He, C. Oakley, P. Chahal, J. Albrecht, and J. Papapolymerou. Aerosol Jet printed 24 GHz end-fire quasi-Yagi-Uda antenna on a 3-D printed cavity substrate. In *2017 International Workshop on Antenna Technology: Small Antennas, Innovative Structures, and Applications (iWAT)*, pages 179–182, March 2017.

[26] A. A. Gupta, A. Bolduc, S. G. Cloutier, and R. Izquierdo. Aerosol Jet Printing for printed electronics rapid prototyping. In *2016 IEEE International Symposium on Circuits and Systems (ISCAS)*, pages 866–869, May 2016.

[27] V. Gjokaj, C. Crump, J. Papapolymerou, J. Albrecht, and P. Chahal. Vivaldi antenna array fabricated using a hybrid process. In *2019 IEEE 69th Electronic Components and Technology Conference (ECTC)*, pages 948–953, 2019.

[28] V. Gjokaj, C. Crump, B. Wright, and P. Chahal. Direct printing of antennas on large 3d printed plastic structures. In *2020 IEEE 70th Electronic Components and Technology Conference (ECTC)*, pages 666–670, 2020.

[29] D. Espalin, D. W. Muse, E. MacDonald, and R. B. Wicker. 3D Printing multifunctionality: structures with electronics. *The International Journal of Advanced Manufacturing Technology*, 72(5-8):963–978, 2014.

[30] M. I. M. Ghazali, S. Karuppuswami, S. Mondal, A. Kaur, and P. Chahal. Embedded Actives Using Additive Manufacturing for High-Density RF Circuits and Systems. *IEEE Transactions on Components, Packaging and Manufacturing Technology*, 9(8):1643–1651, Aug 2019.

[31] S. Biber, J. Schur, A. Hofmann, and L. P. Schmidt. Design of new passive THz devices based on micromachining techniques. In *The Fifth International Kharkov Symposium on Physics and Engineering of Microwaves, Millimeter, and Submillimeter Waves (IEEE Cat. No.04EX828)*, volume 1, pages 26–31 Vol.1, June 2004.

[32] H. Lipson and M. Kurman. *Fabricated: The New World of 3D printing.* John Wiley & Sons, 2013.

[33] A. Kaur, J. C. Myers, M. I. M. Ghazali, J. Byford, and P. Chahal. Affordable terahertz components using 3D printing. In *2015 IEEE 65th Electronic Components and Technology Conference (ECTC)*, pages 2071–2076, May 2015.

[34] M. I. Mohd Ghazali, S. Mondal, S. Karuppuswami, and P. Chahal. 3D Printed Substrates for the Design of Compact RF Systems. In *2019 IEEE 69th Electronic Components and Technology Conference (ECTC)*, pages 113–118, May 2019.

[35] Cobham H-1498. Cobham H-1498. https://www.cobham.com/media/101067/H-1498 [Online; accessed 28-July-20019].

[36] M. Craton, J. A. Byford, V. Gjokaj, J. Papapolymerou, and P. Chahal. 3d printed high frequency coaxial transmission line based circuits. In *2017 IEEE 67th Electronic Components and Technology Conference (ECTC)*, pages 1080–1087, May 2017.

[37] J. A. Byford, Z. Purtill, and P. Chahal. Fabrication of Terahertz Components Using 3D Printed Templates. In *2016 IEEE 66th Electronic Components and Technology Conference (ECTC)*, pages 817–822, May 2016.

[38] J. A. Byford, M. I. M. Ghazali, S. Karuppuswami, B. L. Wright, and P. Chahal. Demonstration of RF and Microwave Passive Circuits Through 3-D Printing and Selective Metalization. *IEEE Transactions on Components, Packaging and Manufacturing Technology*, 7(3):463–471, March 2017.

[39] D.M. Pozar. *Microwave Engineering*. Wiley, 2004.

[40] J. A. Hejase, J. Myers, L. Kempel, and P. Chahal. Design study of electronically steerable half-width microstrip leaky wave antennas. In *2011 IEEE 61st Electronic Components and Technology Conference (ECTC)*, pages 1348–1353, May 2011.

[41] V. Gjokaj, J. Papapolymerou, J. Albrecht, and P. Chahal. A Novel Rigid-Flex Aperture Coupled Patch Antenna Array. In *2018 Asia-Pacific Microwave Conference (APMC)*, pages 597–599, Nov 2018.

[42] M. I. M. Ghazali, E. Gutierrez, J. C. Myers, A. Kaur, B. Wright, and P. Chahal. Affordable 3D printed microwave antennas. In *2015 IEEE 65th Electronic Components and Technology Conference (ECTC)*, pages 240–246, May 2015.

[43] M. I. M. Ghazali, S. Karuppuswami, A. Kaur, and P. Chahal. 3-d printed air substrates for the design and fabrication of rf components. *IEEE Transactions on Components, Packaging and Manufacturing Technology*, 7(6):982–989, June 2017.

[44] V. Gjokaj, P. Chahal, J. Papapolymerou, and J. D. Albrecht. A novel 3d printed vivaldi antenna utilizing a substrate integrated waveguide transition. In *2017 IEEE International Symposium on Antennas and Propagation USNC/URSI National Radio Science Meeting*, pages 1253–1254, July 2017.

[45] Alongkorn Pimpin and Werayut Srituravanich. *Review on Micro- and Nanolithography Techniques and their Applications*. Engineering Journal, 2012.

[46] Constantine A. Balanis. *Antenna Theory Analysis and Design*. Wileyl, 2005.

[47] P. Sullivan and D. Schaubert. Analysis of an aperture coupled microstrip antenna. *IEEE Transactions on Antennas and Propagation*, 34(8):977–984, Aug 1986.

[48] A. Shamim. 3D Inkjet Printed Flexible and Wearable Antenna Systems. In *2017 International Symposium on Antennas and Propagation (ISAP)*, pages 1–2, Oct 2017.

[49] A. Eshkeiti, A. S. G. Reddy, S. Emamian, B. B. Narakathu, M. Joyce, M. Joyce, P. D. Fleming, B. J. Bazuin, and M. Z. Atashbar. Screen Printing of Multilayered Hybrid Printed Circuit Boards on Different Substrates. *IEEE Transactions on Components, Packaging and Manufacturing Technology*, 5(3):415–421, March 2015.

[50] V. Gjokaj, C. Crump, J. Papapolymerou, J. Albrecht, and P. Chahal. Vivaldi Antenna Array Fabricated Using a Hybrid Process. In *2019 IEEE 69th Electronic Components and Technology Conference (ECTC)*, pages 948–953, May 2019.

[51] V. Gjokaj, P. Chahal, J. Papapolymerou, and J. D. Albrecht. A Novel 3D Printed Vivaldi Antenna Utilizing a Substrate Integrated Waveguide Transition. In *2017 IEEE International Symposium on Antennas and Propagation USNC/URSI National Radio Science Meeting*, pages 1253–1254, July 2017.

[52] M. I. M. Ghazali, K. Y. Park, J. A. Byford, J. Papapolymerou, and P. Chahal. 3D Printed Metalized Polymer UWB High Gain Vivaldi Antennas. In *2016 IEEE MTT-S International Microwave Symposium (IMS)*, pages 1–4, May 2016.

[53] T. G. Spence and R. Rodriguez. Additively Manufactured Ultrawideband, Wide Scan, Monolithic Vivaldi Arrays. In *2017 IEEE International Symposium on Antennas and Propagation USNC/URSI National Radio Science Meeting*, pages 1239–1240, July 2017.

[54] B. S. Cook and A. Shamim. Inkjet Printing of Novel Wideband and High Gain Antennas on Low-Cost Paper Substrate. *IEEE Transactions on Antennas and Propagation*, 60(9):4148–4156, Sept 2012.

[55] G. McKerricher, D. Titterington, and A. Shamim. A Fully Inkjet-Printed 3-D Honeycomb-Inspired Patch Antenna. *IEEE Antennas and Wireless Propagation Letters*, 15:544–547, 2016.

[56] R. Bairavasubramanian, D. Thompson, G. DeJean, G. E. Ponchak, M. M. Tentzeris, and J. Papapolymerou. Development of mm-wave dual-frequency multilayer antenna arrays on liquid crystal polymer (lcp) substrate. In *2005 IEEE Antennas and Propagation Society International Symposium*, volume 1B, pages 393–396 vol. 1B, 2005.

[57] G. Wells and P. Pramanick. An accurate dispersion model for shielded microstrip lines. In *Symposium on Antenna Technology and Applied Electromagnetics [ANTEM 1994]*, pages 229–232, Aug 1994.

[58] J. D. Martínez, S. Sirci, V. E. Boria, P. Martín-Iglesias, and H. Leblond. Practical considerations on the design and optimization of substrate integrated coaxial filters. In *2017 IEEE MTT-S International Conference on Numerical Electromagnetic and Multiphysics Modeling and Optimization for RF, Microwave, and Terahertz Applications (NEMO)*, pages 299–301, May 2017.

[59] Simon Ramo, John R Whinnery, and Theodore Van Duzer. *Fields and waves in communication electronics*. John Wiley & Sons, 2008.

[60] D.M. Pozar. *Microwave Engineering*. Wiley, 2004.

[61] D. Hawatmeh and T. Waller. A s/c-band high q resonator architecture for direct print additive manufacturing. In *2017 IEEE 18th Wireless and Microwave Technology Conference (WAMICON)*, pages 1–4, April 2017.

[62] Stratasys 350. Stratasys 350. https://www.stratasys.com/3d-printers/objet-350-500-connex3/, 2020. [Online; accessed 28-July-20019].

[63] Mohd Ifwat Mohd Ghazali, Jennifer A Byford, Saranraj Karuppuswami, Amanpreet Kaur, James Lennon, and Premjeet Chahal. 3D printed out-of-plane antennas for use on high density boards. In *2017 IEEE 67th Electronic Components and Technology Conference (ECTC)*, pages 1835–1842. IEEE, 2017.

[64] D. De, A. Prakash, N. Chattoraj, P. K. Sahu, and A. Verma. Design and analysis of various Wilkinson Power Divider Networks for L band applications. In *2016 3rd International Conference on Signal Processing and Integrated Networks (SPIN)*, pages 67–72, Feb 2016.

[65] C. Ionescu, P. Svasta, A. Vasile, and D. Bonfert. Investigations on organic printed resistors based on pedot:pss. In *2012 IEEE 18th International Symposium for Design and Technology in Electronic Packaging (SIITME)*, pages 85–89, Oct 2012.

[66] C. Sriprachuabwong, C. Srichan, T. Lomas, and A. Tuantranont. Simple rc low pass filter circuit fabricated by unmodified desktop inkjet printer. In *ECTI-CON2010: The 2010 ECTI International Confernce on Electrical Engineering/Electronics, Computer, Telecommunications and Information Technology*, pages 929–932, May 2010.

[67] Byung Ju Kang, Chang Kyu Lee, and Je Hoon Oh. All-inkjet-printed electrical components and circuit fabrication on a plastic substrate. *Microelectronic Engineering*, 97:251–254, 09 2012.

[68] V Correia, K.Y. Mitra, Hélder Castro, J.G. Rocha, Enrico Sowade, Reinhard Baumann, and Senentxu Lanceros-Méndez. Design and fabrication of multilayer inkjet-printed passive components for printed electronics circuit development. *Journal of Manufacturing Processes*, 31:364–371, 01 2018.

[69] J. A. Paulsen, M. Renn, K. Christenson, and R. Plourde. Printing conformal electronics on 3D structures with aerosol jet technology. In *2012 Future of Instrumentation International Workshop (FIIW) Proceedings*, pages 1–4, Oct 2012.

[70] M. Himdi. Tutorial 1: MM-wave antenna design and technologies. In *2014 IEEE Asia-Pacific Conference on Applied Electromagnetics (APACE)*, pages xiv–xiv, Dec 2014.

[71] A. K. Keskin, M. Dagcan Senturk, S. Demirel, A. Kizilay, and A. S. Turk. Front-end design for Ka band mm-Wave radar. In *2016 17th International Radar Symposium (IRS)*, pages 1–4, May 2016.

[72] W. T. Khan, A. Çağrı Ulusoy, G. Dufour, M. Kaynak, B. Tillack, J. D. Cressler, and J. Papapolymerou. A D-Band Micromachined End-Fire Antenna in 130-nm SiGe BiCMOS Technology. *IEEE Transactions on Antennas and Propagation*, 63(6):2449–2459, June 2015.

[73] S. Pan, F. Caster, P. Heydari, and F. Capolino. A 94-GHz Extremely Thin Metasurface-Based BiCMOS On-Chip Antenna. *IEEE Transactions on Antennas and Propagation*, 62(9):4439–4451, Sept 2014.

[74] M. R. Karim, X. Yang, and M. F. Shafique. On chip antenna measurement: A survey of challenges and recent trends. *IEEE Access*, 6:20320–20333, 2018.

[75] Kyutae Lim, A. Obatoyinbo, M. Davis, J. Laskar, and R. Tummala. Development of planar antennas in multi-layer packages for RF-system-on-a-package applications. In *IEEE 10th Topical Meeting on Electrical Performance of Electronic Packaging (Cat. No. 01TH8565)*, pages 101–104, 2001.

[76] S. Kaundinya, E. Arnold, F. Rodriguez-Morales, and A. Patil. A UAS-based ultra-wideband radar system for soil moisture measurements. In *2018 IEEE Radar Conference (RadarConf18)*, pages 0721–0726, April 2018.

[77] Minicircuits AVA-24+ Datasheet. https://www.minicircuits.com/pdfs/AVA-24+.pdf. Accessed: 2018-07-24.

[78] Minicircuits SIM-153+ Datasheet. https://www.minicircuits.com/pdfs/SIM-153+.pdf. Accessed: 2018-07-24.

[79] V. Gjokaj, J. Papapolymerou, J. Albrecht, and P. Chahal. Design and Fabrication of Additively Manufactured Hybrid Rigid-Flex RF Components . In *2018 IEEE CPMT*, June 2018. Unpublished.

[80] Yuxiao He, C. Oakley, P. Chahal, J. Albrecht, and J. Papapolymerou. Aerosol jet printed 24 GHz end-fire quasi-yagi-uda antenna on a 3-D printed cavity substrate. In *2017 International Workshop on Antenna Technology: Small Antennas, Innovative Structures, and Applications (iWAT)*, pages 179–182, March 2017.

[81] F. Cai, S. Pavlidis, J. Papapolymerou, Y. H. Chang, K. Wang, C. Zhang, and B. Wang. Aerosol jet printing for 3-D multilayer passive microwave circuitry. In *2014 44th European Microwave Conference*, pages 512–515, Oct 2014.

[82] Y. Cho, M. Y. Elsayed, and M. N. El-Gamal. A metal-oxide gas sensor based on an aerosol jet printing technology featuring a one second response time. In *2019 20th International Conference on Solid-State Sensors, Actuators and Microsystems Eurosensors XXXIII (TRANSDUCERS EUROSENSORS XXXIII)*, pages 1333–1336, June 2019.

[83] C. Oakley and P. Chahal. Aerosol jet printed quasi-optical terahertz components. *IEEE Transactions on Terahertz Science and Technology*, 8(6):765–772, Nov 2018.

[84] J. Krzeminski, J. Krzeminski, M. Jakubowska, A. Kanthamneni, D. Wagner, M. Detert, and B. Schmidt. Pads and microscale vias with aerosol jet printing technique. In *2017 21st European Microelectronics and Packaging Conference (EMPC) Exhibition*, pages 1–4, Sep. 2017.